GRAVITY CONSTRAINTS ON THE TECTONIC EVOLUTION OF THE SIBUNDOY VALLEY, EASTERN CORDILLERA OF COLOMBIA

By

Stalin Alexander Rosero

December, 2024

Director of thesis: Dr. David Farris

Major Department: Department of Geological Sciences

ABSTRACT

The Sibundoy Valley is a hinterland basin, located in the Eastern Cordillera of Colombia, near the Ecuadorian border. The valley trends to the northeast and has a rhomboidal shape with an approximate area of 100 km^2. The hinterland basin is near the wedge top of a retro-arc basin between the Andean magmatic arc and the Guiana craton. Here, multiple fault types are active due to oblique convergence between the Nazca Plate and South America Plate. The North Andean Block is moving with a slip rate of 21-22 mm/year eastward and a 5-6 mm/year northward. Therefore, two potential models are proposed to explain the tectonic evolution of the Sibundoy Valley. In model 1, a step over between strike-slip faults produced a pull apart basin. In model 2, a system of reverse faults produced a contractional piggyback basin. To distinguish between these models, a combination of surface geology, gravity modeling and density measurements has been used.

Complete Bouguer Anomaly values indicate that the Sibundoy Valley has a negative anomaly of 30 mGal. The density of the basin infill is approximately 1.8 g/cm^3. This density estimate is constrained by measured values of surface rocks and comparison of variable density subsurface gravity models. Overall, the 3-D shape of the basin was determined by gridding together multiple 2-D gravity transect models. These show the basin has a half-

graben shape where the deepest depression (-1300 m) is located at the southwestern side of the basin, and it thins to the northeast. It is likely that a normal fault created most of the accommodation space at the southwestern side of the basin, creating the half-graben shape. The northwest to southeast trending models suggests that a shallowly dipping fault outcrops at the northwestern side of the basin and extends as a master fault underneath the basin to the south. Gravity models also disallow a traditional strike-slip step over geometry as steep strike-slip basin bounding faults do not fit measured gravity data. Unfortunately, the gravity models do not provide the kinematics of the master fault, despite well constraining its geometry so the three different types of basins (piggyback, pull-apart, and hinterland basins) are still possible. Nevertheless, a rifting (or supradetachment) hinterland basin may be the most likely model to describe the tectonic evolution of the basin, considering the shape of the basin, geologic setting, and transtentional kinematics of the faults.

GRAVITY CONSTRAINTS ON THE TECTONIC EVOLUTION OF THE SIBUNDOY VALLEY, EASTERN CORDILLERA OF COLOMBIA

A Thesis

Presented to the Faculty of the Department of Geological Sciences

East Carolina University

In Partial fulfillment of the Requirements for the Degree

Master of Science in Geology

By

Stalin Alexander Rosero

December 2024

Director of Thesis: David Farris, PhD

Thesis Committee Members:

Adriana Heimann-Rios, PhD

Eric Horsman, PhD

Agustín Cardona, PhD

DEDICATION

I dedicate my thesis project to my whole family members: father, mother, sister and grandmother. Despite of the distance, they were always close to me. My dream of studying in the United States was possible thanks to my grandmother, Blanca Pozo. She trusted in me, and I will always be grateful for this gesture that changed my life.

ACKNOWLEDGEMENTS

The dream of studying in the United States became reality due to the help and encouragement of Dr. Rafael Almeida. He persuaded me to attend the 2020 GSA Conference where I was introduced to Dr. Eric Horseman. I will be always grateful to him because I started to trust in my skills and knowledge to conduct research projects.

This present thesis project has been possible because of the constant support of my thesis advisor, Dr. David Farris. He provided the data of the gravity survey, which was conducted in the Sibundoy valley. In addition, he taught me how to use gravity modelling programs along with GIS software. Despite my Hispanic accent, he was so patient and encouraging during the process of sharing ideas. I would like to extend my gratitude to the faculty of the Department of Geological Sciences at East Carolina University, especially Dr. Eric Horseman, Dr. Adriana Heimann-Rios and Dr. David Mallinson. Their lectures were so interesting and enriching that they enabled me to have a broader comprehension of Mineralogy, Petrology and Geophysics.

Finally, I would like to thank my committee members: Dr. Agustin Cardona, Dr. Adriana Heimann-Rios, Dr. Eric Horseman, and Dr. David Farris. They always shared enthusiasm and interest in my research project, especially when they provided edits and comments.

TABLE OF CONTENTS

LIST OF TABLES

LIST OF FIGURES

CHAPTER 1 : INTRODUCTION

Synorogenic basins develop in association with orogens in the foreland or in the hinterland, and they are continuously filled by erosional products of the uplifted topography (Roure, 2008). In South America, hinterland basins (e.g., Tres Cruces basin, Altiplano Basin, Callejon de Huaylas Basin, Cuenca Basin, and Magdalena Valley) are located between the western magmatic arc and the craton-directed fold and thrust belt to the east (Horton, 2011). The location of the Sibundoy basin (**Figure 1**) is complex due to the proximity of the “knot” of Pastos (~62 km) and the beginning of the Magdalena hinterland basin (~200 km). The elevation profile shows that the Sibundoy Basin has a significant elevation, and it is embedded in the orogenic wedge of the Eastern Cordillera of Colombia (**Figure 2B**). The Sibundoy Valley can be considered as a hinterland basin because of the similar structural position compared to the Magdalena Valley, and a relative difference in elevation compared to the orogenic wedge **(Figure 2C**).

Generally, the basins are 10-100 km wide by 10-500 long with Cenozoic fill **(Horton, 2011)**. Sibundoy Valley is an example of a Quaternary hinterland basin, located at the southernmost part of the Eastern Cordillera of Colombia, in the Department of Putumayo. The basin has a significant topographic expression, and its shape is rhombohedral with an approximate area of 100 km^2 (**Figure 1b**). The genesis of hinterland basins is complex because a combination of processes can create the sediment accommodation space of the basin in a retro arc position.

The oblique convergence between the Nazca and South American Plates creates strain partitioning in the upper crust with most of the oblique component absorbed by active strike-slip faults, which run parallel to the plate boundary **(Roure, 2008)**. Generally, strike-slip dominated basins (e.g., pull apart basins) develop between two parallel vertical strike-slip fault segments with a transverse system of oblique extensional faults, creating basin accommodation space. In other cases, thrusting is not restricted to the foreland basin margin and may subdivide the foreland basin to form piggyback basins that lie on top of the thrust sheets. Such piggyback basins are also separated from the foredeep **(Horton, 2011)**. At retro-arc positions within the Andes, defining fault-induced subsidence remains a challenge because a combination of strain partitioning, strike-slip faulting, thrust activation or sub-thrust tectonic accretion, and localized extension may occur at the same time. Finally, fault planes inside the basins are difficult to analyze due to the infilling of sediments.

In summary, the issues outlined above concentrate on the question of how active tectonics can influence the short-term evolution of Quaternary hinterland basins (e.g., Sibundoy Valley) in Andean retro-arc positions. This thesis project combines surface geology, gravity modeling and density measurements to distinguish the best model that describes the tectonic evolution of the Sibundoy Valley. By using gravity data, the dimensions of the basin and the fault steps in the subsurface become recognizable for interpretation. The analysis of faults and basin geometry will determine which tectonic model best fits the observations: Model 1: strike-slip faulting and pull apart basin formation, or Model 2: thrust faulting and hinterland basin formation. Gravity models along multiple transects will enable a better interpretation of the basin geometry and tectonics because the interaction between the infilling sediments, faults and the basement are constrained.

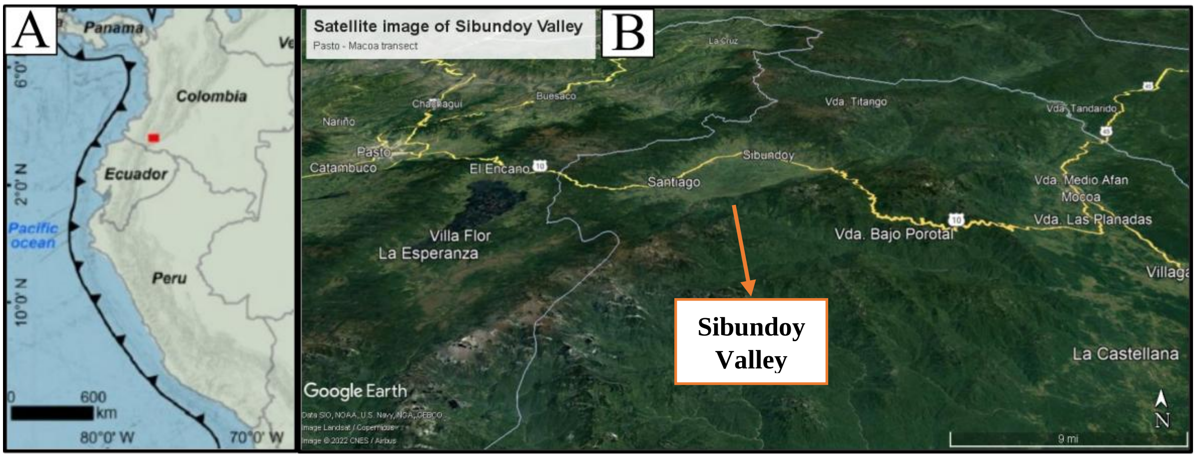

Figure 1 A) Location of the Sibundoy Basin in the southernmost part of Colombia, near Ecuador; taken from ***(Restrepo et al., 2021)***. B) Topographic expression of Sibundoy Valley shows a rhombohedral shape with an approximate area of 100 km^2, next to La Cocha lake and between the towns of Pasto and Mocoa.

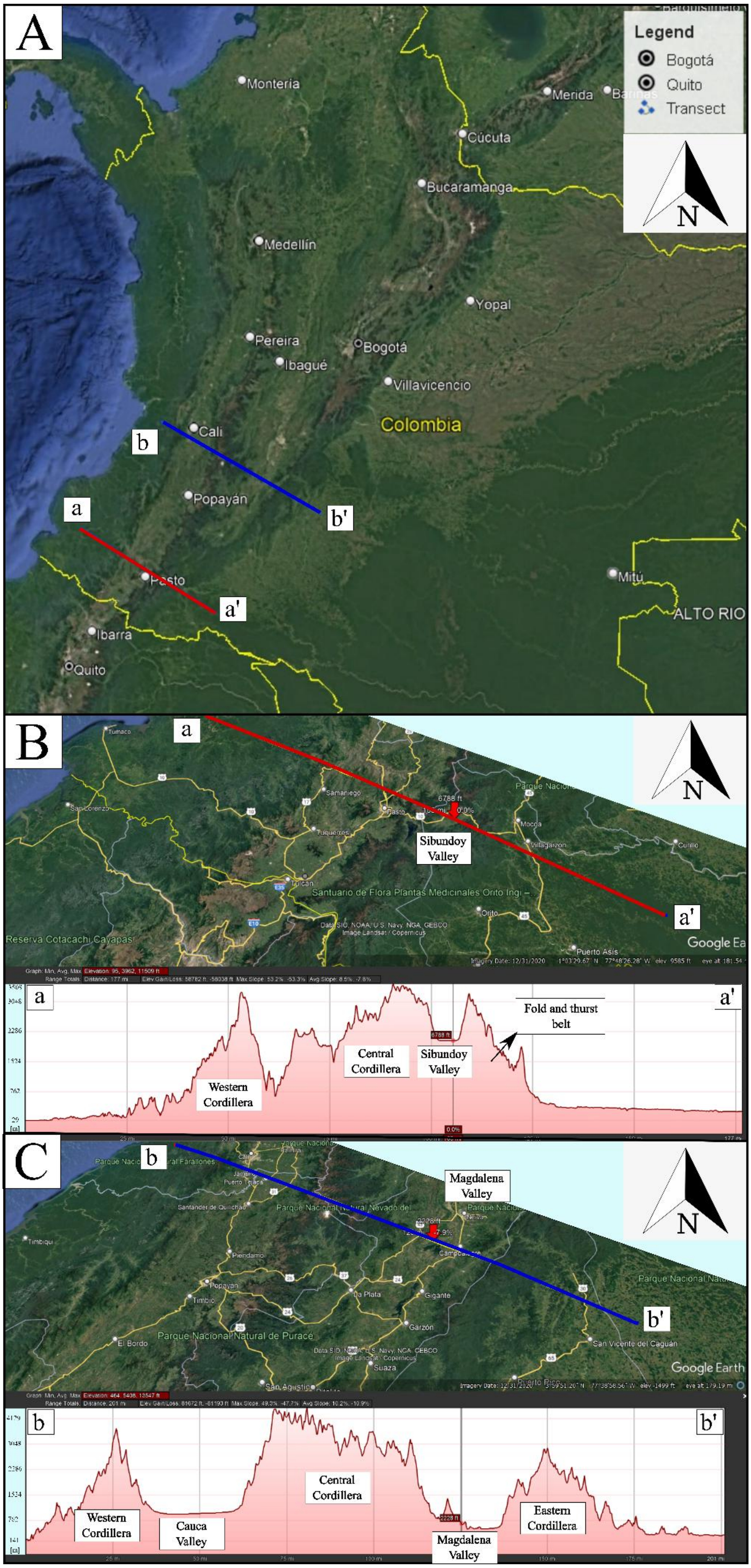
A
Legend
Bogotá
Quito
Transect
N
Monteria
Merida
Cúcuta
Bucaramanga
Medellín
Yopal
Pereira
Bogotá
Ibagué
Villavicencio
Colombia
Cali
b
Popayán
b'
a
Pasto
a'
Mitú
ALTO RIO
Ibarra
Quito
B
a
N
Sibundoy Valley
a'
Google Ea
a
a'
Fold and thurst belt
Central Cordillera
Sibundoy Valley
Western Cordillera
C
b
Magdalena Valley
N
b'
Google Earth
b
b'
Central Cordillera
Eastern Cordillera
Western Cordillera
Cauca Valley
Magdalena Valley

Figure 2 Elevation profiles across the Colombian Andes at two different points: B) Sibundoy Valley and C) Campoalegre (Magdalena Valley). The transect cuts the Andes with a northwest to southeast trend. The elevation is in meter units. We observe that at Sibundoy Valley, the three Cordilleras have not been developed yet. In contrast, three Cordilleras are completely developed at Campoalegre (Magdalena Valley).

1.1.Geologic Setting

The Quaternary Sibundoy basin is located just east of the axis of the Eastern Cordillera of Colombia. However, at this location, the Andean Cordillera bifurcates at the "knot of Pastos", into the Central and the Eastern Cordilleras. Thus, learning the Sibundoy Basin tectonic framework is critical to understanding the tectonic development of the Colombian Andes in general.

Most rocks in the Northern Andes were formed by the subduction of Pacific oceanic lithosphere beneath continental crust of north-western South America since ~209 Ma **(Horton & Folguera, 2019)**. Throughout this time period, slab rollback velocities, changing plate convergence vectors and terrane accretion have all influenced subduction processes. In addition, during the Cretaceous, the Caribbean Large Igneous Province collided and accreted the north-western margin of South American Plate **(Horton & Folguera, 2019)**.

The Eastern, Central, and Western Cordilleras comprise the Northern Andes of Colombia, which are separated by the Cauca and Magdalena Valleys. The Eastern Cordillera constitutes a Precambrian-Paleozoic metamorphic basement, and it is covered by Paleozoic-Cenozoic marine and siliciclastic sedimentary sequences **(Mora et al., 2009) (Restrepo et al., 2021)**. Eastern Cordillera has a fold and thrust belt, which is adjacent to the Putumayo basin (foreland basin). In addition, the Eastern Cordillera is intruded by Cretaceous dikes and sills **(Vásquez, et al., 2010)**. The Central Cordillera also has a metamorphic basement with ages ranging from Paleozoic to Triassic, which was intruded by Jurassic – Cretaceous I-type plutonic bodies **(Cochrane et al., 2014) (Spikings et al., 2015)**. For example, the Ibague, Segovia, and San Lucas Jurassic batholiths outcrop along the eastern and western flanks of the Upper Magdalena Valley within the Central Cordillera of Colombia **(Rodríguez, Arango, Zapata, & Bermúdez, 2018)**. In addition, Jurassic volcanic rock sequences (e.g., Saldana and Norean formations) also outcrop within the westernmost flank of the Central Cordillera **(Vinasco, Cordani, González, Weber, & Pelaez, 2006)**. The basement has been capped by ash and lava derived from ~ 20 volcanoes of the Quaternary Period. Finally, the Western Cordillera includes allochthonous mafic volcanic rocks accreted to the continental margin since the Late Cretaceous **(Villagómez et al., 2011)**.

1.2.Neotectonics

The Central and Eastern Cordillera of Colombia are located at a convergent margin where the Nazca Plate is subducting eastwards beneath South American Plate at a rate of 5-7 cm/year **(Nocquet et al., 2014)**. A recent study estimates that the North Andean Block is moving to the northeast (060°) at a rate of 8.6 mm/year **(Mora-Páez et al., 2019)**. According to **Mora-Páez et al., (2019)**, the total amount of convergence within the upper plate is approximately between 21-22 mm/year eastwards and 5-6 mm/year northwards. The high segmentation of the Nazca Plate along the North Andean margin is caused by crustal heterogeneity on the plate, such as bathymetric differences between the Cocos, Malpelo and Carnegie ridges, and oblique collision with the South American Plate, particularly in southern Colombia and Ecuador **(Gutscher, Malavieille, Lallemand, & Collot, 1999)**. Another component of segmentation is the collision of the Panama Block against the northern part of the North Andean Block, which began at 23-25 Ma **(Farris et al., 2011)**. The width of the North Andean Cordillera widens significantly inboard of the Panama Block collision (**Figure 3**). For example, the Andes width is ~ 284 km along the b – b' transect (**Figure 2**), although the collision zone is significantly far away from this transect. In addition, the North Andean Cordillera experienced a broad episode of exhumation at the Oligocene/Miocene boundary with onset of the Panama arc collision (according to fission track thermochronology), **(Farris et al., 2011)**.

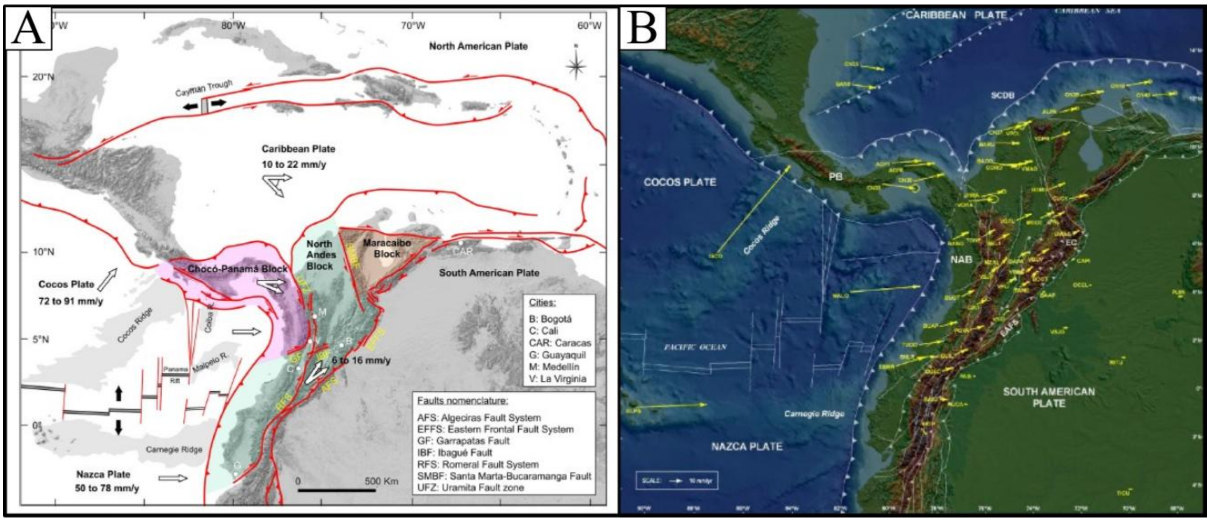

Figure 3 A) The main drivers of deformation of the Andes are the Carnegie Ridge subduction and the collision of the Panama Block **(Farris et al., 2011)**. The width of the North Andean Cordillera widens inboard of the Panama Block collision. B) The total amount of convergence is approximately between 21-22 mm/year eastwards and 5-6 mm/year northwards **(Mora-Páez et al., 2019)**.

According to GPS data, the motion of the convergent margin of the South American Plate occurs in domains. The GPS data suggests an ongoing eastward collision of the Panama arc and Colombia **(Trenkamp, Kellogg, Freymueller, & Mora, 2002)**. The North Andean Block encompasses the Andes from Ecuador to western Venezuela and is moving east to northeastwards in Ecuador and Colombia with a velocity of 7.5 – 9.5 mm yr^{-1} **(Nocquet et al., 2014) (Alvarado et al., 2016)**. In the southernmost part of Colombia, the eastern border of the sliver runs along the Central Cordillera of Colombia, and it has a right-lateral transpressional motion **(Nocquet et al., 2014)**.

The eastern boundary of the North Andean Block correlates with active faults and the location of major historical earthquakes **(Beauval et al., 2013)**. **Tibaldi, Rovida, & Corazzato (2007)** identified a Pleistocene-Holocene right lateral strike-slip motion on the Cayambe – Afiladores – Sibundoy transcurrent fault system with a 7.7 ± 0.4 to 11.9 ± mm year^{-1} slip rate. Active fault systems with high slip rates suggest a significant component of the oblique convergence between Nazca and South American Plates. This fault system accommodates most of the slip between both plates.

1.3. Proposed models

There have been several regional studies where Sibundoy Valley has been studied partially (e.g. **Tibaldi, Rovida, & Corazzato, 2007**; **Velandia, Acosta, Terraza, & Villegas, 2005**) regarding the strike-slip fault systems along the Eastern Cordillera of Ecuador and Colombia (e.g. Algeciras Fault System). They suggested that the Sibundoy Valley is a pull-apart basin that formed by a local overstep of the Sibundoy fault, which is related to the Algeciras Fault System **(Velandia, Acosta, Terraza, & Villegas, 2005)**. In addition to the fault system, the main evidence for the latter interpretation is the rhombohedral shape of the basin. This section provides two tectonic model end members that may describe the tectonic evolution of Sibundoy Valley. These models take into consideration the possibility of significant slip partitioning along strike-slip fault systems on top of a fold and thrust belt in the Andean retro arc.

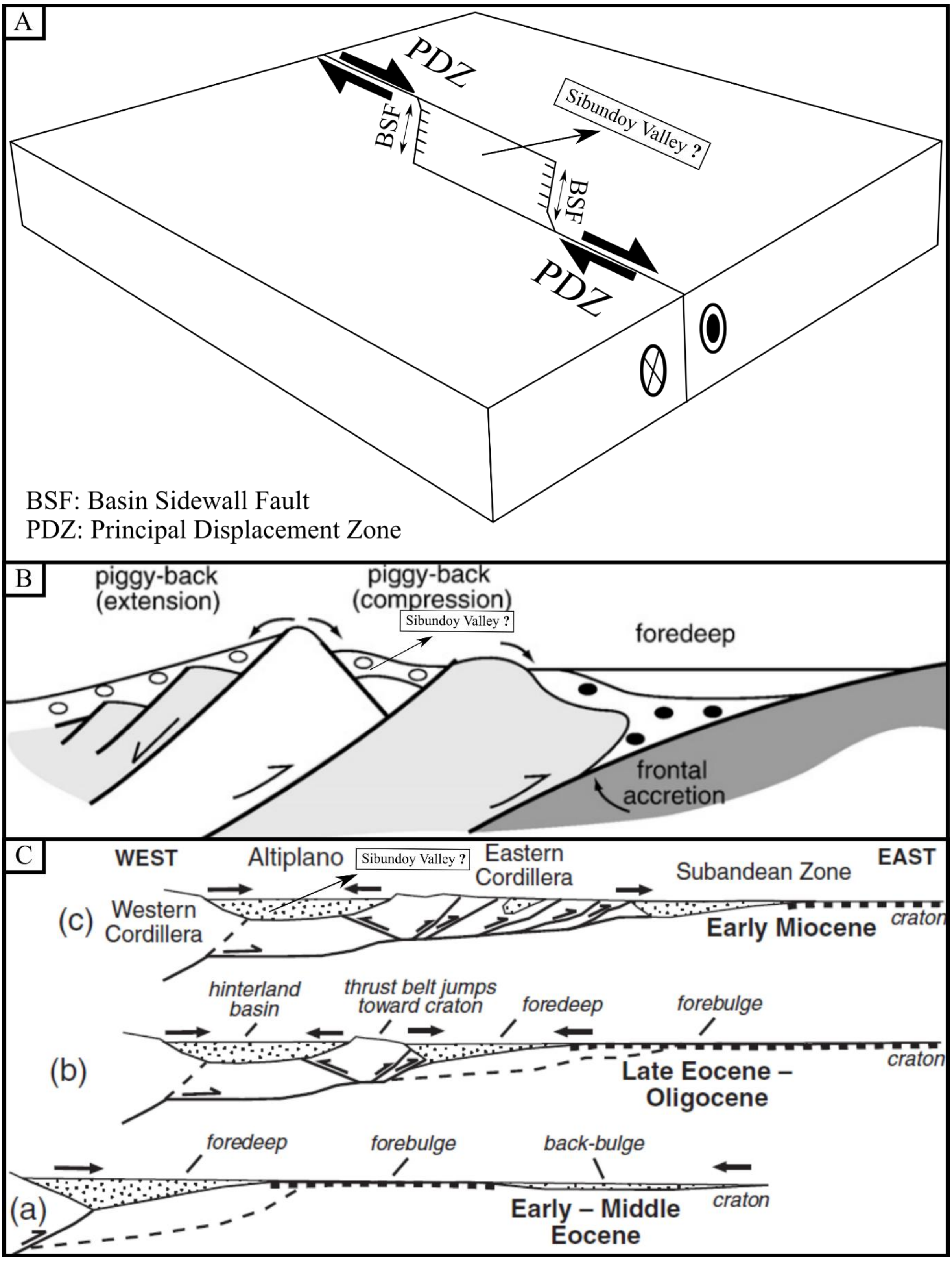

Figure 4 A) Conceptual model of a pure strike-slip pull-apart basin where the depression shows a rhomboidal shape between two sub parallel strike-slip faults, also known as PDZs (Principal Displacement Zones). The depression is bounded by oblique extensional faults, also known as BSFs (Basin Sidewall Faults). Modified from **Farangitakis et al., 2021**. B) Theoretical model of

backthrusting and out-of-sequence thrusting that accompany frontal accretion with possible location of mixed-mode piggy-back basins. Modified from **Alçiçek & ten Veen, 2008a**. C) Schematic reconstruction of Cenozoic foreland and hinterland basin evolution in the Altiplano plateau and neighboring regions of central Andes, showing sediment accumulation (stippled), forebulge zone of erosion or limited accumulation (thick dashed lines), sediment dispersal patterns (large arrows). Taken from **Horton, 2011**.

1.3.1. Pull-Apart Basin

A pull-apart basin is created by two sub parallel strike-slip faults and associated oblique normal faults that create accommodation space (**Figure 4a**). Generally, the shape of pull-apart basins is rhombohedral, similar to the Sibundoy Valley shape. The infilling of sediments inside the basin does not allow the description of the fault plane. However, the strike-slip fault on the western side of the basin is clear because active strike slip faults outcrop next to the basin in a north to south trend. In addition, geologic maps of the study area (**Figure 5**) assure the presence of right lateral strike slip fault systems (e.g. Algeciras Fault system) along the boundary of the Eastern Cordillera of Colombia. The strike slip model would support the idea of significant slip partitioning on the crust which has been accommodated by those active faults.

1.3.2. Piggyback Basin

In ocean-continental arc convergent margin settings, crustal shortening in the overriding continental plate is commonly present. Shortening increases the lithosphere thickness, and it provokes the movement of material outwards from the core of the orogenic belts through thrust faults on the surface **(Nichols, 2009)**. This process transfers mass laterally and results in a loading of the crust causing flexure deformation of the lithosphere, and in turn, creating a retro-arc foreland basin. Thrusting and loading of crust at the margin of the foreland basin continues if the convergent margin is significantly active such as in the Andean margin. Thus, the basin becomes larger and thicker as it evolves through time.

Sometimes thrusting is not restricted to the basin margin, and may subdivide the basin in different sections, creating piggy-back basins that lie on top of the main thrust belt and located away from the foredeep (**Figure 4b**) **(Nichols, 2009)**. In addition, piggyback basins may experience changes from tension to compression and vice versa during the growth of the wedge (**Figure 4b**). The out-of-sequence thrusts are caused by the reactivation of older in-sequence thrusts or by the development of new thrusts faults **(Alçiçek & ten Veen, 2008b)**. Together with backthrusts, they form in response to any obstruction of the thrust sheet movement **(Alçiçek & ten Veen, 2008b)**. According to the available geologic map (**Figure 5**), the type of fault at the eastern border of the basin remains inconclusive. However, a few thrust faults outcrop at eastern side.

1.3.3. Hinterland Basin

Hinterland Basin is a concept that details the location of the basin in the context of a convergent margin. Andean hinterland basins are produced between the western magmatic arc and craton-directed fold and thrust belt to the east (**Figure 4c**) **(Horton, 2011)**. Hinterland basins also form in continent-continent convergent tectonic settings. Even though, tectonic settings are significantly different between oceanic-continent convergent settings and continent-continent convergent settings, some similarities can be found (e.g. high elevation plateaus, parts of internal drainage, areas of active hinterland sedimentation) and two particular modes of hinterland evolution can be present in both systems **(Horton, 2011)**. The first mode explains that the basin evolution is attributed to the initiation of slip on structures related to shortening, extension, and strike-slip deformation within the orogenic interior. For example, fault-induced and flexural subsidence help explain basin evolution in transtensional and transpressional hinterland settings like in central Tibet and Ecuador **(Horton, 2011)**. The second mode consists of the transformation of former foreland basins, including wedge-top depozones, into hinterland basins as the deformation front propagates craton-ward. For example, the hinterland growth of the Magdalena Valley in Colombia is due to a jump in the orogenic front, inducing a shift in sediment patterns where the Magdallena Valley overprinted the former foreland basin. In addition, a topographic barrier or an active uplift may help to shield the succeeding hinterland basins from large-scale erosional processes.

1.4. Regional Geology

The area surrounding Sibundoy Valley was not studied in detail until the research done by **Restrepo et al., (2021)**. Previous studies were focused on creating a geologic map of a wide area without significant input about the geochemistry of the rocks exposed. In general, older Cretaceous and Jurassic sedimentary and crystalline basement rocks exist south of the Sibundoy Valley, whereas Quaternary volcanic rocks from the main axis of the Andean Arc are present to the north.

Metamorphic rocks and plutonic bodies (e.g. Jurassic Sombrerillos and Jurassic Mocoa batholith) crop out in the areas near the Sibundoy Valley (**Figure 5**). The Mocoa batholith yields a crystallization age of 170.7 ± 2.1 Ma to 181.8 ± 1.3 Ma **(Zapata-Garcia, Rodriguez G, & Arango, 2017)**. The La Cocha-Rio Tellez Migmatitic Complex, which includes migmatites, schists, gneisses, and amphibolites, is in fault contact with the Sombrerillos Batholith and Cretaceous sedimentary rocks **(Restrepo et al., 2021)**. The age of this metamorphic complex is still in debate because stratigraphic relationships do not concur with the geochronology found in the southwestern corner, between the La Cocha lake and the municipality of San Francisco **(Restrepo et al., 2021)**. In addition, Quaternary lavas and pyroclastic rocks partially cover the basement rocks.

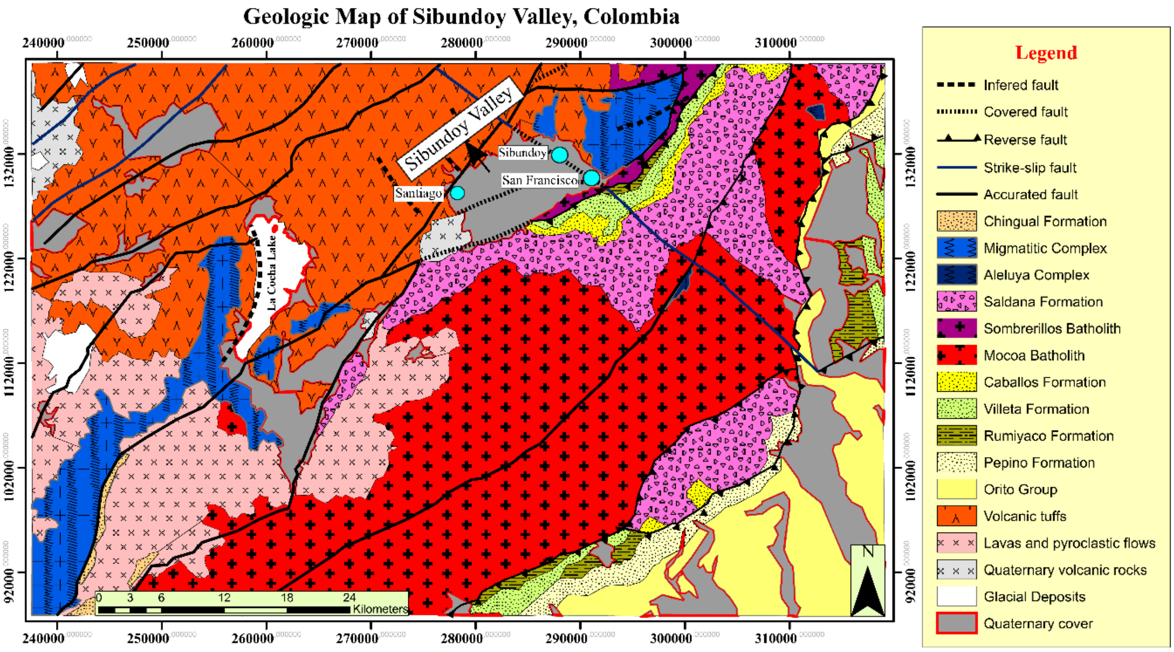

Figure 5 Geological map of Sibundoy Valley, including the La Cocha lake and the San Francisco area. The map shows the following lithology: Precambrian La Cocha-Rio Tellez Migmatitic Complex, Paleozoic Aleluya Complex, Jurassic Mocoa Batholith, Jurassic Sombrerillos Batholith, Jurassic Saldana Formation, Cretaceous Rumiyaco Formation, Cretaceous Villeta Formation, Cretaceous Caballos Formation, Neogene Lavas, pyroclastic flows and volcanic tuffs, Quaternary volcanic rocks and Quaternary cover. The fault traces are also included in the map as black lines. The light blue circles show the location of the towns inside the Sibundoy valley. Modified from **Restrepo et al., (2021)**.

At the eastern corner of the Sibundoy Valley, amphibole schists are in fault contact with plutonic bodies, which are being intruded by mafic dikes **(Restrepo et al., 2021)**. Fault gouge and breccias within a fault zone suggest a brittle behavior. In general, the plutonic rocks are variable in terms of the grain size and percentage of minerals, which includes granites, granodiorites, diorites, and quartz-monzonites. The U-Pb zircon ages of these granitoids yielded a crystallization age of 163.3 ± 0.8 Ma **(Restrepo et al., 2021)**. These granitoids correspond to the Sombrerillos batholith. The found samples of schists are fine to medium- size grains with granolepidoblastic texture with biotite and hornblende defining the main foliation **(Restrepo et al., 2021)**.

At the western side of the Sibundoy Valley, near La Cocha lake, mylonitized to undeformed plutonic rocks are predominant **(Restrepo et al., 2021)**. The deformed plutonic rocks show a phaneritic texture with medium-grain size, dioritic composition, and mylonitic foliation. In contrast, the undeformed rocks (Motilon granodiorite) are weathered granites with phaneritic texture and medium-sized inequigranular crystals **(Restrepo et al., 2021)**. The latter yielded ages of ca. 150 Ma. Most of the Jurassic granitoids are calc-alkaline, and few samples of the Sombrerillos batholith show a high-K calc-alkaline composition **(Restrepo et al., 2021)**.

1.5. Local Lithology

The study area near the Sibundoy Valley shows a wide diversity of rocks in terms of their origin and age (**Figure 5**). The rock sampling has been divided in three different areas: Santiago to Sibundoy Valley (west of the basin), inside the Sibundoy Valley, and San Francisco to Mocoa town (east of the basin). The dense vegetation at both sides of the basin did not allow a wide observation of the lithology. The road cuts provided the best outcrops for interpretation and rock collection. The codes for the lithology and the gravity stations are the same because they share the same location. The geologic mapping is not the main goal of this thesis project. The collected rock samples were mainly used to measure the density of the rocks in order to constrain the structural gravity models (**Appendix A**). Nevertheless, knowing the spatial distribution of geologic units and structures is important because they constrain the origin of the gravity anomalies.

1.5.1. Jurassic Batholiths and Metamorphic Rocks

Jurassic plutonic rocks and metamorphic rocks are found east of the basin. For example, quartz monzonites (**Figure 6a**) and granodiorites (**Figure 6c**) outcropped in the Mocoa Batholith area, according to the cartography on the Restrepo geologic map (**Figure 5**).

The Mocoa Batholith is in fault contact with Cretaceous sedimentary rocks (e.g. Caballos, Villeta and Rumiyaco, and the Paleogene Pepino Formation) **(Nuñez, 2003)**. Mocoa batholith also intrudes the La Cocha-Rio Tellez Migmatitic Complex and the Saldana Formation **(Nuñez, 2003)**. We could not find any metamorphic rock in the San Francisco area where The La Cocha-Rio Tellez Migmatitic Complex is supposed to outcrop so we coincide with Restrepo’s interpretation which suggests that the metamorphic complex does not outcrop in the San Francisco area. We found an amphibolitic gneiss (code: 17-SB-100B) embedded in the Mocoa Batholith. According to the cartography and lithologic description in the literature, this gneiss corresponds to the Aleluya Complex. The Sombrerillos Batholith includes granodiorites, granite, monzogranites that is in fault contact with the Saldana Formation **(Nuñez, 2003)**. Interestingly enough, we were not able to find any intrusive rocks at the San Francisco area, which is just next to the basin at the east side of San Francisco, according to the cartography. If the Sombrerillos batholith outrcops in this area, the extent of this lithology should be limited.

A minority of igneous rocks outcrop at the west of the basin because the Neogene volcanic rocks and flows cover the basement in that side. However, we found a granite in the Santiago town, western side of the basin (**Figure 6b**). It could be related to the Motilon granodiorites that outcrops near La Cocha lake which is relatively close to the Sibundoy Valley. However, we did not do any geochemistry to test this interpretation.

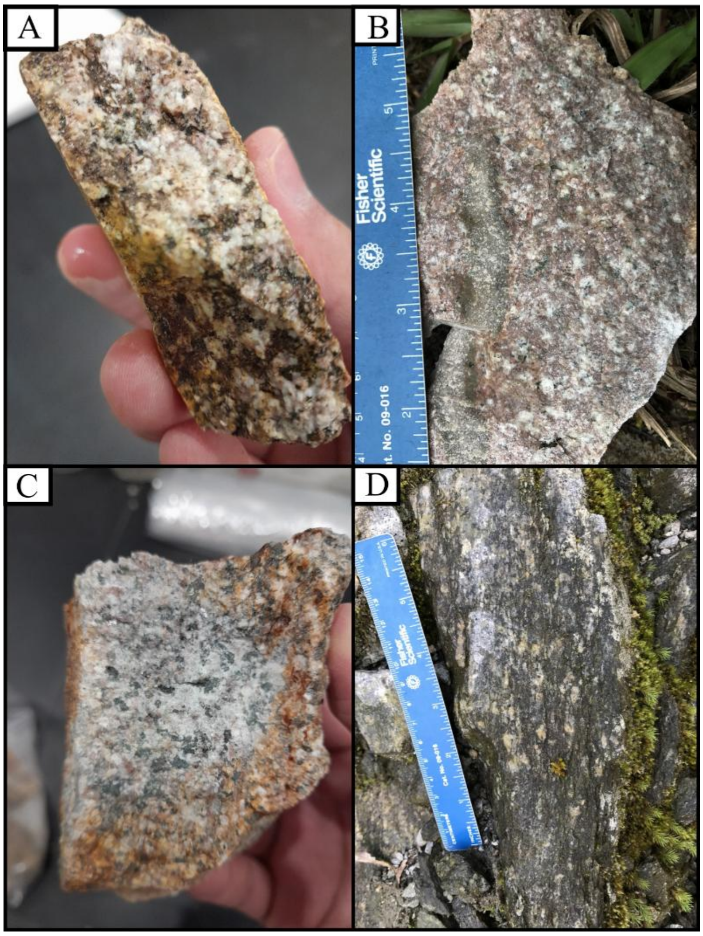

Figure 6 A) quartz monzonite (code: 17-SB-92). B) granite (code: 17-SB-17). C) granodiorite (code:17-SB-94) D) Plutonic rock that shows significant weathering on the surface, next to deep vegetation.

1.5.2. Cretaceous Sedimentary Rocks and Saldana Formation

The Cretaceous sedimentary rocks outcrop at the southeast side of the basin. As mentioned on the previous section, the Sombrerillos Batholith is in fault contact with the Cretaceous sedimentary rocks (e.g. Caballos, Villeta and Rumiyaco, and the Paleogene Pepino Formation) **(Nuñez, 2003)**. We did not find the fault contact between the Sombrerillos Batholith and the sedimentary formations south and west of San Francisco town. The rock found was a micritic limestone (**Figure 7a**) that corresponds to the Villeta Formation.

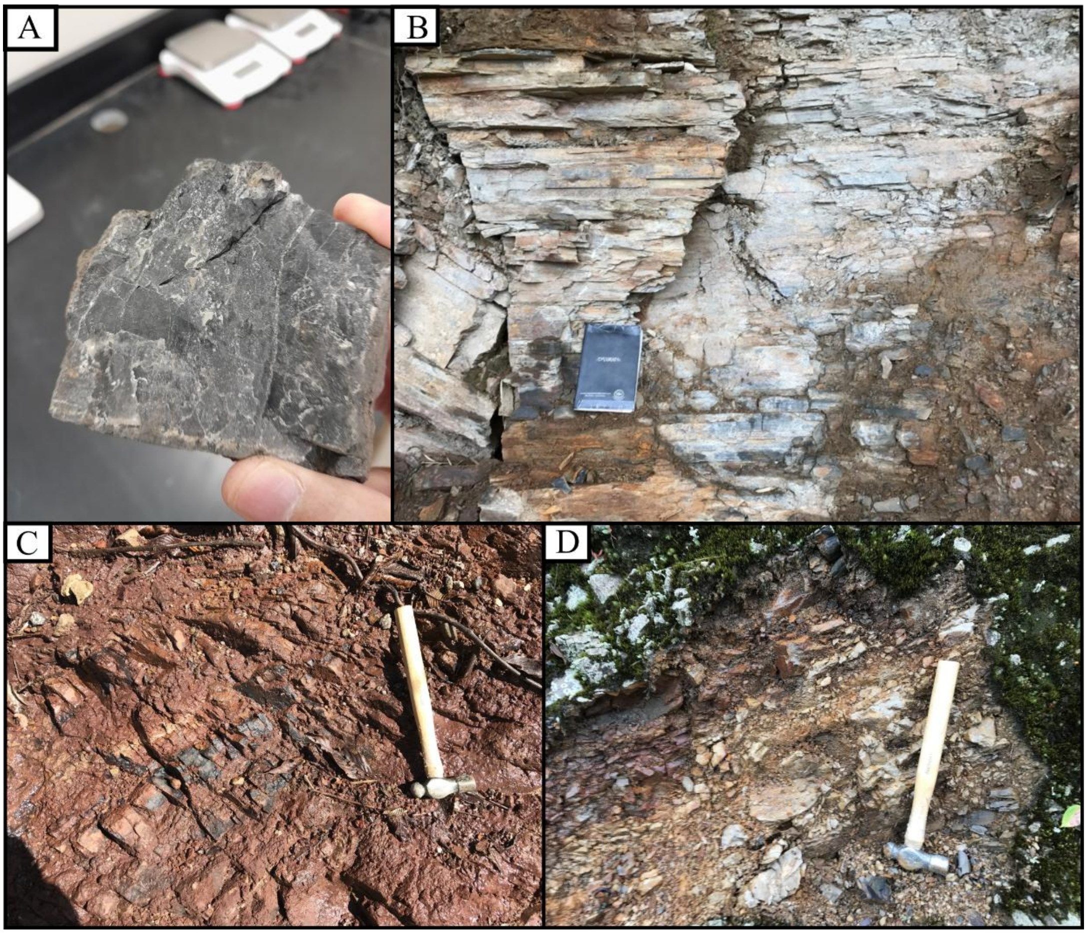

Figure 7 A) Micritic limestone (code: 17-SB-77). B) Outcrop of interbedded fine-grained sandstone with black mudstone. C) Black limestone interbedded with shale layers. D) Similar outcrop from C) but it shows a high number of fractures following the foliation planes.

1.5.3. Neogene lavas, pyroclastic flows and volcanic tuffs

As mentioned in the geologic setting, the Andean convergent margin has been constantly active for millions of years. It has enabled a significant volcanic presence, parallel to the convergent margin. The lavas, pyroclastic flows and falls, and volcanic tuffs outcrop at the west of the basin. There are several active volcanoes (e.g. Galeras volcano) and dormant volcanoes that could have erupted these rocks (**Figure 8**). The closest volcanoes to the study area are the Guamuez-Sibundoy mono-genetic volcanoes, where the last phreatomagmatic eruption may gave rise to lava flows and scoria cones (**Rivera Lara, 2021**). The thick layer of volcanic deposits made it difficult to visualize the basement at the west of the basin. In consequence, the density of the basement rocks was not constrained west and north of the basin.

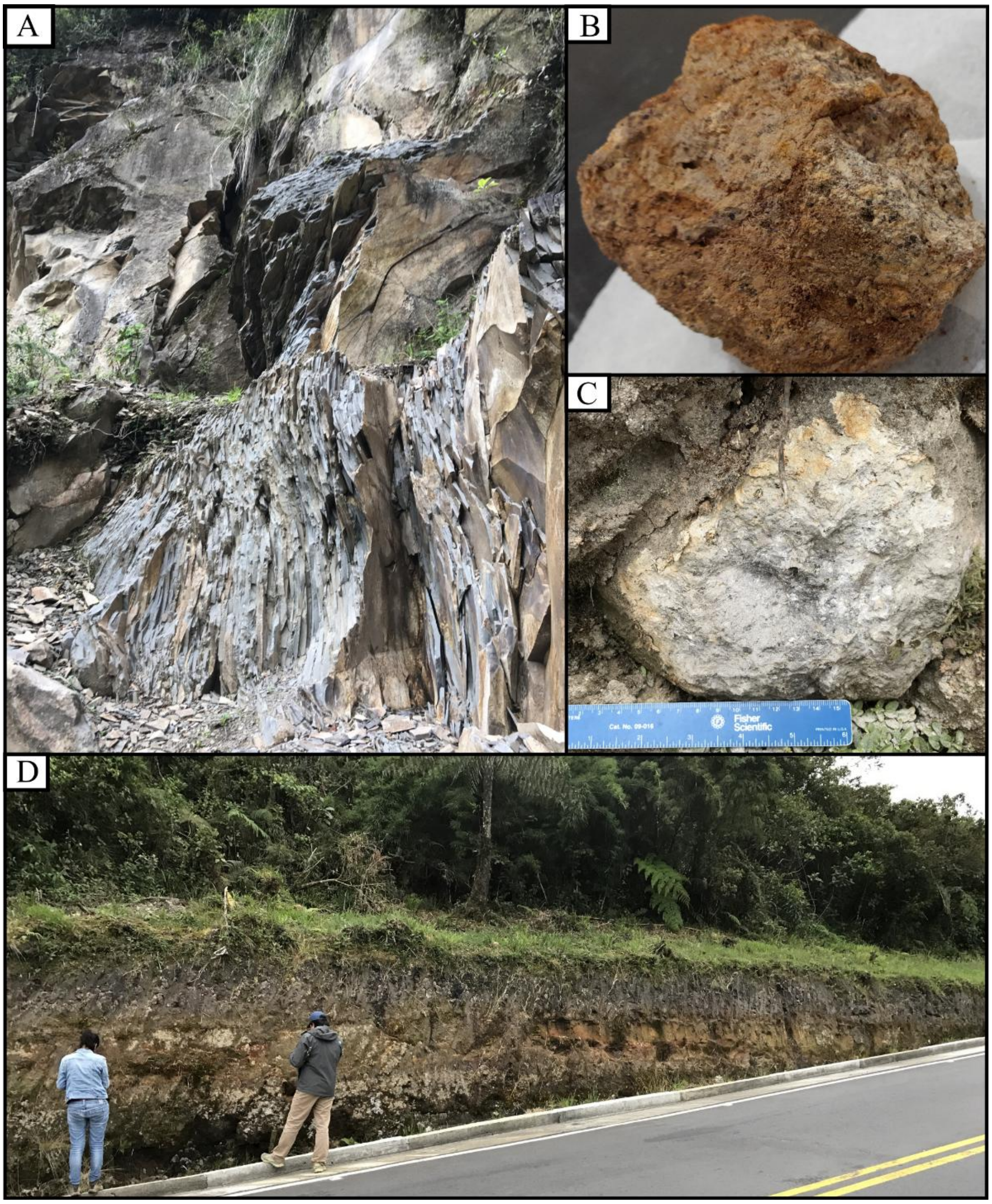

Figure 8 A) Outcrop of lavas found at the west of the basin. The probable age may ne Neogene, according to cartography. B) and C) Volcanic tuffs found at the west of the basin. They have relatively low density and many vesicles (code: 17-SB-18A). D) Outcrop of a pyroclastic flow and fall that cover the basement at the west of the basin. The pyroclastic material varies from lapilli to ash.

1.5.4. Quaternary unconsolidated sediments

The basin infill of the Sibundoy Valley consists of Quaternary unconsolidated sediments that ranges from boulders to fine sand sediments. The outcrops show poor sorting and that the clasts are rounded. However, some big clasts show an angular texture (**Figure 9**). Conglomerates were found next to a stream that is located at a flank of the basin. In general, coarser grained conglomerates are found near the margins of the Sibundoy basin, whereas sediments fine to silt in the center.

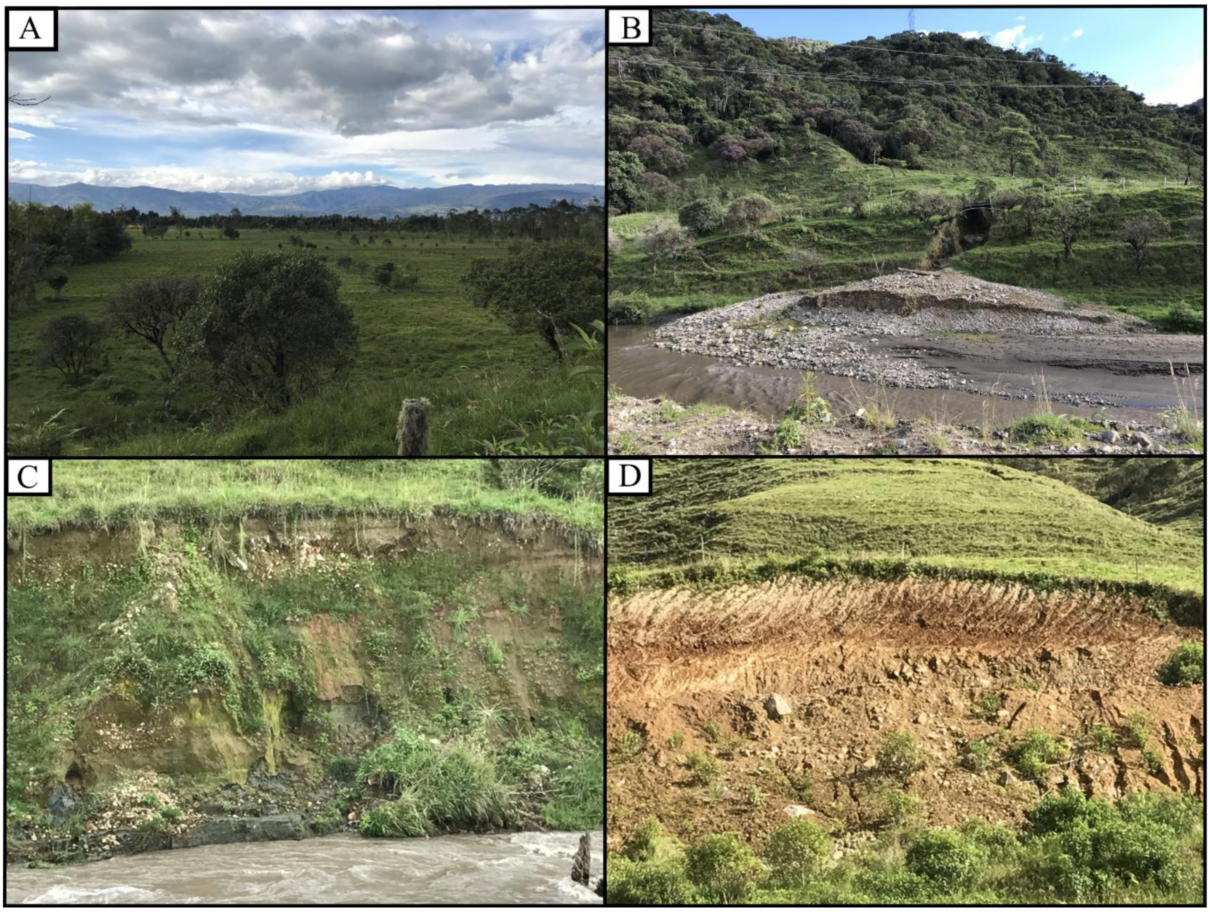

Figure 9 A) General view of the Sibundoy Valley where the basin infill is relatively flat in contrast to the surrounding mountain belts. B) Conglomerates, found at a flank of the basin. C) and D) The basin infill is poorly sorted with clasts that range from boulders to fine sand and silt. Basin sediments are quaternary or younger.

1.6. Existing gravity Data

The International Gravimetric Bureau (BGI) is part of the International Association of Geodesy (IAG) that collects and archives gravity measurements of the Earth's surface. This entity provides Complete Bouguer Anomaly values data for various countries around the world, including Colombia. The abundance of gravity stations was significantly denser in the northern part of Colombia, compared to the southern part. Land based surveys were the method used to collect the data and generally followed the road layout. The BGI gravity data was gridded and interpolated in GRASS GIS and displayed on top of the SRTM topography (**Figure 10a**). BGI gravity data is a helpful tool to get an overview of the tectonostratigraphic regions and their gravity anomaly imprint. For example, positive gravity anomalies appear on top of the accreted oceanic terrains and Guiana Shield, which are located next to the Andean Mountain chain, because thinner but denser rock formations underlie these regions. In the contrary, the Andean Mountain chain exhibits a large negative gravity anomaly due to thicker but less dense rock formations. Nevertheless, the BGI data was not helpful to distinguish the Sibundoy Valley from the surrounding tectonostratigraphic regions (**Figure 10b**). In the profile graph (transect A to A'), we can observe that the Sibundoy Valley did not disrupt the regional gravity trend in the BGI regional dataset. The resolution of the data did not allow the interpretation of the basin because of the insufficient density of gravity measurements in the southern part of Colombia. The BGI data was the only reference found regarding gravity anomalies on the southernmost part of Colombia. This circumstance became the main motivation to carry out a detailed gravity survey on the Sibundoy Valley (See Chapter two and three).

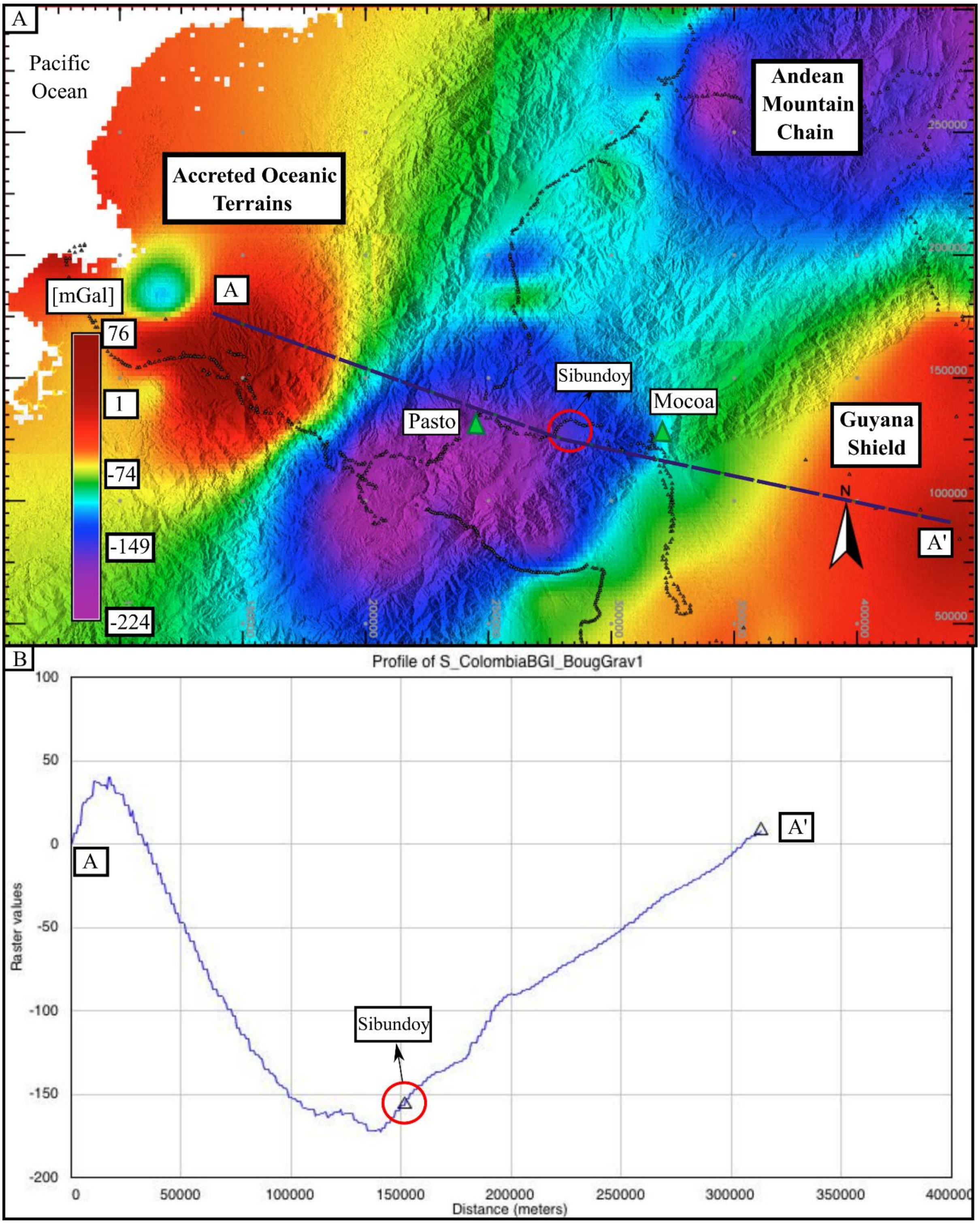

Figure 10 A) Bureau of Gravimetrique International (BGI) Complete Bouguer Anomaly data (black tiny dots) regarding the gravity anomalies of southern Colombia. The data was gridded in GRASS GIS software and draped on top of the SRTM topography shaded relief map. This figure only shows the data of the southern part of Colombia. The red color represents positive gravity anomaly values. Purple and Blue colors represent negative gravity anomaly values. B) Profile graph of BGI Complete Bouguer Anomaly values along the A to A' transect.

CHAPTER 2: METHODOLOGY

2.1. Gravity Method

The gravity method is a geophysical technique that measures small variations (anomalies) in the gravitational field of Earth with the intent of detecting bodies of lesser or greater density than the surrounding formations at a specific location **(Telford, Geldart, & Sheriff, 2004)**. Geometries of lithologic bodies with specific structural styles in the subsurface can be inferred (**Figure 11**), considering that densities (**Appendix A**) affect the gravitational field in distinct styles (e.g. sedimentary rocks are usually less dense than igneous and metamorphic rocks, and they create a relative negative anomaly).

Since Earth is not a uniform sphere, the magnitude of gravity is also affected by other factors besides the density of rocks: earth tides, topography of the surrounding terrain, latitude, and elevation **(Telford, Geldart, & Sheriff, 2004)**. Thus, observed gravity measurements need to be processed by various corrections that involve the resolution of equations and concepts (described in detail in 2.3), in order to analyze the gravity readings as a result of geologic variations in density and subsurface structure.

As with any geophysical technique, the gravity method provides non-unique solutions to any particular anomaly pattern. However, geologic and measured density constraints greatly limit the number of possible models such the gravity data can be used to distinguish between competing geologic models. A gravity model could constrain the countless solutions of geometries of the lithology by reiteratively pairing the observed gravity anomalies, which are taken in the study area, with the calculated anomalies.

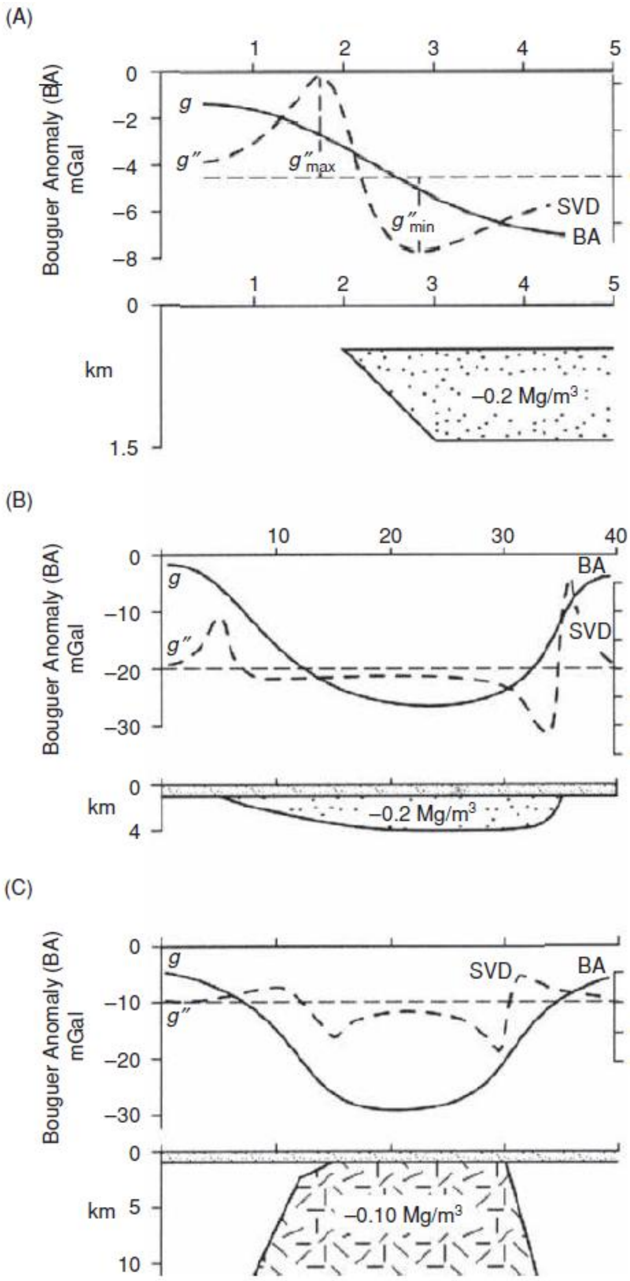

Figure 11 Exemplification of how gravity anomalies vary over A) a horizontal prism, B) a sedimentary basin, and C) a granitic pluton; taken from ***(Reynolds, 2011)***. BA stands for Bouguer Anomaly, SVD stands for Second Vertical Derivative, it is a mathematical calculation where the data is differentiated twice in the vertical direction.

2.2. Gravity survey

The gravity survey was carried out along multiple perpendicular transects that dissect the Sibundoy Valley, and another transect follows a west to east direction from Sibundoy town to Mocoa town (**Figure 15**). Gravity measurements were taken at 100 stations along with latitude, longitude, and elevation data (**Appendix B**). The equipment used was a quartz spring Worden gravimeter and a Trimble Pro XRT differential GPS, respectively (**Figure 12**). The Worden gravimeter has a zero-length spring that records small values of gravity anomalies by following the Hooke's law. The instrument resolution is approximately 0.1 to 0.3 mGal and the spacing of the measurements is 1 km on average. The base station is located near the Sibundoy town square. In addition to the gravity survey, a combination of surface geology and density measurements were carried out, in order to constrain the gravity models (See Chapter 3**).**

Figure 12 Worden gravimeter, next to differential GPS at a station in the Sibundoy Valley, Colombia. Acknowledgement for Nicolas Perez, Andrea Ordonez for help with the field measurements and to Camilo Jaramillo for overall project support.

2.3. Data processing

If properly corrected, gravity anomaly measurements should represent only the lateral variability of rock densities in the field area. However, the raw gravity data, which was obtained by the Worden gravimeter, needs to be processed in several steps and corrections to approach that goal. First, we need to know the difference amount between each station and its base gravity station per day so the average gravity reading of the daily base station is subtracted from the raw gravity dial reading of each station. This procedure decreases the gravimeter reading change (drift) because of the elastic creep in the spring **(Reynolds, 2011)**. The result is multiplied by the gravity dial constant (0.0844). This constant is known as the calibration factor. Then, the observed gravity values (**Appendix B**) are obtained by adding the latter result to the raw gravity dial readings of each station.

Next, the international gravity formula is applied to know the theoretical gravity (g) with respect to the latitude ($\boldsymbol{\theta}$) on a reference ellipsoid. This formula was provided by the International Union of Geodesy and Geophysics (IUGG). Here, the WGS 84 latitude of each station is introduced in the formula to obtain the theoretical gravity, also known as calculated gravity. In the next section, we will start to examine the corrections of the gravity data, also known as the gravity data reduction.

$$\boldsymbol{g = 9.780326.7714\ [\frac{m}{s2}]\left(\frac{1 + 0.001931851381639\ sin^2\theta}{\sqrt{1 - 0.0066943999013\ sin^2\theta}}\right)\ [m/s2]}$$

2.3.1. Free-Air Correction and Anomaly Value

The free-air correction g(f) consists of the reduction of the gravity magnitude with height above the geoid, without considering the rock in between **(Reynolds, 2011)**. In this case, the study area is above sea level, so the free-air correction is positive, and the reference geoid used is EGM96. 3.086 [mGal./m] is the most accepted value for gravity anomalies above the sea level and near the equator **(Reynolds, 2011)**. The following equation obtains the free-air correction g(f) by multiplying 3.086 [mGal/m] and the height (h), which was acquired by the GPS receiver.

$$\boldsymbol{g(f) = 3,086(h)[mgal]}$$

The free air anomaly value for each station was obtained by adding the free air gravity correction g(f) and the observed gravity value. Then, the theoretical gravity value g is subtracted by the latter value (**Appendix B**).

2.3.2. Simple Bouguer Correction and Anomaly Value

The Simple Bouguer correction measures the additional gravitational pull of the rock mass between the station and the sea level (datum), which was ignored in the free-air correction **(Reynolds, 2011)**. The following equation attains the Bouguer Correction g(b) for each station, where *h* represents the thickness in meters of the rock slab; the international gravity constant *G* is 6.67428×10^{-11} [$m^3 kg^{-1} s^{-2}$]; and ρ represents the average density of the rock slab. The GPS receiver measured the height *h* and the EGM 96 was the reference geoid. The chosen value for the rock slab is 2675 [$kg\, m^{-3}$] because this value is assumed to be the average density for crustal rocks **(Telford, Geldart, & Sheriff, 2004)**. The sense of the Bouguer Correction is opposite to the Free Air so it is subtracted when the station is above the sea level (datum) **(Telford, Geldart, & Sheriff, 2004)**.

$$\boldsymbol{g(b) = 2\pi\rho G h * 100000\ [mgal]}$$

Once the Bouguer Correction is obtained, we can calculate the Simple Bouguer Anomaly value by subtracting the Bouguer correction from the free-air anomaly value. Our intent is to know the anomaly value for each station so we just repeat the process for each station (**Appendix B**). The Bouguer correction was possible because two assumptions were made: (1) the rock slab has a uniform density and (2) the length of the rock slab is horizontally infinite **(Telford, Geldart, & Sheriff, 2004)**. Nevertheless, these two assumptions are incorrect because we are aware of the high lateral variability of the different lithologic units in the subsurface with specific dimensions, especially in the Andes. Thus, we need to constrain the density of the different lithologic units by collecting samples and measuring their densities (See Section 2.4). In addition, a gravity model enhances this process by iteratively matching the observed Bouguer anomalies to the calculated Bouguer anomalies (See Chapter 3). The infinite horizontal rock slab (second incorrect assumption) is addressed in the following section.

2.3.4. Terrain Corrections

In general, the Andes show abrupt changes over short distances in its topography. In addition, the distance among gravity stations is greater than 100 meters of elevation. In this scenario, the assumption of semi-infinite horizontal slab is incorrect and needs further calculations to constrain the effects of topography on gravity **(Reynolds, 2011)**. The hills, which have relatively higher elevation than the gravity station, exert an upward pull on the gravimeter **(Telford, Geldart, & Sheriff, 2004)**. In the contrary, valleys, which have relatively lower elevation than the gravity station, exert a less of a downward pull on the gravimeter due to a mass uplift **(Telford, Geldart, & Sheriff, 2004)**. In both cases, the lack or excess of mass underestimates the gravity measurements in the same sense so the terrain correction is added to the gravity readings, in order to approximate to the assumption of the semi-infinite rock slab. Terrain corrections are an important component in this study as individual terrain corrections can exceed > 20 mgal.

The Bullard Method corrects the gravitational attraction of the topography by following three steps **(Nowell, 1999)**. Bullard A (first step) is the same as the Bouguer Simple correction (see Section 2.3.2), where the topography is close to an infinite horizontal thickness, which is equal to the height of the station above sea level **(Nowell, 1999)**. Bullard B (second step) reduces the infinite horizontal slab to a spherical cap with same thickness, to a radius of 166.735 [km] **(Nowell, 1999)**. Here, the spherical cap pulls downwards, increasing the observed value of gravity, in the contrary, the truncation of the infinite Bouguer slab at

166.735 km decreases the observed value of gravity. Bullard B correction (**Appendix B**) is subtracted from the gravity readings and the equation is the following, where h stands for the height of the gravity station and the letters from A to B are called as the Bullard Coefficients: A= 1464,139 x10^{-3}, B = 3533,047 x10^{-7}, C= 1002,709 x10^{-13} and D= 3002,407 x10^{-18} **(Nowell, 1999)**.

$$BB = Ah0 - Bh^2 + Ch^3 + Dh^4$$

Bullard C (third step) corrects the undulations of the topography relative to the spherical cap at the height of the gravity station **(Nowell, 1999)**. In the contrary of Bullard B, Bullard C needs to be added to the final readings because the hills above the gravity station exert an upwards attraction and the valleys below the gravity station exert a downwards attraction.

A traditional terrain correction technique is the Hammer method which determines the gravity at the center of two concentric circles that have an inner and outer radius **(Reynolds, 2011)**. The circles are segmented concentric rings that are superimposed over a topographic map, where the average elevation of each segment is estimated and the terrain correction in [mGal] are derived **(Reynolds, 2011)**. However, the Hammer method was not used in this research project.

Instead, we followed the Blais and Ferland **(1984)** method that works well for gridded DEM elevation data. The Blais and Ferland (1984) method uses the gravity attraction of a right rectangular prism in each DEM cell with respect to a particular gravity station. It is calculated by the formula for the gravitational attraction (g), where height (h) is center at a grid point; s is the cross-sectional area, d is the horizontal distance from the gravity station to the DEM point, which also coincides with the middle of the prism; and d' is the distance between the gravity station and the top of the prism **(Nowell, 1999)**.

$$g = G\rho s\left(\frac{1}{d} - \frac{1}{d'}\right);$$

$$d' = \sqrt{d^2 + h^2}$$

An inner and outer terrain correction was used to get a higher resolution terrain correction while also taking into account far field effects. The inner terrain correction is the nearest area with respect to the gravity station that represents a significant part of the terrain correction, while the outer terrain correction is the furthest zone with respect to the gravity station. The inner terrain correction used 90-meter SRTM data out to a distance of 30 km, whereas the outer terrain correction used 1km DEM data from 39-167 km. The distance of stopping the inner or outer terrain calculation is subjective but the limit for the inner terrain correction was 30 km and the limit for the outer terrain correction was 167 km. According to Bullard, the gravity attraction further 167 km is insignificant, in the contrary, La Fehr claimed that beyond 167 km is sometimes worth to analyze the topographic effects on gravity **(Nowell, 1999)**. The total terrain correction is the sum of the inner and outer terrain correction. This value was added to the simple Bouguer anomaly (**Appendix B**).

In summary, the final gravity reading, also known as the Complete Bouguer Anomaly (**Appendix B**), consists of the final product of the reduction and correction process. This final value is the result of adding the values of the Simple Bouguer anomaly and the total terrain corrections and subtracting the spherical cap correction.

2.3.5. Regional and residual gravity anomalies

Now, the gravity data only relates to lateral variations of density in the subsurface where a high-density geologic feature should result on a relative positive Bouguer anomaly **(Reynolds, 2011)**. In the contrary, a low-density geologic feature should result on a relative negative Bouguer anomaly. The Complete Bouguer Anomaly gravity data shows a subtle trend that reflects a long-wavelength gravity anomaly **(Reynolds, 2011)**. We could detect this signal by observing the Complete Bouguer anomaly maps (**Figure 14**). Here, the gravity data is displayed as mgal areas with a specific color. This regional signal is strongly influenced by deep geological features, possibly related to the bulk of the Andean basement. In contrast, the shorter-wavelength anomalies from shallower geologic features (e.g. Sibundoy Valley) are overlapping with the regional anomalies. Considering that the object of study is a shorter-wavelength anomaly, the regional signal should be removed, in order to obtain the data that portraits the residual gravity anomalies.

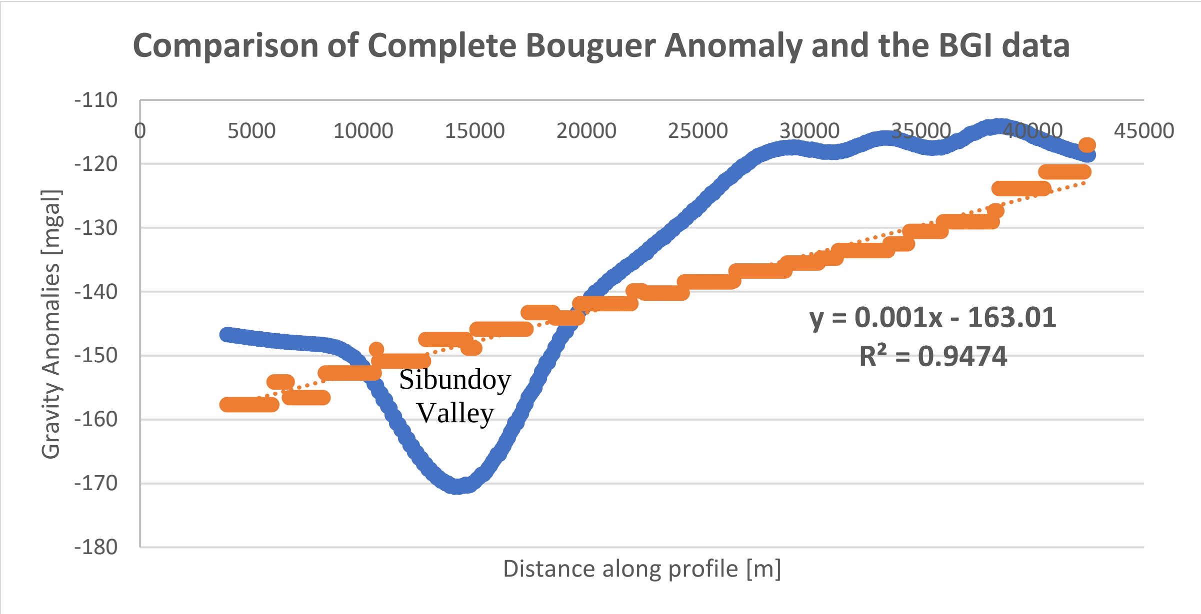

Figure 13 Comparison between the Complete Bouguer Anomaly (blue curve) and the International Gravimetric Bureau data (orange curve). The data was extracted from a profile that had a North West to South East direction. It went across the Sibundoy Valley and its surrounding areas. The orange curve shows an increasing, constant, and linear behavior along the profile. The BGI gravimetry data does not register the depression of the Basin. Thus, it only records the regional signal from the bulk of the Andean basement. In the graph, the linear regression equation of the BGI gravimetry data is displayed with a strong R square value.

The BGI gravimetry data and the Complete Bouguer Anomaly data were introduced into the GRASS software. Here, a surface interpolation was performed from the vector points map by splines. In addition to portray the data as a floating-point raster, GRASS enabled us to extract the data with respect to a northwest to southeast profile. This profile covered the

Sibundoy Valley and the surrounding geological features. Then, the information was plotted in a graph (**Figure 13**) and a linear regression was done on the BGI data because we consider that it reflects the regional trend from the bulk of the Andean basement. It is evident when we compared both curves, the Sibundoy Valley was not registered on the BGI data. The curve of the BGI data behaves as a linear function so a first-grade polynomial equation best describes the curve (**Figure 13**). The regional correction consisted of the application of the linear equation on the Complete Bouguer anomalies (**Appendix C**). This latter correction highlights the shorter-wavelength anomalies that are strongly correlated to shallow geologic features (e.g. Sibundoy Valley).

2.4. Density values

Once corrections have been made, the primary control on gravity variations is rock density. However, idealized rock density does not always match the actual rock density. Therefore, density measurements were carried out on rocks that were located at the gravity stations (**Appendix A**). We could not get one sample per gravity station because of dense vegetation or because the infrastructure overlayed the rock exposures. Densities of rocks (ρ) are defined by the ratio between the mass and volume. The mass of the rock is obtained by measuring the rock in a digital balance. The volume of rock is measured by immersing it in a water container without touching the sides nor the bottom. Since one gram of water occupies 1 cubic centimeter, the mass of water displaced on the digital balance is the volume of the rock.

$$\boldsymbol{\rho} = \frac{\textit{Weight in air}}{\textit{Weight of the displaced water}} \ \mathbf{[g/cm^3]}$$

Density measurements will be used to adjust the accuracy of the gravity models in the following chapter.

CHAPTER 3: RESULTS

3.1. Representation of the observed gravity values.

After the correction process to the observed gravity values, we obtained the Complete Bouguer Anomaly Values (CBA) which reflect the lateral variation of densities in the subsurface (**Appendix B**). We can identify this lateral variation by displaying and interpolating the data in Oasis Montaj (**Figure 14**). The most relevant observation from the CBA values consists on the area of lowest negative gravity anomalies (color blue and light blue). This area corresponds to the Sibundoy Valley and the values range from -140.0 to -170.2 mGal, a negative anomaly of 30 mGals. Here, we can observe an elliptical shape where the main axis has a southwest to northeast trend. The bottom of the basin shows the lowest gravity values. We can also observe that the gravity values are progressively increasing until -111.0 mGal along the Sibundoy to Mocoa Transect (east of the Sibundoy Valley). This area has a variety of lithology. For example, the Mocoa Batholith, Saldana Formation, etc. In order to contextualize these values, the BGI data shows negative gravity values for the entire bulk of the Andes in the range of -74 to -224 mGal (**Figure 10**). The Andes shows negative gravity values due to a thicker but less dense rock formations. A free air and simple bouguer anomaly maps were also created and located in the **Appendix D**.

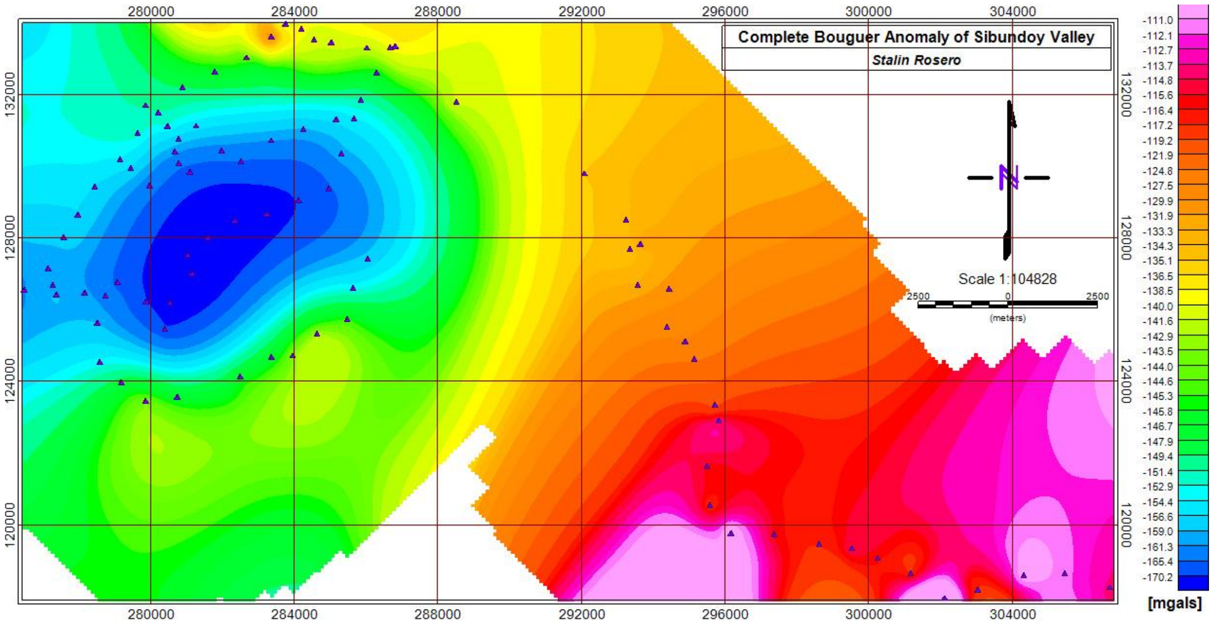

Figure 14 Complete Bouguer Anomaly map of the Sibundoy Valley. The basin is in dark blue. The triangles show the 100 gravity stations. The colors show different gravity values in mgals.

3.2. Structural Modeling

The findings of density and thickness regarding the Sibundoy Valley in the subsurface are the main objective for the gravity modelling. At the same time, the geological observations in the surface need to be coherent with the subsurface geology. The importance of knowing the shape of the basin consists on the potential insights of the Quaternary deformation style that created the accommodation space in the basin. Overall, gravity modeling can provide support for thrust dominated vs strike-slip dominated tectonics at the Eastern margin of the North Andean Sliver.

The creation of the structural models starts by the upload and interpolation of the Complete Bouguer anomaly values from each gravity station into the Oasis Montaj and GrassGIS software. In Oasis Montaj, the data was gridded, in order to visualize the areas of lower and higher gravity anomalies in a map (**Figure 14**). In GrassGIS, the gridded Complete Bouguer anomaly values were extracted along 6 transects; 3 transects follow a southwest to northeast trend and 3 transects follow a northwest to southeast trend (**Figure 15**). These trends are perpendicular to the main fault traces on both sides of the basin because our intent is to observe the interaction between the fault planes and lithology by analyzing the gravity models.

The gravity models are 2D transects across the basin. If we join the dimensions of the basin from each gravity model and we add control points in the intersections of each model and at the boundary of the basin, it is possible to build a 3D model that can portrait the dimensions of the basin by applying a gridding method on the basin depth values derived from the gravity models.

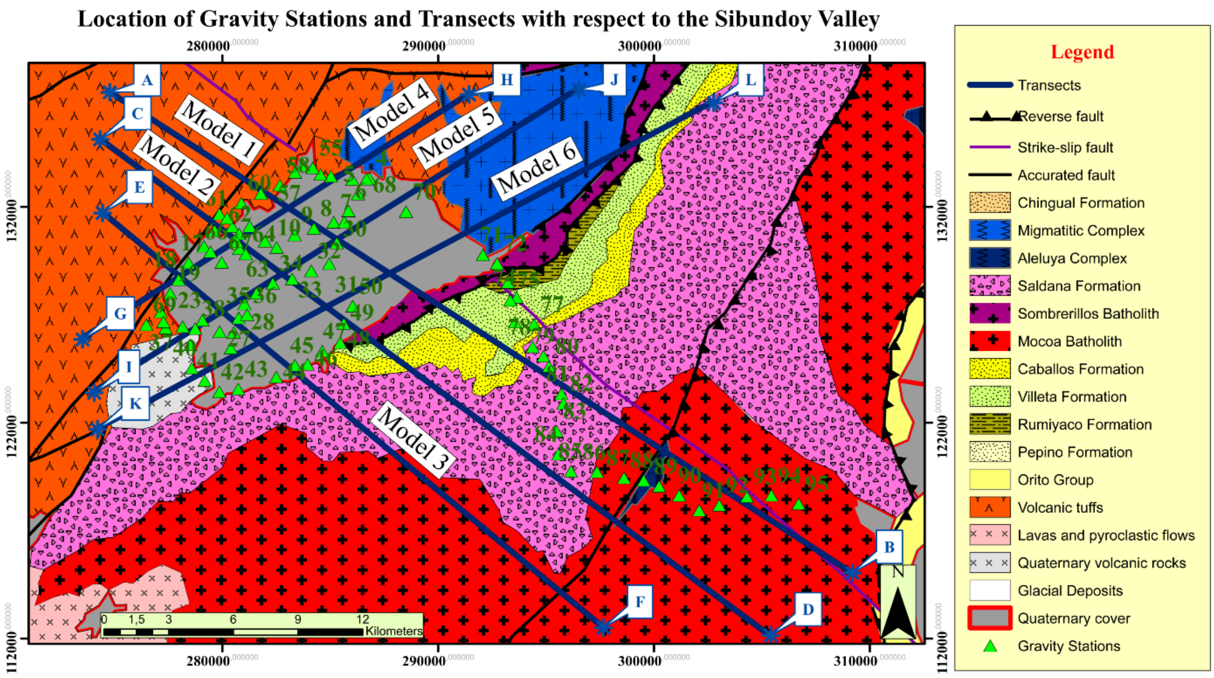

Figure 15 Location of gravity stations (green color triangles) and transects with respect to the Sibundoy Valley. Table 1 explains the nomenclature of each model, the source data, and the density for the basin.

Table 1 Description of the nomenclature used for each gravity model.

Model	Description	Figure
Model 2a	Model that follows C to D end points, the source data is CBA, and the basin infill is 1.8 g/cm^3.	Figure 16
Model 2b	Model that follows C to D end points, the source data is CBA without regional trend, the basin infill is 1.8 g/cm^3.	Figure 17
Model 3b	Model that follows E to F end points, the source data is CBA without regional trend, the basin infill is 1.8 g/cm^3.	Figure 18
Model 5b	Model that follows I to J end points, the source data is CBA without regional trend, the basin infill is 1.8 g/cm^3.	Figure 19
Model 2e	Model that follows C to D end points, the source data is CBA without regional trend, the basin infill is 1.8 g/cm^3. Strike-slip arrangement.	Figure 20
Model 3c	Model that follows E to F end points, the source data is CBA, the basin infill is 2.0 g/cm^3.	Figure 21
Model 2d	Model that follows C to D end points, the source data is CBA without regional trend, the basin infill is 2.0 g/cm^3.	Figure 22
Model 3d	Model that follows E to F end points, the source data is CBA without regional trend, the basin infill is 2.0 g/cm^3.	Figure 23
Model 5d	Model that follows I to J end points, the source data is CBA without regional trend, the basin infill is 2.0 g/cm^3.	Figure 24

3.2.2. Gravity models of the Sibundoy Basin

The goal of gravity modeling building is to evaluate different tectonic geometries and density constraints in the Sibundoy basin. Models were created along the above transects for different geologic scenarios (see below). Models were also created with the Complete Bouguer Anomaly values with and without regional trend consists of the observed gravity values. Once the gravity values were projected along a transect in GrassGIS, we proceed to insert the data in GravMag software. Then, we need to create the calculated gravity curve artificially in Grav Mag software to compare both curves. If both curves match, it means that the model generates identical values as the observed gravity values. The calculated gravity curve depends on the geometry of the blocks that represents the lithology and the density of each block. The extent of each block on the surface follows the dimensions provided by the Restrepo geologic map (**Figure 15**). The dimensions of the blocks in the subsurface are unknown so the multiple arrangements of the blocks arise. Since we are attempting to test the strike-slip dominated versus the thrust-up dominated tectonic scenarios, we accommodated the geometry of the blocks, depending on both scenarios, as long as the calculated gravity curve approaches to the observed gravity curve. The density of each block is fixed with the exception of the unconsolidated sediments in the basin. We measured the density of rocks that were collected in the study area (Appendix A) and included the values in the settings for each block. The unconsolidated sediments were also density measured but the results show a variety of values that were not consistent because of water saturation in the samples. Thus, we assigned two value variations for the unconsolidated sediments in the basin: a) 1.8 g/cm^3 (low density model) and b) 2.0 g/cm^3 (high density model). Another variable for the models comes from the source of data. The regional trend in the Andes is significant so the proposed model is going to change if we use the Complete Bouguer Anomaly values with or without the regional trend.

3.2.3. Low Density models

As mentioned on the previous section, the low-density models consist of the models where the basin infill is 1.8 g/cm^3. In **Figure 16**, we can observe a gravity model that used Complete Bouguer Anomaly data along a northwest to southeast transect that cuts the basin in half. Here, the geometry of the lithology mimics a thrust-up dominated arrangement where the Cretaceous formation and Saldana Formation block the southeastern side of the basin. The Volcanic Neogene cover a thin layer at northwest of the basin. The Aleluya Complex (blue color) is next to the Mocoa Batholith (red color) at southeast of the basin. If we compare the observed and calculated gravity curves, there is a decent agreement among them. However, there is a significant gap on the margins of the basin. The observed gravity curve shows an abrupt bulge at the southeast of the basin. The location of the bulge matches the Aleluya Complex outcrop.

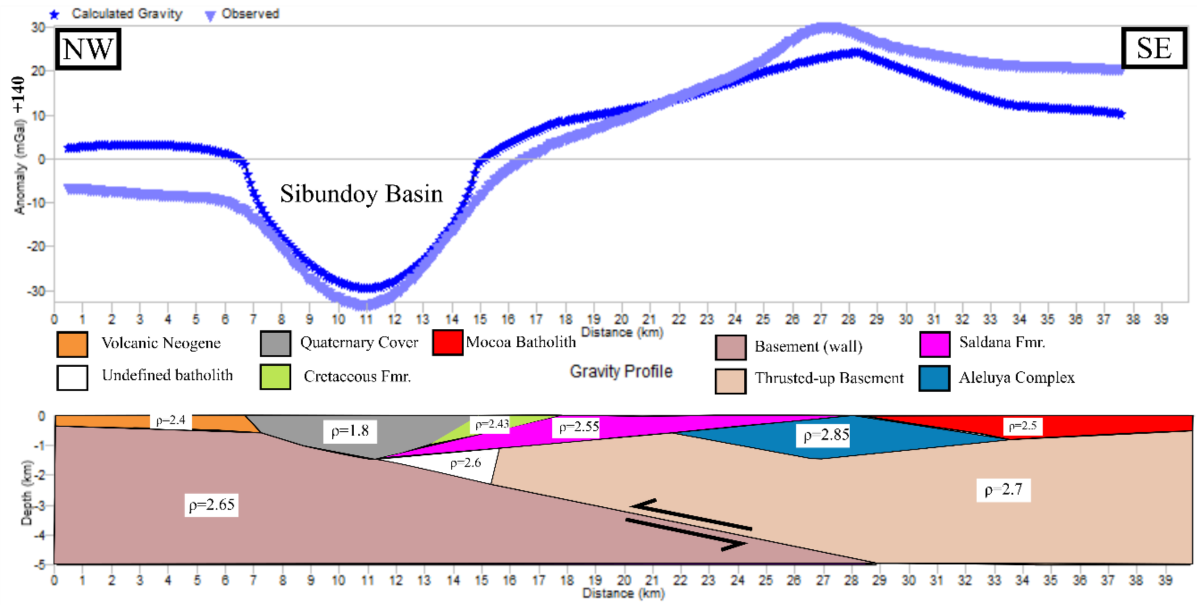

Figure 16 Model 2a shows the Complete Bouguer Anomaly values along a transect from point C and D that overlays the central part of the Sibundoy Valley with a NW to SE trend. The transect is approximately 38 km long. The calculated density measurements and the geology map were used to constrain this model, considering that the average of the basin infill is 1.8 g/cm^3. The geometries were

changed until the calculated gravity best matches the observed gravity. The values on the y axis were added 140 mGal because we only want to model the upper part of the crust on the GravMag software.

Figure 17 also shows a low-density model that is using the Complete Bouguer Anomaly without the regional trend as observed gravity data. **Figure 17 and 16** models are following the same transect. Despite of using the same thrust dominated arrangement for the geometry of the blocks, this model (**Figure 17**) shows a stronger agreement between the observed and calculated gravity curves, if we compare to the model that used the Complete Bouguer Anomaly values with the regional trend included (**Figure 16**). In addition, **Figure 18 and 19** are also showing a strong agreement between the observed and calculated gravity curves. We can conclude that the removal of the regional trend was important to enhance the gravity signal that comes from the Sibundoy Valley.

Figure 17 and 18 models follow a northwest to southeast transect, and they are separated for few kilometers. They have a thrust-up dominated arrangement for the geometry of the blocks where the thrust fault trace reaches the northwesternmost side of the basin. It seems that the thrust fault may be considered as thick-skinned tectonics. The hanging wall thrust-up to the point of blocking the southeast side of the basin with the Cretaceous Formations and Saldana Formation. As mentioned before, the calculated and observed gravity curves show a strong agreement for both models. However, there is a small disparity among the curves at the northwestern of the basin where the volcanic Neogene outcrops. In this area, the observed gravity has more positive anomalies than the calculated gravity curve. We presume that a denser rock may outcrop in this area, for example, a metamorphic complex. Another interpretation is that an edge effect may disrupt the observed curve at the northwestern margin of the model. Edge effect often happens when data is close to the edge of the model.

The main difference between **Figure 17 and 18** models consists on the absence of the bulge and an overall more positive gravity anomalies on the **Figure 18** model. A possible interpretation is that the Aleluya Complex does not outcrop in this area. In addition, a denser rock formation than the Saldana and Cretaceous Formations may lie below these formations. We suggest the presence of an undefined batholith below these formations that increase the overall positive anomalies in the area.

Figure 19 model follows a southwest to northeast trend and it is perpendicular to the **Figure 17 and 18** models. Here, the volcanic Neogene covers the southwest and northeast of the basin. The shape of the basin is uneven where the deepest depression lies on the southwestern part of the basin and the basin gets thinner towards the northeastern side. The Mocoa Batholith, Saldana and Cretaceous Formations do not outcrop in this area. The calculated and observed gravity show a strong agreement with the exception at the southwest side. A denser metamorphic rock may be present underneath the Quaternary volcanics and Volcanic Neogene. Another interpretation is that an edge effect is disrupting the observed gravity curve on the southwestern margin of the model.

Figure 20 model shows a new variation on the arrangement of the blocks while keeping the same density of them. The strike slip arrangement of the blocks does not generate a decent agreement between the observed and calculated gravity curves. It is even more evident especially at the flanks of the basin. The model has a northwest to southeast trend and it uses the Complete Bouguer Anomaly without the regional trend as the source of data.

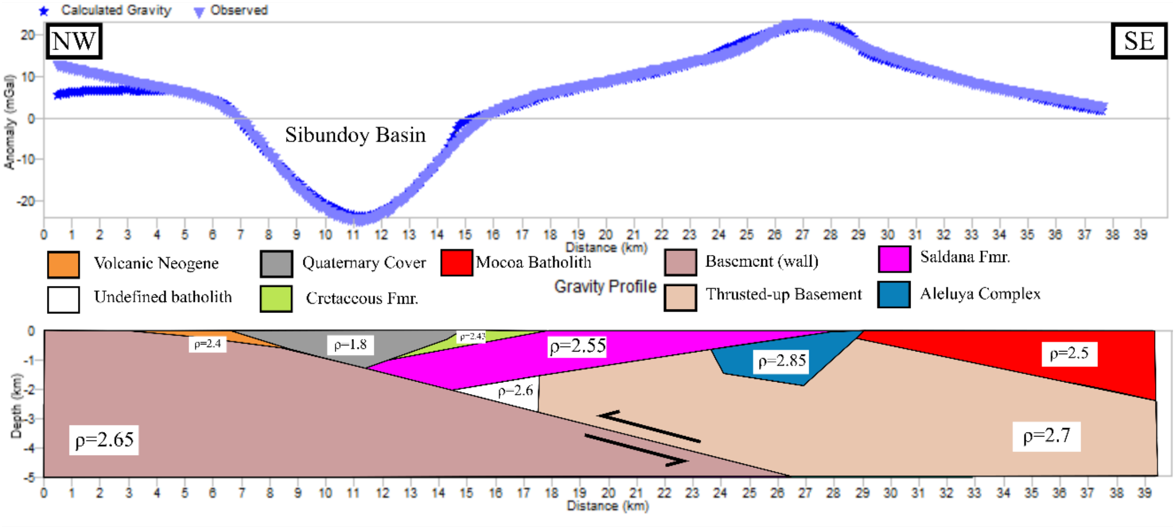

Figure 17 Model 2b shows the Complete Bouguer Anomaly values without the regional gravitational signature (taken from the best fit line from the BGI data), along a transect from point C and D that overlays the central part of the Sibundoy Valley with a NW to SE trend. The transect is approximately 38 km long. The calculated density measurements and the geology map were used to constrain this model, considering that the average of the basin infill is 1.8 g/cm^3. The geometries were changed until the calculated gravity best matches the observed gravity. Models using lower density basin fill and with the regional trend removed provide the best fit.

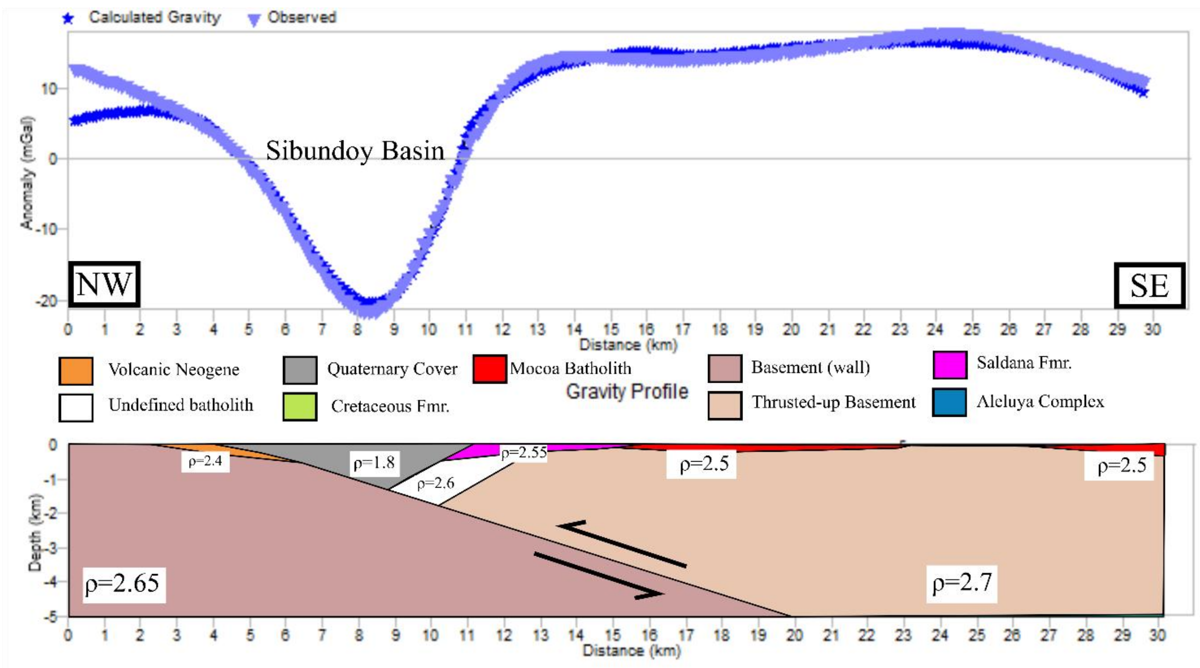

Figure 18 Model 3b shows the Complete Bouguer Anomaly values without the regional gravitational signature (taken from the best fit line from the BGI data), along a transect from point E and F that

overlays the southern part of the Sibundoy Valley with a NW to SE trend. The transect is approximately 30 km long. The calculated density measurements and the geology map were used to constrain this model, considering that the average of the basin infill is 1.8 g/cm^3. The geometries were changed until the calculated gravity best matches the observed gravity.

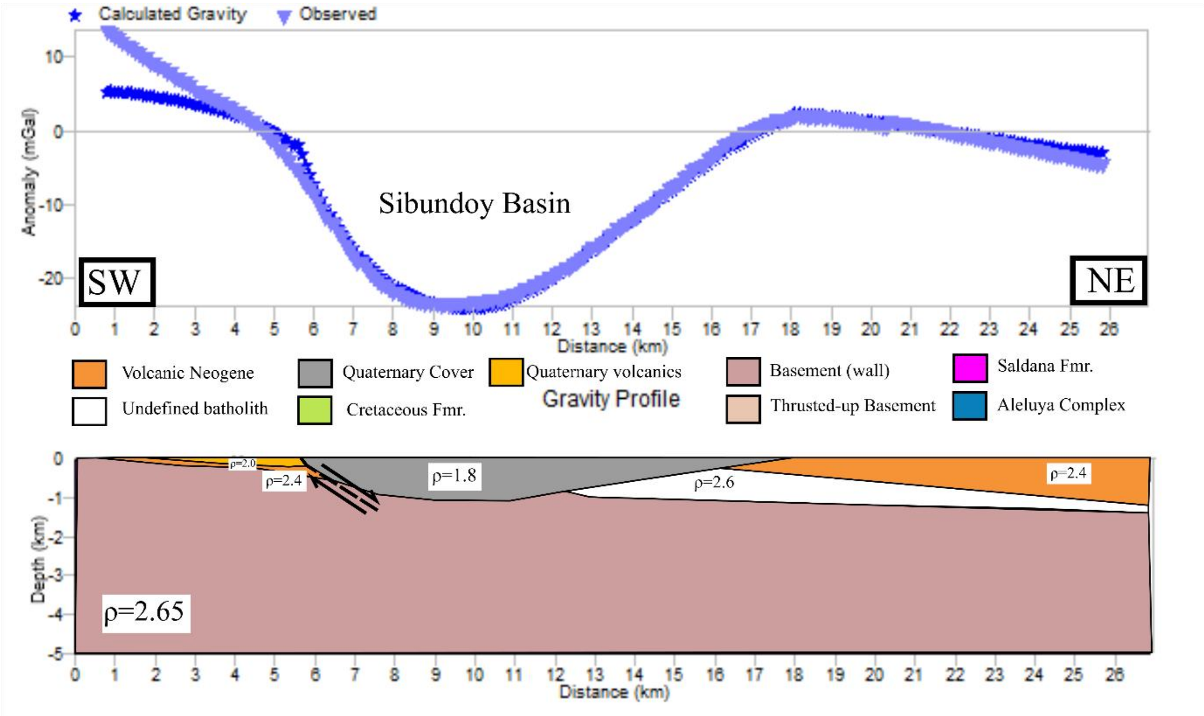

Figure 19 Model 5b shows the Complete Bouguer Anomaly values without the regional gravitational signature (taken from the best fit line from the BGI data), along a transect from the point I and J that overlays the central part of the Sibundoy Valley with a SW to NE trend. The transect is approximately 26 km long. The calculated density measurements and the geology map were used to constrain this model, considering that the average of the basin infill is 1.8 g/cm^3. The geometries were changed until the calculated gravity best matched the observed gravity.

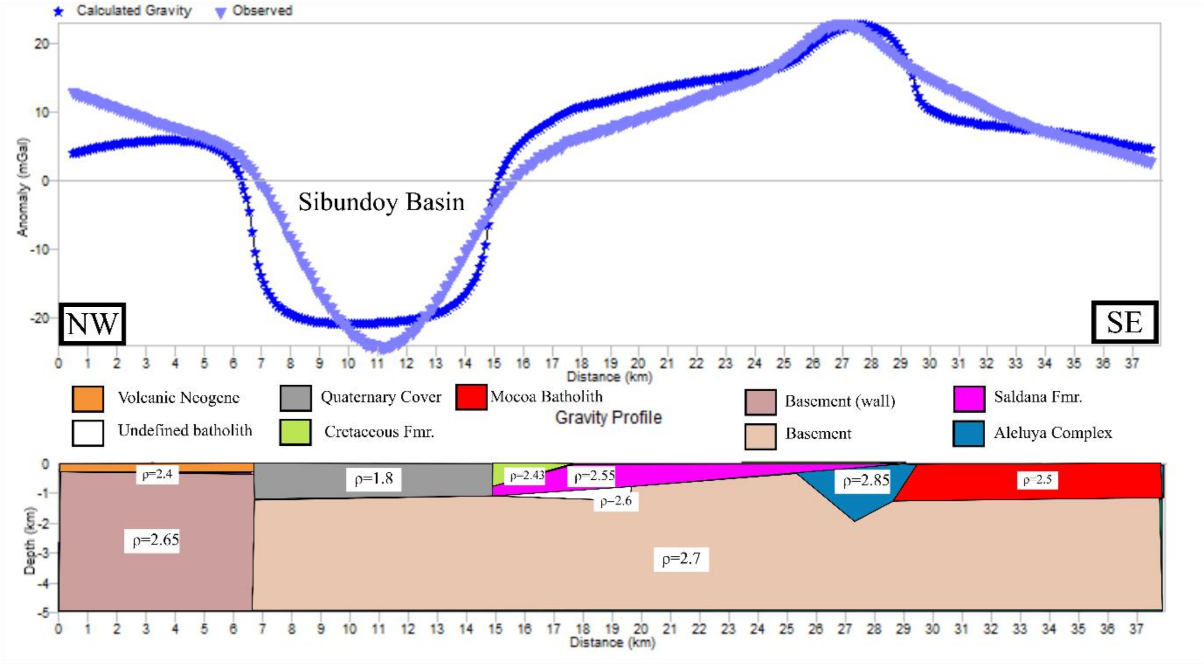

Figure 20 Model 2e shows the Complete Bouguer Anomaly values without the regional signature (taken from the best fit line from the BGI data), along a transect from point Cand D that overlays the central part of the Sibundoy Valley with a NW to SE trend. The transect is approximately 38 km long. The calculated density measurements and the geology map were used to constrain this model, considering that the average of the basin infill is 1.8 g/cm^3. **The geometry of the blocks follows a strike-slip arrangement.** The geometries were changed until the calculated gravity best matches the observed gravity. This model overall provides a poor fit to the gravity data.

3.1.2. High Density models

As mentioned before, the high-density models consist of models where the basin infill is 2.0 g/cm^3. **Figure 21** model follows a northwest to southeast trend, and it uses the Complete Bouguer Anomaly values for the observed gravity curve. The lithologic polygons mimic a thrust-up dominated arrangement where the hanging wall is blocking the southeast side of the basin, specifically, the Saldana Formation. In this specific transect, the Mocoa Batholith and the Saldana Formation outcrop at the southeast of the basin. The Neogene volcanics outcrop at the northwest of the basin. The agreement between the observed and calculated curve is decent at the basin but the curves do not show any agreement on the southeast and northwest of the basin. **Figure 23** model is also a high-density model and follow the same transect as **Figure 21 model,** but it uses Complete Bouguer Anomaly values without the regional trend for the observed gravity curve. Despite having the same thrust-up arrangement, **Figure 23** model shows a stronger agreement between the observed and calculated gravity curves with an exception at the northwesternmost side. We again can conclude that the source data without a regional trend enhanced the Sibundoy Valley signal. It is possible that a denser metamorphic rock may appear underneath the Neogene Volcanics that overall increases the observed gravity at the northwesternmost side margin. Another explanation is that an edge effect is disturbing the values.

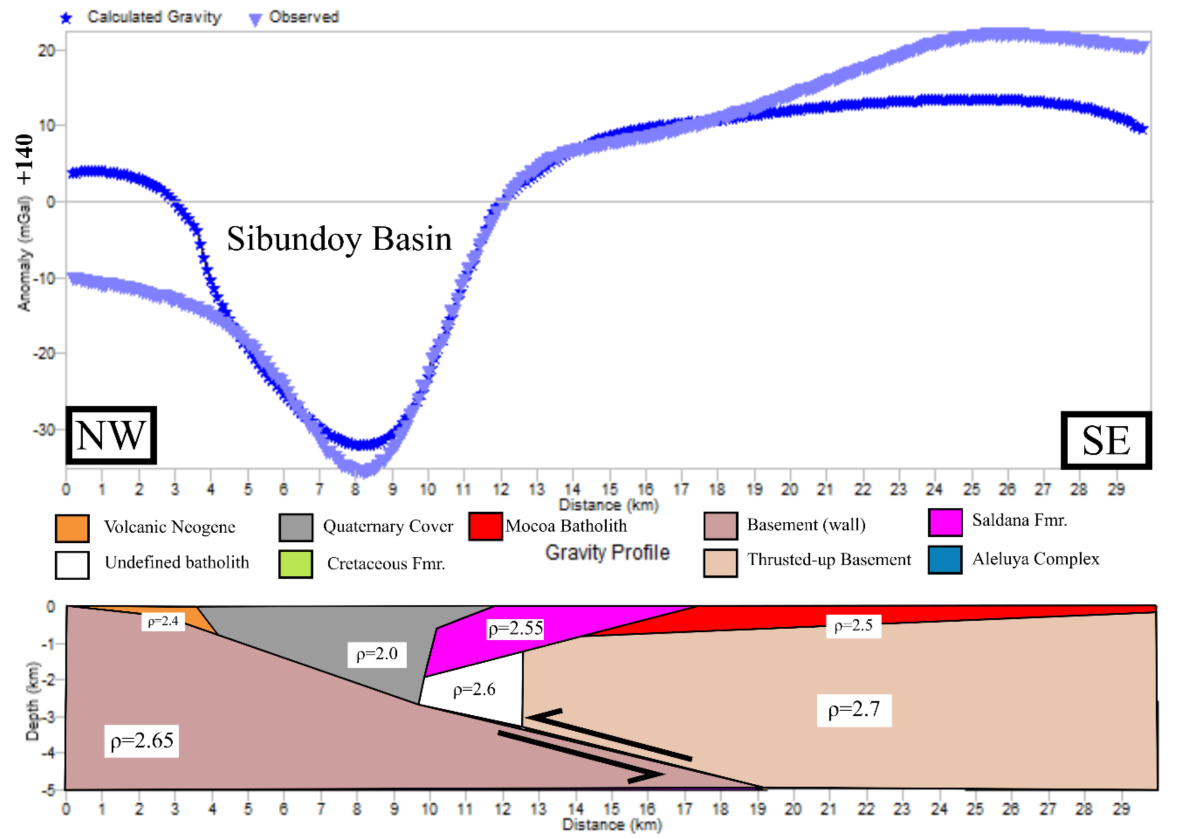

Figure 21 Model 3c shows the Complete Bouguer Anomaly values along a transect from point E and F that overlays the southern part of the Sibundoy Valley with a NW to SE trend. The transect is approximately 29 km long. The calculated density measurements and the geology map were used to constrain this model, considering that the average of the basin infill is 2.0 g/cm^3. The geometries were changed until the calculated gravity best matches the observed gravity.

Figure 22, 23, and 24 models are high-density models where the Complete Bouguer Anomaly values without the regional trend are used for the observed gravity curve. **Figure 22**

and 23 models follow a northwest to southeast trend, and they are separated by few kilometers. Both of them share a thrust-up arrangement for the geometry of the blocks. The shape of the basin is uneven and triangular. **Figure 23** model shows a bulge at the southwest of the basin. Here, the positive anomaly matches with the Aleluya Metamorphic Complex outcrop. In addition, the southeastern flank of the basin is blocked by the Saldana and Cretaceous Formations. In contrast, the **Figure 23** model did not show a positive anomaly bulge but an overall positive anomaly increments at the southeast of the basin.

Figure 21 model is a high-density model that uses the Complete Bouguer Anomaly values without the regional trend. It follows a southwest to northeast trend. From this perspective, the basin shows a half-graben shape that gets thinner towards the northwestern flank of the basin. The Neogene Volcanics outcrops at both sides of the basin.

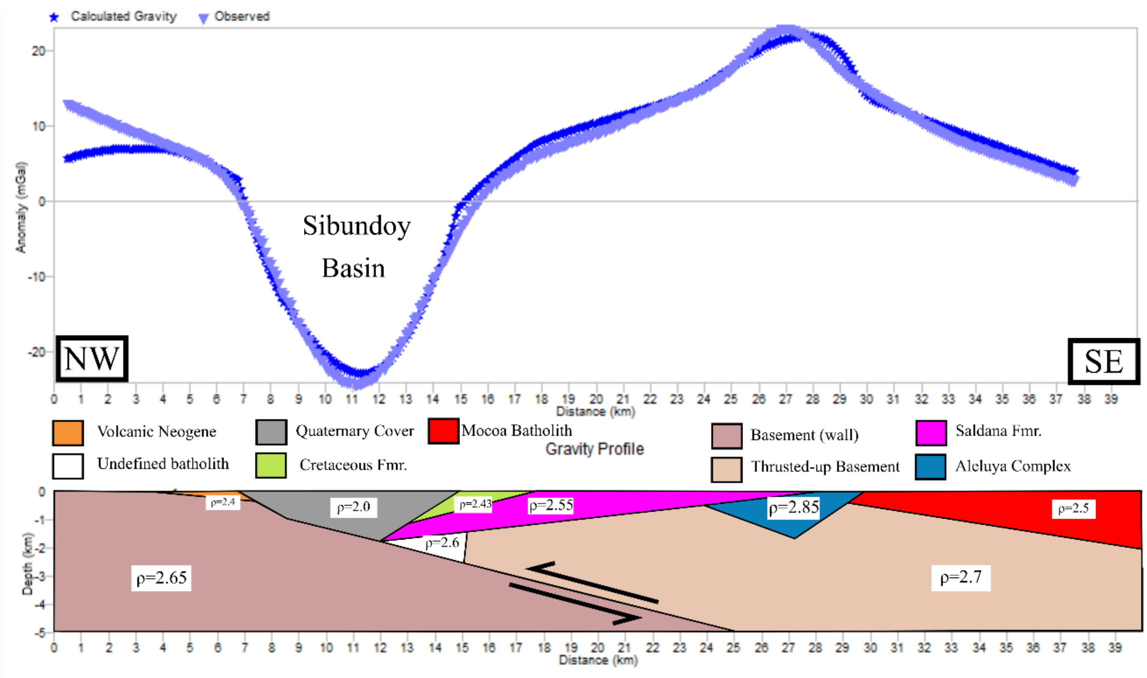

Figure 22 Model 2d shows the Complete Bouguer Anomaly values without the regional gravitational signature (taken from the best fit line from the BGI data), along a transect from point C and D that overlays the central part of the Sibundoy Valley with a NW to SE trend. The transect is approximately 38 km long. The calculated density measurements and the geology map were used to constrain this

model, considering that the average of the basin infill is 2.0 g/cm^3. The geometries were changed until the calculated gravity best matches the observed gravity.

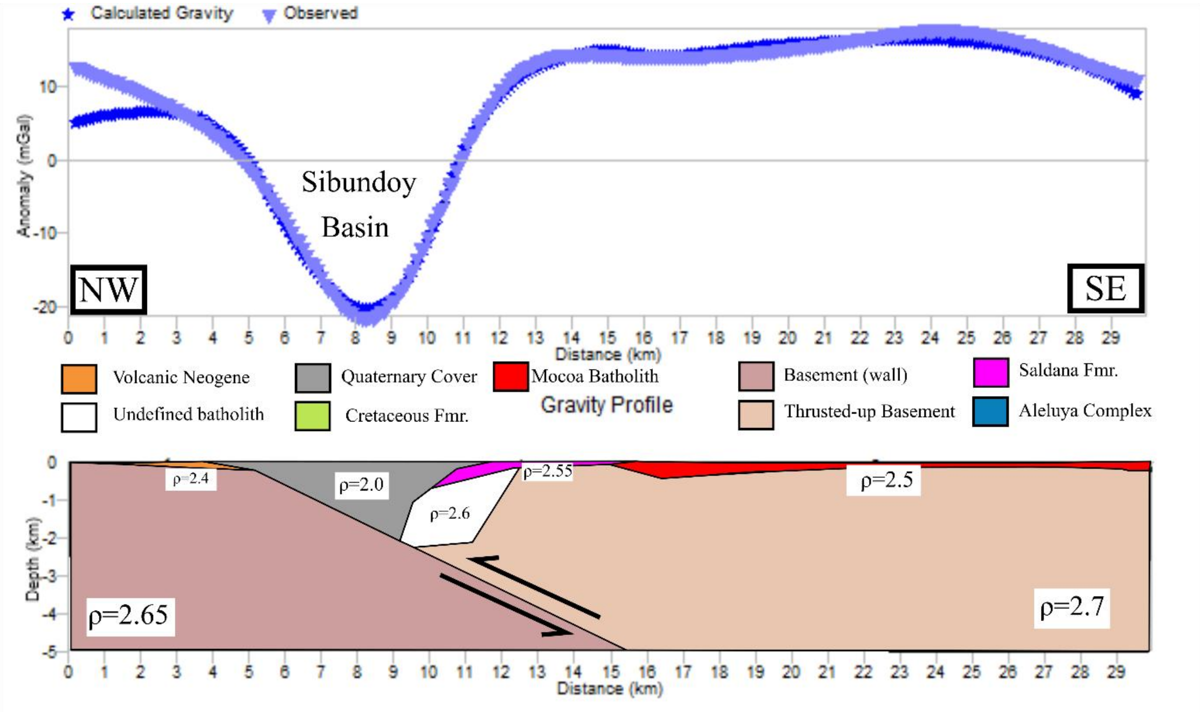

Figure 23 Model 3d shows the Complete Bouguer Anomaly values without the regional gravitational signature (taken from the best fit line from the BGI data), along a transect from point E and F that overlays the southern part of the Sibundoy Valley with a NW to SE trend. The transect is approximately 30 km long. The calculated density measurements and the geology map were used to constrain this model, considering that the average of the basin infill is 2.0 g/cm^3. The geometries were changed until the calculated gravity best matches the observed gravity.

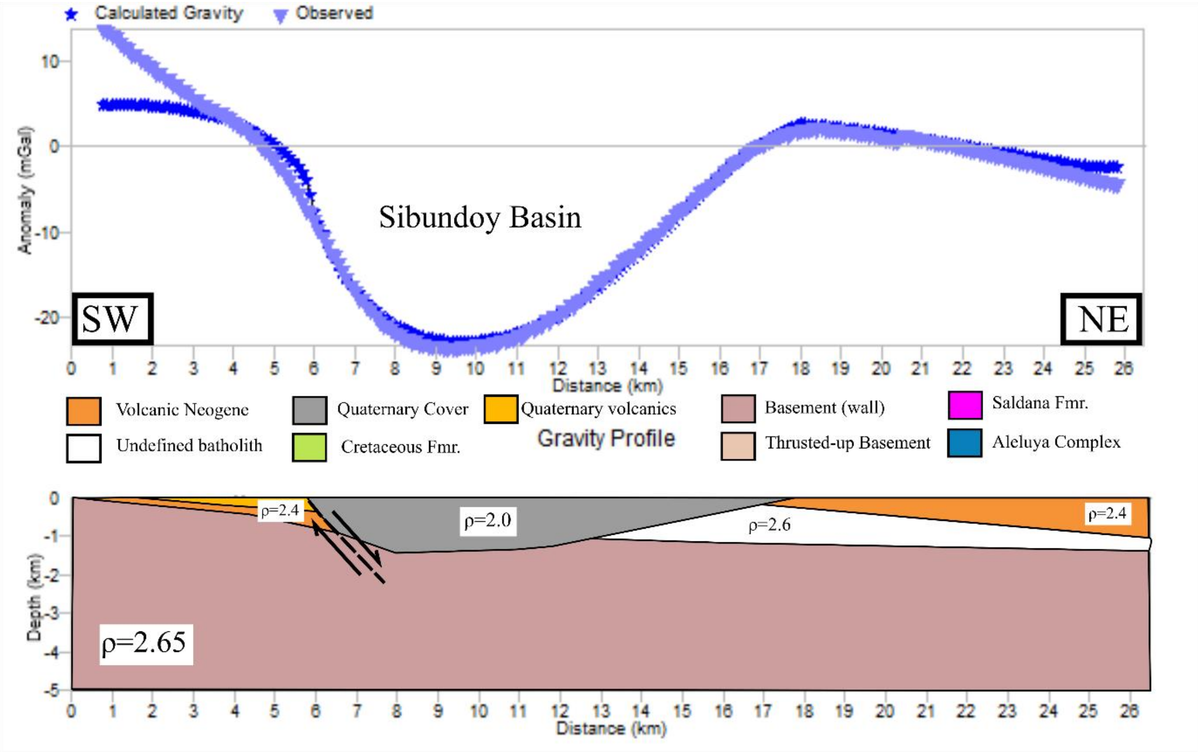

Figure 24 Model 5d shows the Complete Bouguer Anomaly values without the regional gravitational signature (taken from the best fit line from the BGI data), along a transect from point I and J that overlays the central part of the Sibundoy Valley with a SW to NE trend. The transect is approximately 26 km long. The calculated density measurements and the geology map were used to constrain this model, considering that the average of the basin infill is 2.0 g/cm^3. The geometries were changed until the calculated gravity best matched the observed gravity.

CHAPTER 4: DISCUSSION

In this chapter, we provide a 3D view reconstruction and a contour map of the basin shape which were obtained from the information collected on the gravity models. We will also review the geologic evidence found in the gravity models, in order to choose the best tectonic model that explains the shape and accommodation space of the Sibundoy Valley. In addition, we will discuss the implications of the chosen tectonic model in the regional geologic setting. Prior to that, we will emphasize the key points during the correction process of the gravity data since this technique helped to enhance the gravity signal from the Sibundoy Valley.

Accuracy of our data

The main technique used in this thesis project has been gravity modeling in order to interpret the best tectonic model that could explain the Sibundoy Valley evolution. Thus, the importance of the gravity survey and gravity correction play an important role. The gravity survey carried out approximately 100 gravity stations along the Mocoa transect and within the basin in multiple directions. The separation between stations did not exceed 1 km apart so the resolution and distribution of our raw data (absolute gravity values) can be considered as acceptable. The correction process on the gravity data followed the normal protocol to obtain the Complete Bouguer Anomalies, for example, the application of the Bullard coefficients, the international gravity formula, etc. It was uncertain that the Complete Bouguer Anomalies would provide an accurate signal from the basin especially after looking at the BGI data, where the basin signal was not detected in a context of an overall negative gravity anomaly from the bulk of the Andes. The Complete Bouguer Anomalies on this study detected the basin signal but also contained the regional trend. Thus, the removal of the regional trend become the best method to enhance the gravity signal from the basin. At the same time, the fact that BGI data did not detect the Sibundoy Valley, the BGI data became the best source of data for regional trend representation. We created several models by using both sources of data while the other variables remained constant on the models (e.g. density, geometry, and arrangement of the blocks). When the removal of the regional trend was used, the observed and calculated gravity curves show a stronger agreement.

3D view and contour map of the basin

The 3D views and contour map provide accurate dimensions of the basin in the subsurface with a good visualization (**Figure 25, 26, 27, 28, 29**). The 3D views were created by a minimum curvature gridding method in Oasis Montaj. The data for the 3D views consists of the depth and distance of the basin from the previous models, specifically on the intersection among the models. This was possible because the models are perpendicular to each other. In addition, the control points along the contour of the basin are another source of data for the 3D views since the shape of the basin on the surface has already been mapped. The contour map was created with the same information from the 3D view visualization, but using contour lines as the representation technique for elevation data.

The shape of the basin is better visualized in 3D views. We can conclude that the basin has a half-graven shape where the main axis of longitude has a southwest to northeast trend. The deepest depression of the basin is located at the southwestern side of the basin with a value of approximate 1300 meters, considering that the basin infill of the basin is 1.8 g/cm3. The basin gets thinner towards the northeastern side of the basin. Along the minor axis of longitude, the basin shows symmetrical and subtle angles on both flanks.

The high-density models did not show the best agreement between the observed and calculated gravity curves if we compared them to the low-density models. Therefore, a 3D view and a contour map were not produced for a basin infill of 2.0 g/cm^3.

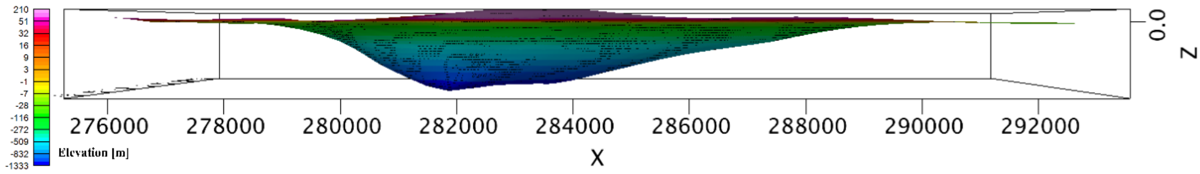

Figure 25 The thickness of the basin was created by a minimum curvature gridding method in Oasis Montaj. The data was provided by the depth and distance of the basin from the previous models. The positive values are artifacts from the interpolation method. 2D view of the basin from the south towards the north.

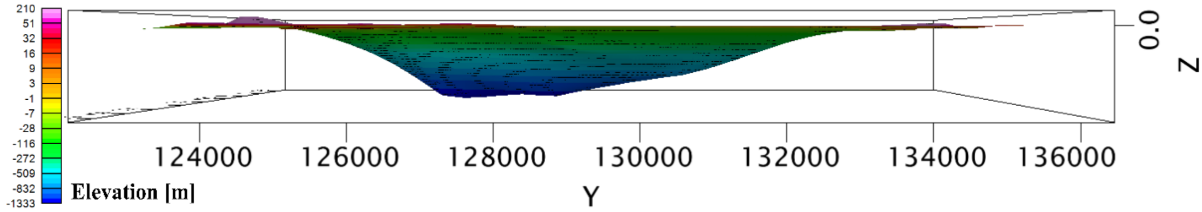

Figure 26 The thickness of the basin was created by a minimum curvature gridding method in Oasis Montaj. The data was provided by the depth and distance of the basins from the previous models. The positive values are artifacts from the interpolation method. 2D view of the basin from the west towards the east.

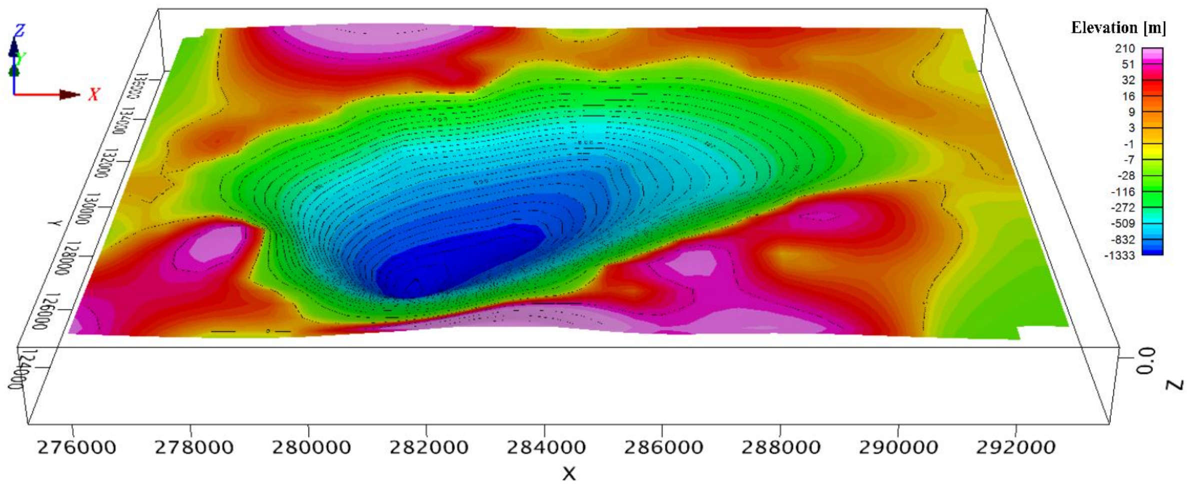

Figure 27 3D view of the basin from the south towards the north. It shows that the deepest depression is located in the southern section of the basin.

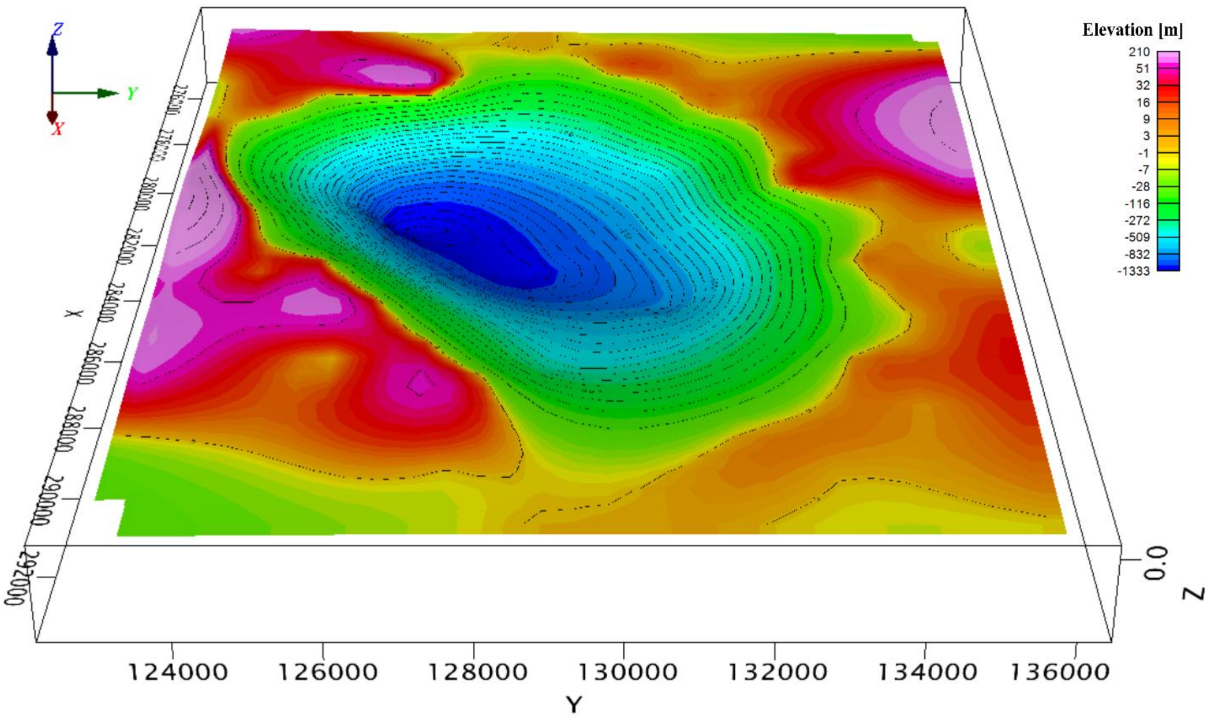

Figure 28 3D view of the basin from the east towards the west. It shows that the deepest depression is located at the western part of the basin.

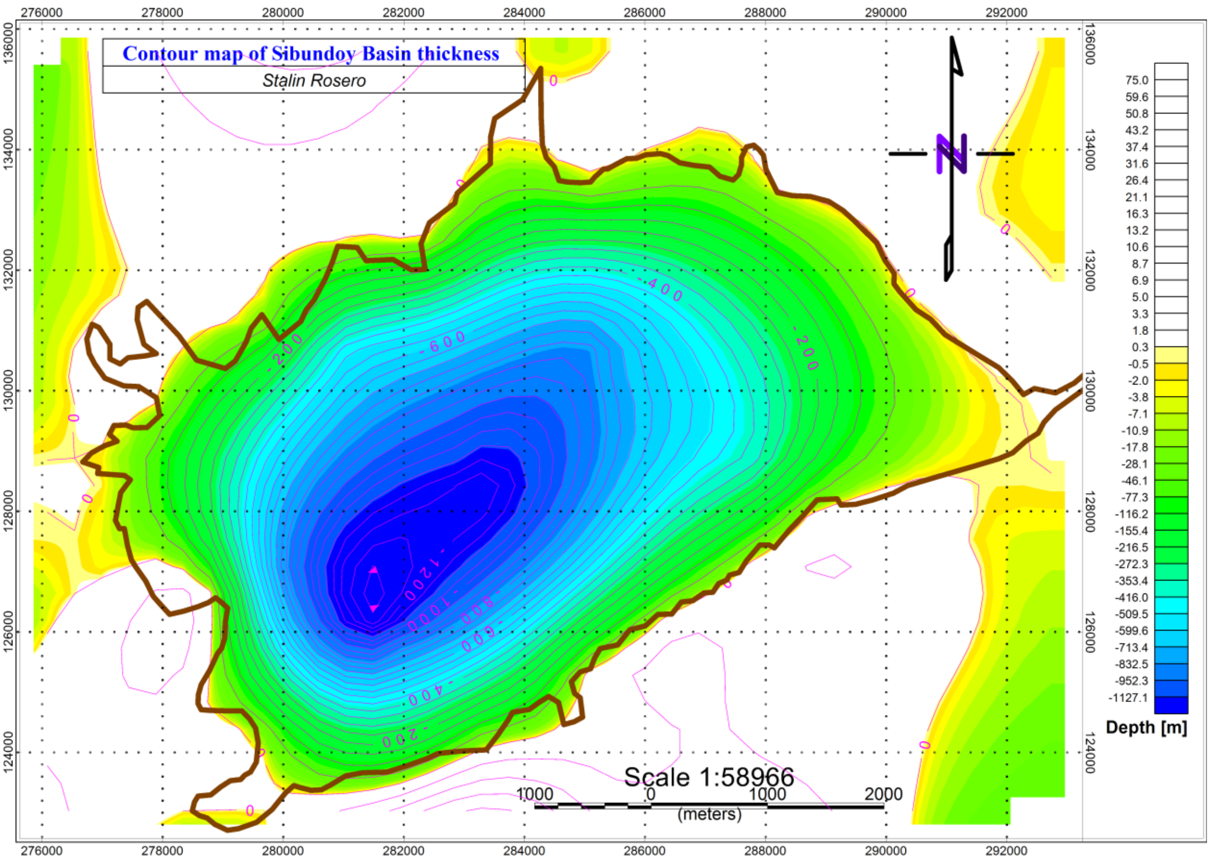

Figure 29 Contour map of Sibundoy Basin thickness. Contour interval is 50 m with a maximum estimated basin depth of 1300 m in the southwestern corner.

Interpretation of the shape of the basin

The shape of the basin is the direct result how Quaternary brittle faults have created the accommodation space in the basin. Unfortunately, the shape of the basin suggests, but does not uniquely constrain, the fault kinematics. However, the shape of the basin does provide insights to discard a type of fault. For example, the half-graben shape of the basin has subtle and shallow angles on their flanks so it suggests that a steep strike-slip fault may not be a good fit on the flanks, particularly on the north side. In addition, the vertical strike -slip fault model (**Figure 20**) shows a low agreement between the calculated and observed gravity curves, particularly when a sharp and steep geometry of the basin was used along the northwest to southeast trend gravity models. Instead, the gravity models suggest that a southwest to northeast trending fault is present at the western flank of the basin. They suggest a thick-skinned fault with a moderate slip angle (**Figure 21 and 22**). Colon fault is the name of the surface expression of this fault. We interpret three different possibilities, depending on the kinematics of the fault (**Figure 30 and 31**). The first option is shallowly dipping strike-slip fault with a step over to the south side of the basin. The second option is the presence of a reverse slip component on the fault. It would create a transpressional zone perpendicular to the deformation zone. The third option is the presence of a normal sense component on the fault. It would create a transtensional zone. In addition, the gravity models do not show a fault at the eastern flank of the basin. Instead, we observe a conformable contact between the Cretaceous sedimentary rocks and the basin.

The deepest depression of the basin occurs at the southwestern side of the basin, and it gets progressively thinner towards the northeastern side of the basin. We can infer that a northwest to southeast trending normal fault at the southwestern side of the basin is responsible for creating the half-graben shape. In addition, we can infer that no fault is present at the northeastern side of the basin.

Potential tectonic models

In this section, we discuss the arguments in favor and against tectonic models that explain the basin shape, based on the known faults present, according to the 3D views and gravity models. Since the kinematics of the faults are not certain, three possible tectonic interpretations arise for the basin: pull-apart, piggyback, or hinterland basin.

According to Velandia, et al., (2005)**.** Sibundoy Valley is a pull-apart basin, based on regional GPS data and the geometric arrangement of the faults in map view. The pure pull apart tectonic model explains that two parallel strike slip faults create an area of crustal extension where the normal faults or bounding basin sidewall faults connect the two opposite principal displacement zones (PDZ). So far, the normal fault at the southwestern side of the basin is the best interpretation for the half-graben shape of the basin. The pull apart model agrees on the presence of the normal fault with a northwest to southeast trend at the southwestern side of the basin. The pull apart model also agrees on a strike slip fault with moderate dip angle that potentially would drive the principal displacement zone. The idea of a moderate dip angle on a strike slip angle should not be considered as an extreme idea because moderate slip angles appear along the bend zones of the San Andreas Fault (Fuis, Scheirer, Langenheim, & Kohler, 2012). However, our model suggests the absence of any fault at the southeastern side of the basin. Instead, our gravity models show a conformable contact between the basin and the Cretaceous sedimentary formations. Thus, our model does not support the idea of a parallel strike slip fault inside the basin but we cannot confirm or deny a possible occurrence of a strike slip fault further north of the basin since the Algeciras fault system is active and accommodating the slip from the oblique convergence between the Nazca and South American Plate.

A piggyback basin is formed at convergent plate boundaries when the thrusting is not restricted to the foreland basin margin, and a thrust fault may subdivide the former foreland basin in different sections, creating a piggyback basin on the wedge top. Thrusting and loading of the crust at the margin of the foreland basin happens when the convergent margin is significantly active like the Andean margin. Most thrust faults on the North Andean fold and thrust belt have an eastern vergence towards the craton. According to the gravity model, there is a possibility that the fault at the western flank of the basin has a transpressional component. This means a thick-skinned back thrust with a western vergence. If this is the case, the back-thrust is creating an obstruction to the thrust sheet.

The Andean hinterland basins are produced between the western magmatic arc and the craton-directed fold-thrust belt to the east. The location of the Sibundoy basin is complex due to the proximity of the “knot” of Pastos (62 km away) and the beginning of the Magdalena hinterland basin (~200 km away). The profile graph (**Figure 1**) shows that the Sibundoy Basin has a significant elevation, and it is embedded in the orogenic wedge of the

Eastern Cordillera. Here, the Central Cordillera has not been differentiated from the other Cordilleras yet and the Interandean depression is not well formed. However, the Sibundoy Valley can be considered as a hinterland basin due to the similar structural position compared to the Magdalena Valley, and a relative difference in elevation compared to the orogenic wedge.

There are two common modes of hinterland basin formation (Horton et al. 2011). Sibundoy Basin follows the development of new activated features in regions that had recently been experiencing erosion and deformation like the Eastern Cordillera of Colombia. The basin evolution can be attributed to the initiation of slip on particular structures associated with shortening, extension, and strike-slip deformation within the orogenic interior (Horton et al. 2011). According to the gravity model, there is a possibility that the fault at the western flank of the basin has a transtentional component. This means a normal fault activated a former fault and induced rifting (or supradetachment) basin. One example of this scenario occurred in the Peruvian Andes (e.g. Callejon de Huaylas Basin).

Strain partitioning is a key part in the geologic setting of the Northern Andes due to oblique plate convergence between the Nazca and South American Plate. The ENE slip vector has been accommodated by a combination of right lateral NNE strike slip fault systems in the North Andean Block, and perpendicular retro arc thrusting (Dewey, Holdsworth, & Strachan, 1998). In addition, the collision between the Panamanian isthmus and the North Andean Block is another key factor in the Northern Andes because it is considered to be the event that has widen the Colombian Andes into three Cordilleras. The possible transtentional component may be influenced by this event despite of the distance between the basin and the collision site. The best tectonic model tries to fit the kinematics of faults, the shape of the basin, and the geologic setting.

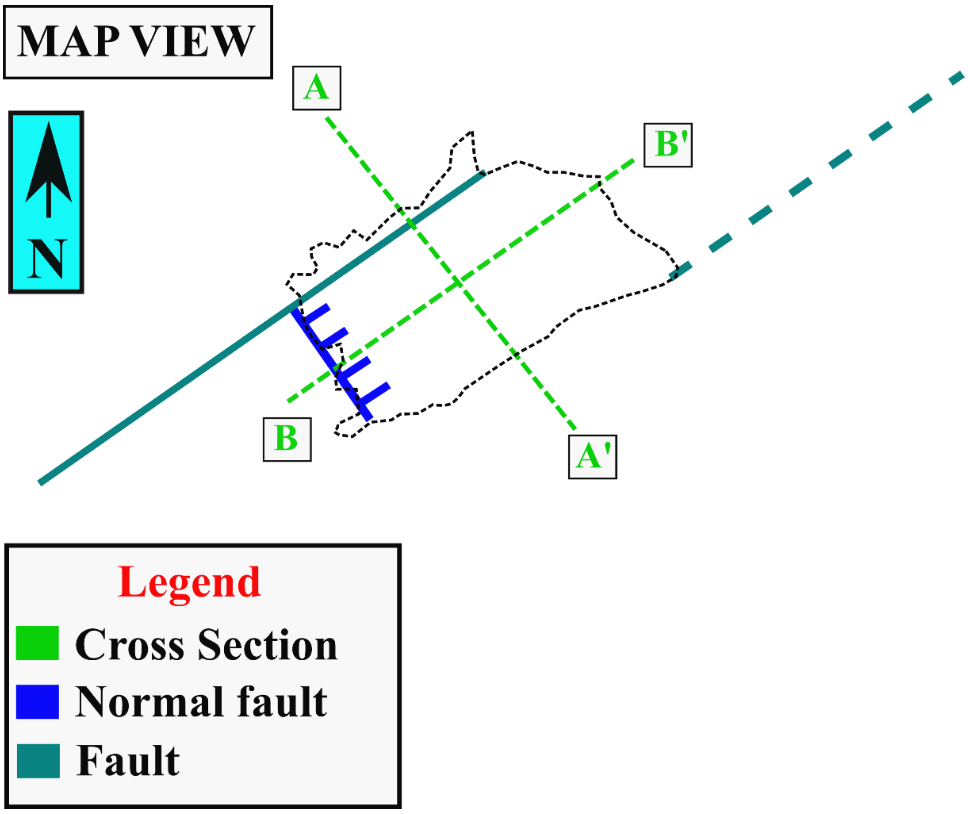

Figure 30 Map view sketch that describes the faults found during gravity modeling. It also shows the two perpendicular transects for the cross section in figure 31.

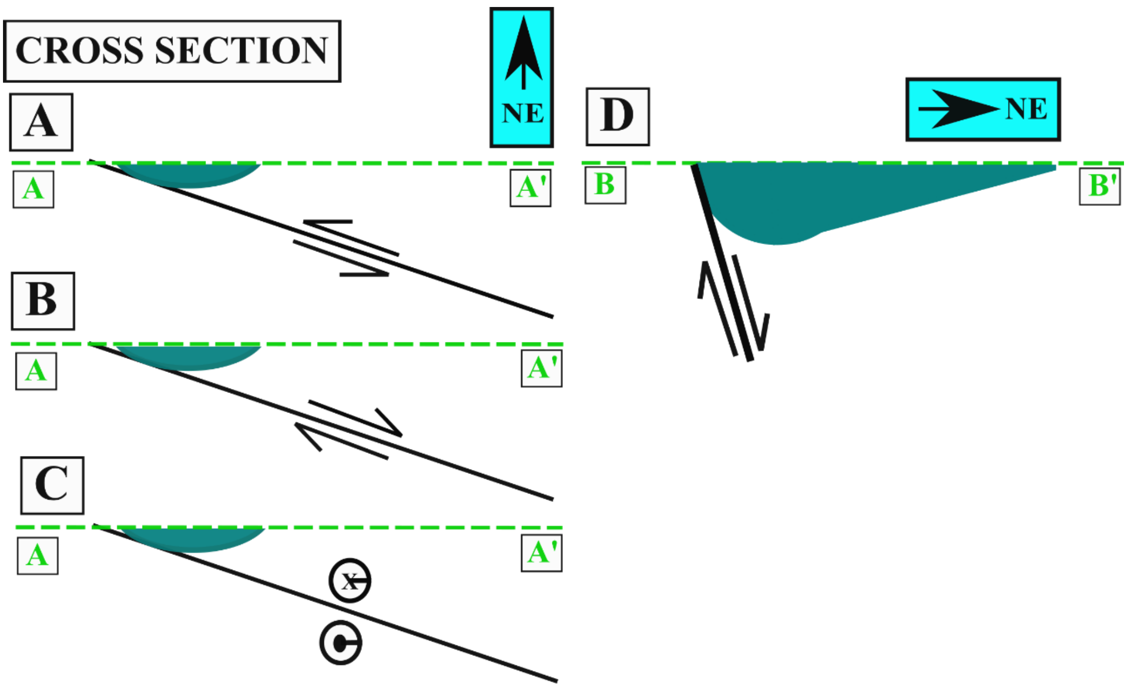

Figure 31 Cross section of the Sibundoy Basin shows the found faults during the gravity modeling. Three different alternatives arise from the kinematics of the fault: normal, reverse, or pure strike slip fault.

CONCLUSIONS

1. The Complete Bouguer Anomaly values suggest that the Sibundoy Valley has a negative anomaly of 30 mGal. This area of lowest negative Bouguer gravity values in the study area ranges from -140.0 to -170.2 mGal.
2. Sibundoy Valley has a half-graben shape where the deepest depression (-1300 m) is located at the southwestern side of the basin, and it gets thinner towards the northeastern side of the basin, according to the 3D views and the contour map.
3. The southwest to northeast trend models suggest that the basin has a half-graben shape where a normal fault creates the accommodation space at the southern flank of the basin. The basin gets thinner towards the northern flank of the basin so it is unlikely the presence of a fault at the mentioned flank.
4. The thrust-up arrangement of the blocks in the models generate the strongest agreement between the calculated and observed gravity curves, especially along the northwest to southeast trend models. The strike-slip arrangement of the blocks does not show any agreement along the same trend models. The same trend models show that the Saldana and Cretaceous Formations block the eastern flank of the basin, forming a conformable contact. The same trend models also suggest that a fault outcrops at the western flank of the basin and has a thick-skinned behavior. Colon fault is the name of the surface expression of this fault. The shape of the basin has lower angles on their flanks so it is unlikely the presence of a vertical bounding strike-slip fault.
5. Since, the kinematics of the thick-skinned fault is not certain, the piggyback, pull-apart, and the hinterland models are possible. Arguments in favor and against were presented in the discussion. A rifting (or supradetachment) hinterland basin may be the most likely model that best describes the tectonic evolution of the basin,

considering the shape of the basin, geologic setting, and transtentional kinematics of the faults.

6. The high-density and low-density models show a slight difference in terms of the agreement between the calculated and observed gravity curves. The low-density models show a better agreement, so it is likely that the basin infill is 1.8 g/cm^3.

7. The removal of the regional trend on the Complete Bouguer Anomaly values enhanced the signal from the Sibundoy Valley. In addition, it reduced the edge effect on the model margins. The calculated and observed gravity curves started to have a stronger agreement without any change in the geometry of the blocks.

8. The Aleluya metamorphic Complex shows a significant positive anomaly with respect to the rest of the rocks which made it feasible to track and map the extent of this geologic unit at the east of the basin (Mocoa transect).

9. The Migmatitic Complex was included in the referenced map. However, this unit does not appear on the gravity models.

REFERENCES

Alçiçek, M. C., & ten Veen, J. H. (2008). The late early Miocene Acıpayam piggy-back basin: Refining the last stages of lycian nappe emplacement in SW Turkey. *Sedimentary Geology*, *208*(3), 101–113. doi:10.1016/j.sedgeo.2008.05.003

Alvarado, A., Audin, L., Nocquet, J. M., Jaillard, E., Mothes, P., Jarrín, P., . . . Cisneros, D. (2016). Partitioning of oblique convergence in the Northern Andes subduction zone: Migration history and the present-day boundary of the north Andean sliver in Ecuador. *Tectonics (Washington, D.C.), 35*(5), 1048–1065. doi:10.1002/2016TC004117

Beauval, C., Yepes, H., Palacios, P., Segovia, M., Alvarado, A., Font, Y., . . . Vaca, S. (2013). An earthquake catalog for seismic hazard assessment in Ecuador. *Bulletin of the Seismological Society of America*, *103*(2A), 773–786. doi:10.1785/0120120270

Blais, J. A. R., & Ferland, R. (1984). Optimization in gravimetric terrain corrections. *Canadian Journal of Earth Sciences, 21*(5), 505–515. doi:10.1139/e84-055

Cochrane, R., Spikings, R., Gerdes, A., Winkler, W., Ulianov, A., Mora, A., & Chiaradia, M. (2014). Distinguishing between in-situ and accretionary growth of continents along active margins. *Lithos, 202-203,* 382–394. doi:10.1016/j.lithos.2014.05.031

Dewey, J. F., Holdsworth, R. E., & Strachan, R. A. (1998). Transpression and transtension zones. *Continental transpressional and transtensional tectonics* (pp. 1–14) The Geological Society of London. doi:10.1144/GSL.SP.1998.135.01.01 Retrieved from https://www.lyellcollection.org/doi/10.1144/GSL.SP.1998.135.01.01

Farangitakis, G., McCaffrey, K. J. W., Willingshofer, E., Allen, M. B., Kalnins, L. M., Hunen, J., . . . Sokoutis, D. (2021). The structural evolution of pull-apart basins in response to changes in plate motion. *Basin Research, 33*(2), 1603–1625. doi:10.1111/bre.12528

Farris, D. W., Jaramillo, C., Bayona, G., Restrepo-Moreno, S. A., Montes, C., Cardona, A., . . . Valencia, V. (2011). Fracturing of the Panamanian Isthmus during initial collision with South America. *Geology (Boulder), 39*(11), 1007–1010. doi:10.1130/G32237.1

Fuis, G. S., Scheirer, D. S., Langenheim, V. E., & Kohler, M. D. (2012). A new perspective on the geometry of the San Andreas fault in southern California and its relationship to lithospheric structure. *Bulletin of the Seismological Society of America, 102*(1), 236–251. doi:10.1785/0120110041

Gutscher, M. -., Malavieille, J., Lallemand, S., & Collot, J. -. (1999). Tectonic segmentation of the north Andean margin: Impact of the Carnegie ridge collision. *Earth and Planetary Science Letters, 168*(3), 255–270. doi:10.1016/S0012-821X(99)00060-6

Horton, B. K. (2011). Cenozoic evolution of hinterland basins in the andes and tibet. *Tectonics of sedimentary basins* (pp. 427–444). Chichester, UK: John Wiley & Sons, Ltd. doi:10.1002/9781444347166.ch21 Retrieved from https://onlinelibrary.wiley.com/doi/abs/10.1002/9781444347166.ch21

Horton, B. K., & Folguera, A. (2019). *Andean tectonics*. Amsterdam: Elsevier. doi:10.1016/C2017-0-04053-3

Kellogg, J. N., Vega, V., Stailings, T. C., & Aiken, C. L. V. (1995). *Tectonic development of Panama, Costa rica, and the Colombian Andes: Constraints from global positioning system geodetic studies and gravity* The_Geological_Society_of_America. doi:10.1130/SPE295-p75

Mora, A., Gaona, T., Kley, J., Montoya, D., Parra, M., Quiroz, L. I., . . . Strecker, M. R. (2009). The role of inherited extensional fault segmentation and linkage in contractional Orogenesis: A reconstruction of lower cretaceous inverted rift basins in the Eastern Cordillera of Colombia. *Basin Research, 21*(1), 111–137. doi:10.1111/j.1365-2117.2008.00367.x

Mora-Páez, H., Kellogg, J. N., Freymueller, J. T., Mencin, D., Fernandes, R. M. S., Diederix, H., . . . Corchuelo-Cuervo, Y. (2019). Crustal deformation in the Northern Andes – A new GPS velocity field. *Journal of South American Earth Sciences, 89,* 76–91. doi:10.1016/j.jsames.2018.11.002

Nichols, G. (2009). *Sedimentology and stratigraphy* (2. edition, 1. publ. ed.). Chichester [u.a.]: Wiley-Blackwell. Retrieved from http://bvbr.bib-bvb.de:8991/F?func=service&doc_library=BVB01&local_base=BVB01&doc_number=016392246&sequence=000002&line_number=0001&func_code=DB_RECORDS&service_type=MEDIA

Nocquet, J., Villegas-Lanza, J. C., Chlieh, M., Mothes, P. A., Rolandone, F., Jarrin, P., . . . Yepes, H. (2014). Motion of continental slivers and creeping subduction in the northern andes. *Nature Geoscience, 7*(4), 287–291. doi:10.1038/NGEO2099

Nowell, D. A. G. (1999). Gravity terrain corrections — an overview. *Journal of Applied Geophysics, 42*(2), 117–134. doi:10.1016/S0926-9851(99)00028-2

Nuñez, A. (2003). Reconocimiento geologico regional de las planchas 411 la cruz, 412 san Juan de Villalobos, 430 Mocoa, 431 Piamonte, 448 Monopamba, 449 orito y 465 Churuyaco Departamento de Caqueta, Cauca, Huila, Nariño y Putumayo escala

1:100000. *INGEOMINAS*, , 92–98. Retrieved from https://catalogo.sgc.gov.co/cgi-bin/koha/opac-detail.pl?biblionumber=48504%20thumbnail-shelfbrowser

Restrepo, M., Bustamante, C., Cardona, A., Beltrán-Triviño, A., Bustamante, A., Chavarría, L., & Valencia, V. A. (2021). Tectonic implications of the Jurassic magmatism and the metamorphic record at the southern Colombian Andes. *Journal of South American Earth Sciences*, *111*, 103439. doi:10.1016/j.jsames.2021.103439

Reynolds, J. M. (2011). *An introduction to applied and Environmental Geophysics* (2. ed., 1. publ. ed.). Chichester [u.a.]: Wiley-Blackwell. Retrieved from http://bvbr.bib-bvb.de:8991/F?func=service&doc_library=BVB01&local_base=BVB01&doc_number=022530835&sequence=000002&line_number=0001&func_code=DB_RECORDS&service_type=MEDIA

Rivera Lara, V. (2021). Estudio morfométrico y geomorfológico del campo volcánico mono genético Guamuez – Sibundoy, Colombia. *Universidad de Caldas*. Disponible en: https://repositorio.ucaldas.edu.co/handle/ucaldas/16978

Rodríguez, G., Arango, M. I., Zapata, G., & Bermúdez, J. G. (2018). Petrotectonic characteristics, geochemistry, and U-Pb geochronology of Jurassic plutons in the upper Magdalena valley-Colombia: Implications on the evolution of magmatic arcs in the NW Andes. *Journal of South American Earth Sciences*, *81*, 10–30. doi:10.1016/j.jsames.2017.10.012

Roure, F. (2008). Foreland and hinterland basins: What controls their evolution? *Swiss Journal of Geosciences*, *101*(Suppl 1), 5–29. doi:10.1007/s00015-008-1285-x

Spikings, R., Cochrane, R., Villagomez, D., Van der Lelij, R., Vallejo, C., Winkler, W., & Beate, B. (2015). The geological history of northwestern South America: From Pangaea to the early collision of the Caribbean large igneous province (290–75Ma). *Gondwana Research, 27*(1), 95–139. doi:10.1016/j.gr.2014.06.004

Telford, W. M., Geldart, L. P., & Sheriff, R. E. (2004). *Applied geophysics* (2 ed.)

Tibaldi, A., Rovida, A., & Corazzato, C. (2007). Late quaternary kinematics, slip-rate and segmentation of a major cordillera-parallel transcurrent fault: The Cayambe-Afiladores-Sibundoy system, NW South America. *Journal of Structural Geology, 29*(4), 664–680. doi:10.1016/j.jsg.2006.11.008

Trenkamp, R., Kellogg, J. N., Freymueller, J. T., & Mora, H. P. (2002). Wide plate margin deformation, Southern Central America and northwestern South America, CASA GPS observations. *Journal of South American Earth Sciences, 15*(2), 157–171. doi:10.1016/s0895-9811(02)00018-4

Vásquez, M., Altenberger, U., Romer, R. L., Sudo, M., & Moreno-Murillo, J. M. (2010). Magmatic evolution of the Andean Eastern Cordillera of Colombia during the Cretaceous: Influence of previous tectonic processes. *Journal of South American Earth Sciences, 29*(2), 171–186. doi:10.1016/j.jsames.2009.02.003

Velandia, F., Acosta, J., Terraza, R., & Villegas, H. (2005). The current tectonic motion of the Northern Andes along the Algeciras fault system in SW Colombia. *Tectonophysics, 399*(1), 313–329. doi:10.1016/j.tecto.2004.12.028

Villagómez, D., Spikings, R., Magna, T., Kammer, A., Winkler, W., & Beltrán, A. (2011). Geochronology, geochemistry and tectonic evolution of the Western and Central Cordilleras of Colombia. *Lithos, 125*(3), 875–896. doi:10.1016/j.lithos.2011.05.003

Vinasco, C. J., Cordani, U. G., González, H., Weber, M., & Pelaez, C. (2006). Geochronological, isotopic, and geochemical data from Permo-Triassic granitic gneisses and granitoids of the Colombian Central Andes. *Journal of South American Earth Sciences, 21*(4), 355–371. doi:10.1016/j.jsames.2006.07.007

Zapata-Garcia, G., Rodriguez G, & Arango, M. I. (2017, Petrografia, geoquimica y geocronologia de rocas metamorficas aflorantes en San Francisco Putumayo y la via Palermo-San Luis asociadas a los complejos la Cocha-rio Tellez y Aleluya. *Boletin De Ciencias De La Tierra 41*, 47–64.

APPENDIX A: DENSITY DATA TABLE OF COLLECTED ROCK SAMPLES

Station Name	Lithology	Mass [g] ± 0.01	Mass of water displaced [g] ± 0.01	Average Density [g/cm3]	Image
17-SB-70	Hornblende dacite	494.09	191.34	2.58	
17-SB-88	Andesite	265.39	104.28	2.55	
17-SB-100B	Amphibolitic Gneiss	191.02	68.58	2.79	
17-SB-100A	Amphibolitic Gneiss	465.51	165.15	2.82	

17-SB-77	Micritic Limestone	372.54	141.57	2.63	
17-SB-80	Black Mudstone	177.10	73.20	2.42	
17-SB-93	-----	320.77	119.40	2.69	
17-SB-81	------	174.81	68.73	2.54	

17-SB-57	Andesite	429.99	183.34	2.35	
17-SB-45.5	------	379.08	143.49	2.64	
17-SB-82	Quartzite	422.86	170.41	2.48	

17-SB-83	Crystalline Dacite	222.49	86.33	2.58	
17-SB-17	Granite	127.37	49.00	2.60	
17-SB-92	Quartz Monzonite	157.00	62.40	2.52	

17-SB-94	Granodiorite	263.92	100.21	2.63	
17-SB-78	Black Mudstone	109.55	49.19	2.23	
17-SB-99	Aplite	402.35	159.72	2.52	
17-SB-87	Basalt	133.71	50.82	2.63	

17-SB-84	Alkalic granite	370.86	139.14	2.67	
17-SB-18A	Hornblende Andesite	327.81	301.98	1.09	
17-SB-18B	Volcanogenic Sediment	21.56	9.13	2.36	--
17-SB-95	Granite	76.87	30.01	2.56	
17-SB-40	Matrix and cobble	94.23	35.67	2.64	
17-SB-72	Saturated Lapilli Tuff	146.64	110.97	1.32	

17-SB-72	Unsaturated Lapilli Tuff	71.62	120.82	0.59	
17-SB-71	Saturated Dacite tuff	44.63	33.93	1.32	
17-SB-71	Unsaturated Dacite tuff	27.02	50.21	0.54	
17-SB-34	Saturated River sediment	179.47	110.97	1.62	
17-SB-34	Unsaturated River sediment	124.27	120.82	1.03	

APPENDIX B: GRAVITY SURVEY DATA TABLE

Station	*UTM Zone 18*		*EGM 96*	*Vertical*	*Absolute*	*Calculated*	*Free-Air*	*Simple Bouguer*	*Free-Air*	*Simple Bouguer*	*Inner Terrain*	*Outer Terrain*	*Complete Bouguer*
Name	Easting [m]	Northing [m]	GPS Height [m]	Precision [m]	Gravity [mGal]	Gravity [mGal]	Correction [mGal]	Gravity Correction [mGal]	Anomaly [mGal]	Anomaly [mGal]	Correction [mGal]	Correction [mGal]	Anomaly [mGal]
17SB001	245236.208	154316.76	1798.593	0.1	977585.716	978035.7373	555.0457998	201.762744	105.0245	-96.7382445	2.53	0.398	-95.2958453
17SB002	245965.789	150316.52	1990.116	0.3	977535.076	978035.5808	614.1497976	223.2474301	113.645037	-109.602393	4.997	0.393	-105.721035
17SB004	286808.819	133331.392	2140.581	0.1	977471.0924	978034.9628	660.5832966	240.1263078	96.7128447	-143.413463	5.552	0.499	-138.870974
17SB005	286287.285	132596.497	2099.025	0.1	977472.8648	978034.9377	647.759115	235.4646347	85.6861987	-149.778436	4.655	0.484	-146.149587
17SB006	285843.427	131814.929	2085.49	0.1	977470.7885	978034.9111	643.582214	233.9463042	79.4596345	-154.48667	4.03	0.481	-151.48609
17SB007	285158.227	131289.549	2080.318	0.1	977467.5054	978034.8933	641.9861348	233.366119	74.5981813	-158.767938	3.72	0.481	-156.077427
17SB008	284241.806	131009.683	2076.989	0.1	977464.9058	978034.8839	640.9588054	232.9926782	70.9807904	-162.011888	3.649	0.478	-159.395412
17SB009	283350.468	130699.237	2074.535	0.1	977463.5217	978034.8734	640.201501	232.7173931	68.8497913	-163.867602	3.618	0.474	-161.286146
17SB010	282510.063	130120.677	2072.274	0.1	977459.7068	978034.854	639.5037564	232.4637584	64.3565846	-168.107174	3.6	0.472	-165.545733
17SB011	281973.949	130409.756	2072.618	0.1	977462.357	978034.8636	639.6099148	232.5023477	67.1032341	-165.399114	3.839	0.467	-162.603671
17SB012	281261.815	131106.365	2075.983	0.1	977467.9864	978034.887	640.6483538	232.879827	73.7477519	-159.132075	4.541	0.46	-155.641608
17SB013	280461.224	131085.827	2081.747	0.1	977468.4675	978034.8863	642.4271242	233.5264215	76.0083137	-157.518108	5.231	0.459	-153.33858
17SB014	279859.791	131677.658	2134.986	0.4	977459.0654	978034.9063	658.8566796	239.4986714	83.0157333	-156.482938	6.266	0.466	-151.259741
17SB015	279635.439	130900.56	2082.096	0.5	977467.5054	978034.8801	642.5348256	233.5655717	75.1601142	-158.405458	6.932	0.455	-152.528926
17SB016	279146.019	130170.93	2090.931	0.3	977463.4457	978034.8556	645.2613066	234.5566652	73.8514529	-160.705212	7.274	0.46	-154.48154
17SB017	278432.329	129409.713	2093.849	0.1	977461.3864	978034.8302	646.1618014	234.8840009	72.7180047	-162.165996	6.296	0.46	-156.920266
17SB018	277963.919	128630.133	2089.855	0.3	977460.9475	978034.8043	644.929253	234.4359616	71.0724456	-163.363516	7.854	0.463	-156.556864
17SB019	277579.127	127995.797	2086.254	0.4	977460.6605	978034.7834	643.8179844	234.0320082	69.6951512	-164.336857	7.722	0.462	-157.663266
17SB020	277144.203	127132.773	2108.184	0.1	977453.5287	978034.755	650.5855824	236.492074	69.3592623	-167.132812	7.129	0.472	-161.041706
17SB021	277368.332	126387.519	2096.666	0.1	977459.8756	978034.7308	647.0311276	235.2000066	72.1759691	-163.024038	5.511	0.475	-158.548245
17SB022	278154.013	126453.27	2081.743	0.1	977461.3188	978034.7329	642.4258898	233.5259728	69.0118166	-164.514156	4.781	0.475	-160.768629
17SB023	279073.836	126748.205	2074.386	0.9	977457.6728	978034.7425	640.1555196	232.7006786	63.085746	-169.614933	4.234	0.476	-166.415478
17SB024	279867.221	126218.405	2071.469	0.5	977454.7188	978034.7253	639.2553334	232.373455	59.2487701	-173.124685	4.08	0.483	-170.072248
17SB025	280391.74	125451.7	2067.478	0.1	977455.9594	978034.7005	638.0237108	231.9257523	59.2826202	-172.643132	3.93	0.491	-169.732711
17SB026	280527.259	126182.996	2068.532	0.1	977451.5791	978034.7242	638.3489752	232.043988	55.2038661	-176.840122	3.733	0.487	-174.130698
17SB027	280757.2	126853.742	2068.155	0.1	977449.4016	978034.746	638.232633	232.0016968	52.888181	-179.113516	3.614	0.484	-176.526093

17SB028	281024.158	127502.352	2070.863	0.5	977449.7476	978034.7672	639.0683218	232.3054751	54.048696	-178.256779	4.097	0.483	-175.187346
17SB029	285652.869	131300.57	2082.266	0.1	977468.6785	978034.8937	642.5872876	233.584642	76.3721104	-157.212532	3.768	0.483	-154.471997
17SB030	285300.634	130327.444	2080.332	0.6	977463.9268	978034.861	641.9904552	233.3676895	71.0562956	-162.311394	3.489	0.488	-159.844883
17SB031	284949.216	129365.435	2075.47	0.1	977459.116	978034.8288	640.490042	232.8222796	64.7772066	-168.045073	3.365	0.492	-165.69861
17SB032	284116.681	129036.996	2075.267	0.1	977454.8538	978034.8179	640.4273962	232.7995075	60.46329	-172.336217	3.307	0.489	-170.050756
17SB033	283234.768	128660.844	2072.158	0.1	977452.3978	978034.8054	639.4679588	232.4507458	57.0602938	-175.390452	3.278	0.487	-173.136012
17SB034	282334.912	128464.933	2070.262	0.1	977451.5116	978034.7989	638.8828532	232.2380561	55.5954844	-176.642572	3.36	0.482	-174.311141
17SB035	281581.289	127999.528	2069.346	0.1	977450.7013	978034.7836	638.6001756	232.1353009	54.5179276	-177.617373	3.455	0.48	-175.192946
17SB036	281141.044	127002.453	2068.636	0.1	977448.8276	978034.7509	638.3810696	232.0556545	52.4578361	-179.597818	3.528	0.486	-177.094394
17SB037	277265.307	126678.101	2096.385	0.1	977457.7318	978034.7402	646.944411	235.1684846	69.9360422	-165.232442	5.736	0.472	-160.534656
17SB038	278738.161	126363.569	2086.055	0.2	977459.9347	978034.73	643.756573	234.0096848	68.9612417	-165.048443	4.368	0.479	-161.711855
17SB039	278506.085	125608.673	2095.953	0.5	977460.6521	978034.7056	646.8110958	235.1200236	72.7576209	-162.362403	4.474	0.486	-158.912626
17SB040	278578.46	124530.649	2084.813	0.1	977466.3069	978034.6709	643.3732918	233.8703596	75.0092788	-158.861081	6.13	0.492	-153.749512
17SB041	279179.066	123953.586	2083.872	0.1	977472.7719	978034.6525	643.0828992	233.7648	81.2023457	-152.562454	5.276	0.501	-148.295899
17SB042	279857.033	123429.841	2070.264	0.1	977476.494	978034.6358	638.8834704	232.2382804	80.7415979	-151.496683	5.676	0.505	-146.826252
17SB043	280735.214	123559.122	2072.05	0.5	977475.574	978034.64	639.43463	232.4386305	80.368674	-152.069957	6.23	0.511	-146.839517
17SB044	282494.419	124116.215	2077.195	0.1	977474.806	978034.6577	641.022377	233.0157868	81.1706062	-151.845181	6.407	0.517	-146.431703
17SB045	283360.333	124660.083	2077.219	0.1	977475.2533	978034.6751	641.0297834	233.0184791	81.6079206	-151.410559	5.954	0.521	-146.44608
17SB046	283945.742	124702.236	2084.119	0.1	977475.4812	978034.6765	643.1591234	233.792508	83.9637768	-149.828731	7.637	0.525	-143.177172
17SB047	284629.385	125317.694	2083.477	0.1	977472.6453	978034.6963	642.9610022	233.7204897	80.9100194	-152.81047	6.253	0.522	-147.54592
17SB048	285462.262	125712.859	2080.537	0.1	977474.7131	978034.7091	642.0537182	233.390686	82.0577649	-151.332921	7.188	0.52	-145.135408
17SB049	285626.958	126595.487	2083.643	0.1	977465.792	978034.7377	643.0122298	233.7391112	74.0665642	-159.672547	6.94	0.516	-153.726995
17SB050	286035.261	127401.455	2083.37	0.1	977464.104	978034.764	642.927982	233.7084866	72.2679903	-161.440496	4.355	0.51	-158.085948
17SB051	286809.552	133330.952	2140.511	0.1	977471.0924	978034.9628	660.5616946	240.1184554	96.6912577	-143.427198	5.55	0.499	-138.886713
17SB052	286020.061	133278.088	2112.804	0.1	977473.5315	978034.961	652.0113144	237.0103368	90.5818684	-146.428468	5.328	0.483	-142.127211
17SB053	285027.06	133422.27	2101.408	0.1	977476.0466	978034.9659	648.4945088	235.7319552	89.5752637	-146.156692	6.039	0.476	-141.151781
17SB054	284542.153	133504.352	2112.827	0.1	977474.232	978034.9687	652.0184122	237.0129169	91.2817624	-145.731155	5.858	0.476	-140.906896
17SB055	284189.95	133809.806	2118.23	0.1	977474.4768	978034.9792	653.685778	237.6190151	93.1834004	-144.435615	5.715	0.473	-139.75716
17SB056	283744.016	133940.441	2112.693	0.1	977474.5021	978034.9837	651.9770598	236.997885	91.4955169	-145.502368	6.051	0.469	-140.492115
17SB057	283362.188	133597.244	2100.778	0.1	977476.764	978034.9719	648.3000908	235.661283	90.0922804	-145.569003	6.867	0.465	-139.747109
17SB058	282661.122	133006.079	2098.67	0.1	977474.6625	978034.9516	647.649562	235.4248115	87.3604689	-148.064343	5.309	0.465	-143.800502

17SB059	281782.287	132616.755	2100.368	0.1	977471.3287	978034.9383	648.1735648	235.6152899	84.5639867	-151.051303	5.385	0.462	-146.71442
17SB060	280879.641	132175.685	2095.012	0.1	977468.8895	978034.9232	646.5207032	235.014464	80.4870004	-154.527464	5.972	0.457	-149.608708
17SB061	280209.273	131477.856	2107.883	0.2	977464.7202	978034.8996	650.4926938	236.4583084	80.3132978	-156.145011	5.646	0.461	-151.547915
17SB062	280771.373	130747.581	2072.273	0.9	977466.4166	978034.875	639.5034478	232.4636462	71.0450945	-161.418552	4.691	0.46	-157.778111
17SB063	280781.759	130062.564	2069.28	0.1	977460.7196	978034.852	638.579808	232.1278972	64.4474206	-167.680477	4.269	0.463	-164.45905
17SB064	281083.777	129819.04	2068.677	0.1	977458.829	978034.8439	638.3937222	232.0602538	62.3789031	-169.681351	4.005	0.467	-166.719926
17SB065	280669.084	130388.231	2071.077	0.1	977463.8086	978034.8629	639.1343622	232.3294812	68.080114	-164.249367	4.511	0.46	-160.788933
17SB066	279445.71	129923.755	2074.555	0.1	977465.8764	978034.8473	640.207673	232.7196367	71.2367962	-161.482841	5.38	0.458	-157.155384
17SB067	279967.67	129428.121	2067.858	0.1	977461.3779	978034.8308	638.1409788	231.9683799	64.6880934	-167.280287	4.517	0.462	-163.811864
17SB068	286668.496	133287.632	2131.936	0.2	977472.0208	978034.9613	657.9154496	239.1565282	94.9749009	-144.181627	5.466	0.494	-139.73058
17SB069	276474.813	126538.621	2189.819	0.1	977439.1892	978034.7357	675.7781434	245.6497331	80.2316526	-165.418081	5.151	0.498	-161.274065
17SB073	288509.464	131775.737	2116.826	0.1	977473.7341	978034.9098	653.2525036	237.4615171	92.0767494	-145.384768	4.961	0.504	-141.429366
17SB074	292068.813	129777.419	2195.901	0.3	977461.9096	978034.8427	677.6550486	246.3320003	104.721967	-141.610033	7.548	0.564	-135.002463
17SB075	292727.233	129377.693	2292.799	0.1	977441.4342	978034.8294	707.5577714	257.2018337	114.162553	-143.039281	8.408	0.62	-135.503336
17SB076	293225.6	128499.002	2382.412	0.1	977424.934	978034.8003	735.2123432	267.2544498	125.346046	-141.908404	8.269	0.679	-134.435095
17SB077	293630.009	127811.416	2509.128	1.4	977402.7621	978034.7776	774.3169008	281.4692098	142.301373	-139.167837	7.212	0.77	-132.626266
17SB078	293335.682	127670.891	2564.492	0.1	977389.7223	978034.773	791.4022312	287.6798381	146.351525	-141.328313	7.027	0.809	-134.914202
17SB079	293557.909	126664.726	2677.56	0.1	977369.787	978034.7401	826.295016	300.3635914	161.341926	-139.021666	6.469	0.907	-133.022948
17SB080	294433.155	126552.751	2767.169	0.4	977353.5232	978034.7365	853.9483534	310.4157587	172.73501	-137.680749	7.119	0.994	-130.903249
17SB081	294374.013	125513.935	2668.18	0.2	977374.4712	978034.7028	823.400348	299.3113608	163.168752	-136.142609	8.376	0.92	-128.227937
17SB083	294876.169	125090.078	2572.786	0.1	977393.0814	978034.6892	793.9617596	288.6102432	152.354009	-136.256234	9.607	0.852	-127.216159
17SB085	295129.456	124610.089	2504.118	0.2	977408.0793	978034.6738	772.7708148	280.9071975	146.176349	-134.730849	10.441	0.805	-124.926848
17SB086	295708.823	123337.796	2371.791	0.2	977434.294	978034.6332	731.9347026	266.0630062	131.595424	-134.467582	15.543	0.727	-119.674629
17SB087	295803.91	122895.261	2283.008	0.8	977450.7435	978034.6192	704.5362688	256.103498	120.660558	-135.44294	16.139	0.679	-120.118548
17SB088	295480.424	121611.774	2150.43	0.1	977475.2448	978034.5789	663.622698	241.2311499	104.288662	-136.942488	21.907	0.615	-115.928431
17SB089	295564.791	120538.717	2169.481	0.1	977477.2536	978034.5455	669.5018366	243.3682549	112.209928	-131.158327	14.463	0.628	-117.573977
17SB090	296151.035	119757.044	2204.75	0.1	977472.7804	978034.5213	680.38585	247.3246643	118.64488	-128.679784	21.336	0.654	-108.19336
17SB091	297356.134	119727.623	2098.582	0.2	977491.0952	978034.5204	647.6224052	235.4149399	104.197119	-131.217821	15.977	0.609	-116.141983
17SB092	298605.2	119447.264	1981.877	0.2	977511.2921	978034.5118	611.6072422	222.3231948	88.3874748	-133.93572	17.787	0.567	-117.089906
17SB093	299518.294	119328.86	1897.366	0.7	977527.7416	978034.5082	585.5271476	212.8429114	78.7605586	-134.082353	20.407	0.539	-114.637083
17SB094	300233.206	119056.505	1874.232	0.2	977532.6622	978034.4999	578.3879952	210.2477833	76.5502613	-133.697522	18.251	0.537	-116.407329

17SB095	301159.584	118627.501	1850.773	0.5	977539.9796	978034.4868	571.1485478	207.6161973	76.6413883	-130.974809	14.651	0.531	-117.287264
17SB096	302093.297	117944.378	1981.562	0.3	977511.0726	978034.466	611.5100332	222.2878587	88.1166369	-134.171222	17.602	0.576	-117.50139
17SB097	303021.672	118176.698	2119.908	0.5	977482.5708	978034.4731	654.2036088	237.80725	102.301263	-135.505987	19.15	0.644	-117.221467
17SB098	304307.949	118575.162	2198.167	0.7	977468.0371	978034.4853	678.3543362	246.5861959	111.906157	-134.680039	25.57	0.685	-109.929255
17SB099	305438.447	118636.328	2263.305	0.9	977453.8748	978034.4871	698.455923	253.8932529	117.843539	-136.049714	25.099	0.726	-111.72124
17SB100	306700.702	118242.897	2110.926	0.1	977477.8444	978034.4752	651.4317636	236.7996663	94.8009412	-141.998725	28.568	0.648	-114.292531

The measurements of the base stations are the following: 17SB001, 17SB002 and 17SB004.

APPENDIX C: APPLICATION OF REGIONAL CORRECTION

					Regional Correction	
Stations	**X**	**Y**	**Z**	**CBA on grid**	**G=0.001*X - 163.01**	**CBA- G**
17SB001.cor	245236.208	154316.76	1798.593	-95.29584531	82.226208	-13.0696373
17SB002.cor	245965.789	150316.52	1990.116	-105.7210351	82.955789	-22.7652461
17SB004.cor	286808.819	133331.39	2140.581	-138.8709743	123.798819	-15.0721553
17SB005.cor	286287.285	132596.5	2099.025	-146.1495869	123.277285	-22.8723019
17SB006.cor	285843.427	131814.93	2085.49	-151.4860904	122.833427	-28.6526634
17SB007.cor	285158.227	131289.55	2080.318	-156.0774273	122.148227	-33.9292003
17SB008.cor	284241.806	131009.68	2076.989	-159.3954117	121.231806	-38.1636057
17SB009.cor	283350.468	130699.24	2074.535	-161.2861459	120.340468	-40.9456779
17SB010.cor	282510.063	130120.68	2072.274	-165.5457328	119.500063	-46.0456698
17SB011.cor	281973.949	130409.76	2072.618	-162.6036706	118.963949	-43.6397216
17SB012.cor	281261.815	131106.37	2075.983	-155.6416078	118.251815	-37.3897928
17SB013.cor	280461.224	131085.83	2081.747	-153.3385803	117.451224	-35.8873563
17SB014.cor	279859.791	131677.66	2134.986	-151.2597412	116.849791	-34.4099502
17SB015B.cor	279635.439	130900.56	2082.096	-152.5289256	116.625439	-35.9034866
17SB016.cor	279146.019	130170.93	2090.931	-154.4815402	116.136019	-38.3455212
17SB017.cor	278432.329	129409.71	2093.849	-156.9202656	115.422329	-41.4979366
17SB018.cor	277963.919	128630.13	2089.855	-156.5568639	114.953919	-41.6029449
17SB019.cor	277579.127	127995.8	2086.254	-157.663266	114.569127	-43.094139
17SB020.cor	277144.203	127132.77	2108.184	-161.0417062	114.134203	-46.9075032
17SB021.cor	277368.332	126387.52	2096.666	-158.5482447	114.358332	-44.1899127
17SB022.cor	278154.013	126453.27	2081.743	-160.7686288	115.144013	-45.6246158
17SB023.cor	279073.836	126748.21	2074.386	-166.4154778	116.063836	-50.3516418
17SB024.cor	279867.221	126218.41	2071.469	-170.0722484	116.857221	-53.2150274
17SB025.cor	280391.74	125451.7	2067.478	-169.7327106	117.38174	-52.3509706
17SB026.cor	280527.259	126183	2068.532	-174.1306975	117.517259	-56.6134385
17SB027.cor	280757.2	126853.74	2068.155	-176.5260927	117.7472	-58.7788927

17SB028.cor	281024.158	127502.35	2070.863	-175.1873456	118.014158	-57.1731876
17SB029.cor	285652.869	131300.57	2082.266	-154.4719974	122.642869	-31.8291284
17SB030.cor	285300.634	130327.44	2080.332	-159.8448834	122.290634	-37.5542494
17SB031.cor	284949.216	129365.44	2075.47	-165.69861	121.939216	-43.759394
17SB032.cor	284116.681	129037	2075.267	-170.050756	121.106681	-48.944075
17SB033.cor	283234.768	128660.84	2072.158	-173.1360117	120.224768	-52.9112437
17SB034.cor	282334.912	128464.93	2070.262	-174.3111409	119.324912	-54.9862289
17SB035.cor	281581.289	127999.53	2069.346	-175.1929462	118.571289	-56.6216572
17SB036.cor	281141.044	127002.45	2068.636	-177.0943938	118.131044	-58.9633498
17SB037.cor	277265.307	126678.1	2096.385	-160.5346561	114.255307	-46.2793491
17SB038.cor	278738.161	126363.57	2086.055	-161.7118551	115.728161	-45.9836941
17SB039.cor	278506.085	125608.67	2095.953	-158.9126262	115.496085	-43.4165412
17SB040.cor	278578.46	124530.65	2084.813	-153.7495117	115.56846	-38.1810517
17SB041.cor	279179.066	123953.59	2083.872	-148.2958986	116.169066	-32.1268326
17SB042.cor	279857.033	123429.84	2070.264	-146.8262517	116.847033	-29.9792187
17SB043.cor	280735.214	123559.12	2072.05	-146.8395168	117.725214	-29.1143028
17SB044.cor	282494.419	124116.22	2077.195	-146.4317027	119.484419	-26.9472837
17SB045.cor	283360.333	124660.08	2077.219	-146.4460803	120.350333	-26.0957473
17SB046.cor	283945.742	124702.24	2084.119	-143.177172	120.935742	-22.24143
17SB047.cor	284629.385	125317.69	2083.477	-147.5459201	121.619385	-25.9265351
17SB048.cor	285462.262	125712.86	2080.537	-145.1354082	122.452262	-22.6831462
17SB049.cor	285626.958	126595.49	2083.643	-153.7269945	122.616958	-31.1100365
17SB050.cor	286035.261	127401.46	2083.37	-158.0859476	123.025261	-35.0606866
17SB051.cor	286809.552	133330.95	2140.511	-138.8867125	123.799552	-15.0871605
17SB052.cor	286020.061	133278.09	2112.804	-142.1272111	123.010061	-19.1171501
17SB053.cor	285027.06	133422.27	2101.408	-141.1517814	122.01706	-19.1347214
17SB054.cor	284542.153	133504.35	2112.827	-140.9068964	121.532153	-19.3747434
17SB055.cor	284189.95	133809.81	2118.23	-139.7571598	121.17995	-18.5772098
17SB056.cor	283744.016	133940.44	2112.693	-140.4921147	120.734016	-19.7580987
17SB057.cor	283362.188	133597.24	2100.778	-139.7471089	120.352188	-19.3949209

17SB058.cor	282661.122	133006.08	2098.67	-143.8005022	119.651122	-24.1493802
17SB059.cor	281782.287	132616.76	2100.368	-146.7144202	118.772287	-27.9421332
17SB060.cor	280879.641	132175.69	2095.012	-149.608708	117.869641	-31.739067
17SB061.cor	280209.273	131477.86	2107.883	-151.5479145	117.199273	-34.3486415
17SB062.cor	280771.373	130747.58	2072.273	-157.7781108	117.761373	-40.0167378
17SB063.cor	280781.759	130062.56	2069.28	-164.4590498	117.771759	-46.6872908
17SB064.cor	281083.777	129819.04	2068.677	-166.719926	118.073777	-48.646149
17SB065.cor	280669.084	130388.23	2071.077	-160.7889326	117.659084	-43.1298486
17SB066.cor	279445.71	129923.76	2074.555	-157.1553844	116.43571	-40.7196744
17SB067.cor	279967.67	129428.12	2067.858	-163.8118641	116.95767	-46.8541941
17SB068.cor	286668.496	133287.63	2131.936	-139.7305803	123.658496	-16.0720843
17SB069.cor	276474.813	126538.62	2189.819	-161.274065	113.464813	-47.809252
17SB073.cor	288509.464	131775.74	2116.826	-141.4293659	125.499464	-15.9299019
17SB074.cor	292068.813	129777.42	2195.901	-135.0024629	129.058813	-5.9436499
17SB075.cor	292727.233	129377.69	2292.799	-135.5033361	129.717233	-5.7861031
17SB076.cor	293225.6	128499	2382.412	-134.4350952	130.2156	-4.2194952
17SB077B.cor	293630.009	127811.42	2509.128	-132.6262662	130.620009	-2.0062572
17SB078.cor	293335.682	127670.89	2564.492	-134.9142023	130.325682	-4.5885203
17SB079.cor	293557.909	126664.73	2677.56	-133.0229484	130.547909	-2.4750394
17SB080.cor	294433.155	126552.75	2767.169	-130.903249	131.423155	0.519906
17SB081.cor	294374.013	125513.94	2668.18	-128.2279369	131.364013	3.1360761
17SB083.cor	294876.169	125090.08	2572.786	-127.2161589	131.866169	4.6500101
17SB085.cor	295129.456	124610.09	2504.118	-124.9268483	132.119456	7.1926077
17SB086.cor	295708.823	123337.8	2371.791	-119.6746286	132.698823	13.0241944
17SB087.cor	295803.91	122895.26	2283.008	-120.1185475	132.79391	12.6753625
17SB088.cor	295480.424	121611.77	2150.43	-115.9284306	132.470424	16.5419934
17SB089.cor	295564.791	120538.72	2169.481	-117.5739765	132.554791	14.9808145
17SB090.cor	296151.035	119757.04	2204.75	-108.1933596	133.141035	24.9476754
17SB091.cor	297356.134	119727.62	2098.582	-116.1419825	134.346134	18.2041515
17SB092.cor	298605.2	119447.26	1981.877	-117.0899063	135.5952	18.5052937

17SB093.cor	299518.294	119328.86	1897.366	-114.6370831	136.508294	21.8712109
17SB094.cor	300233.206	119056.51	1874.232	-116.4073289	137.223206	20.8158771
17SB095.cor	301159.584	118627.5	1850.773	-117.2872641	138.149584	20.8623199
17SB096.cor	302093.297	117944.38	1981.562	-117.5013896	139.083297	21.5819074
17SB097.cor	303021.672	118176.7	2119.908	-117.221467	140.011672	22.790205
17SB098.cor	304307.949	118575.16	2198.167	-109.9292547	141.297949	31.3686943
17SB099.cor	305438.447	118636.33	2263.305	-111.7212404	142.428447	30.7072066
17SB100.cor	306700.702	118242.9	2110.926	-114.2925314	143.690702	29.3981706

APPENDIX D: FREE AIR AND SIMPLE BOUGUER ANOMALY MAP

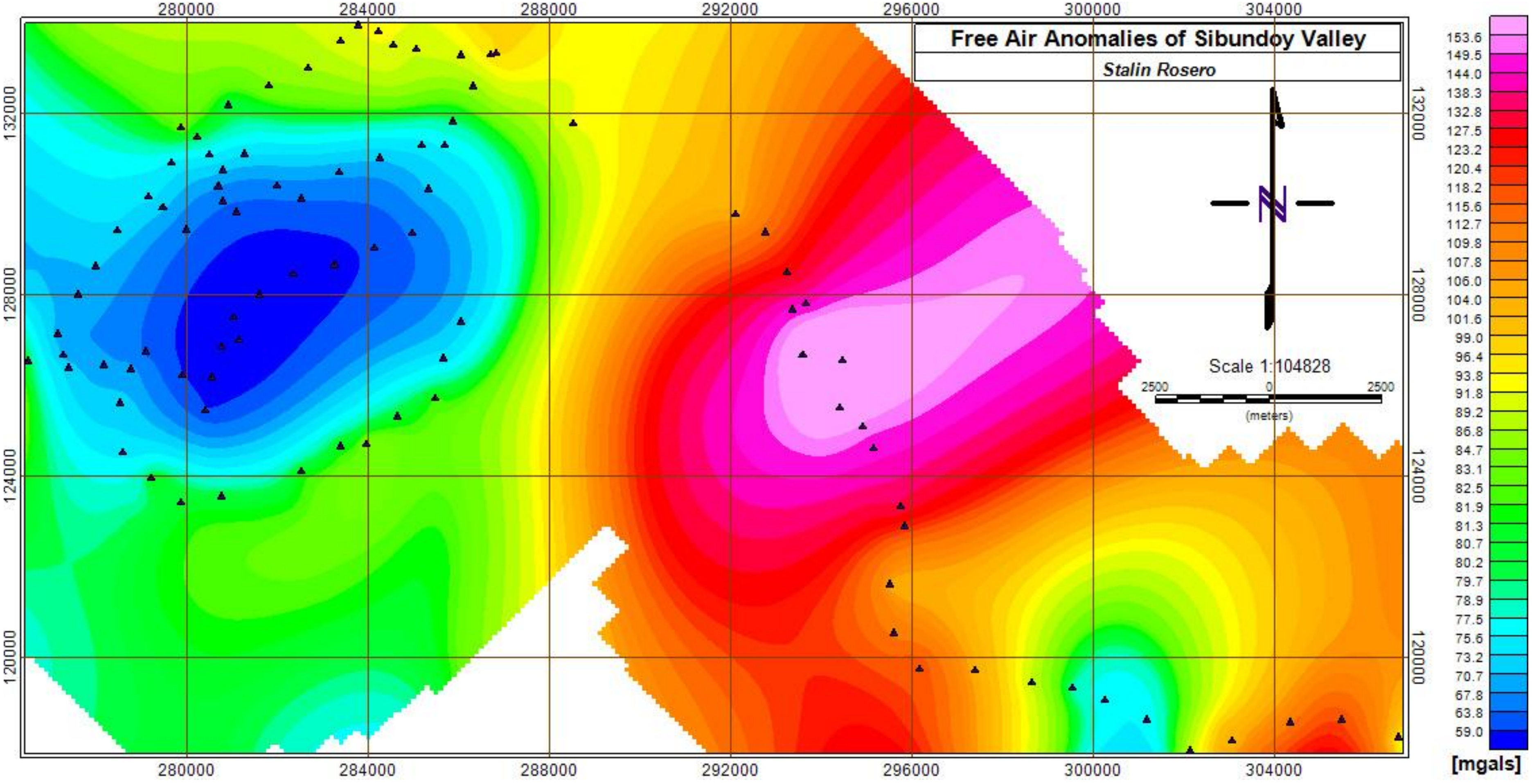

Figure 32 Free air Anomaly map of the Sibundoy Valley.

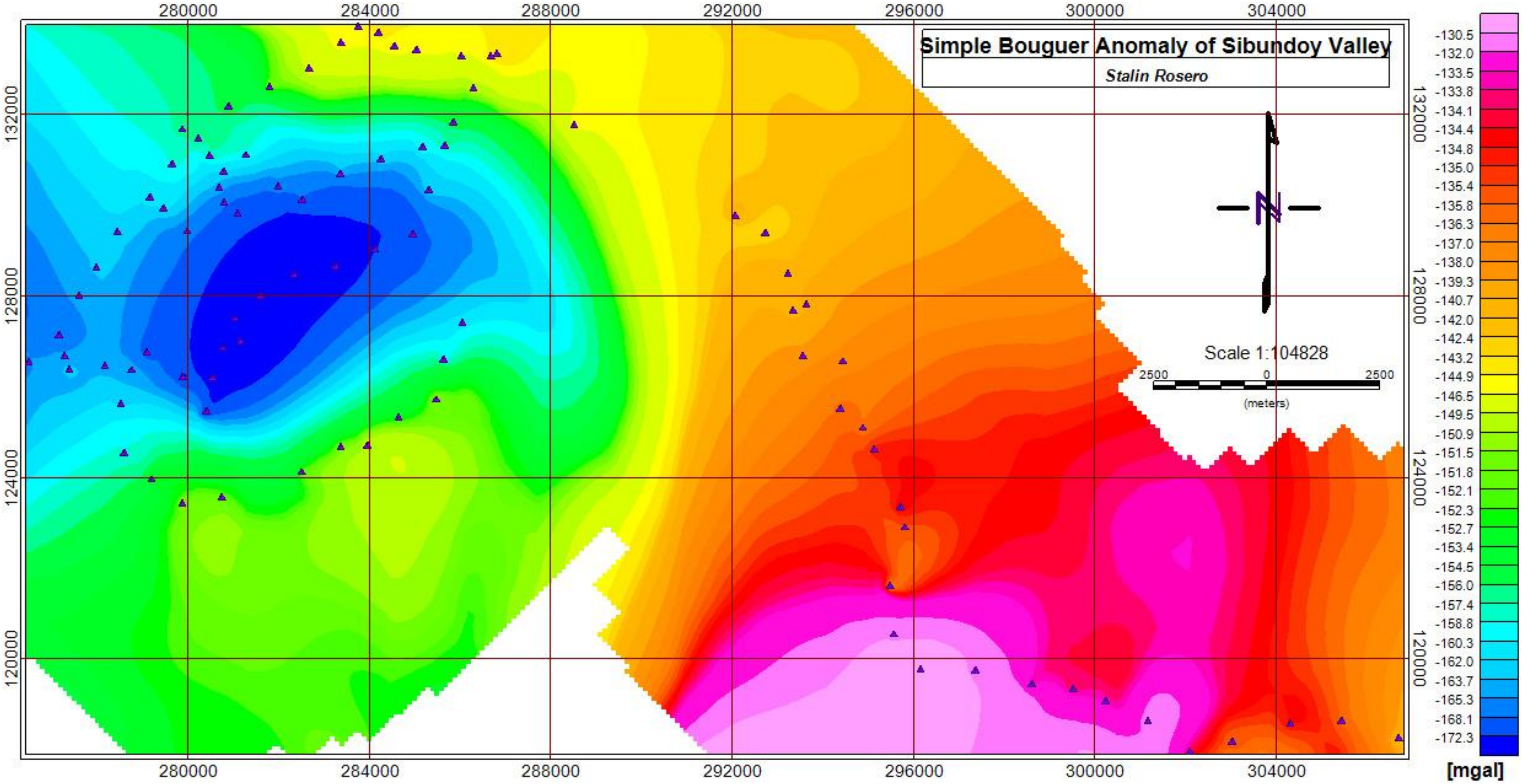

Figure 33 Simple Bouguer Anomaly of the Sibundoy Valley.

APPENDIX E: GRAVITY MODELS

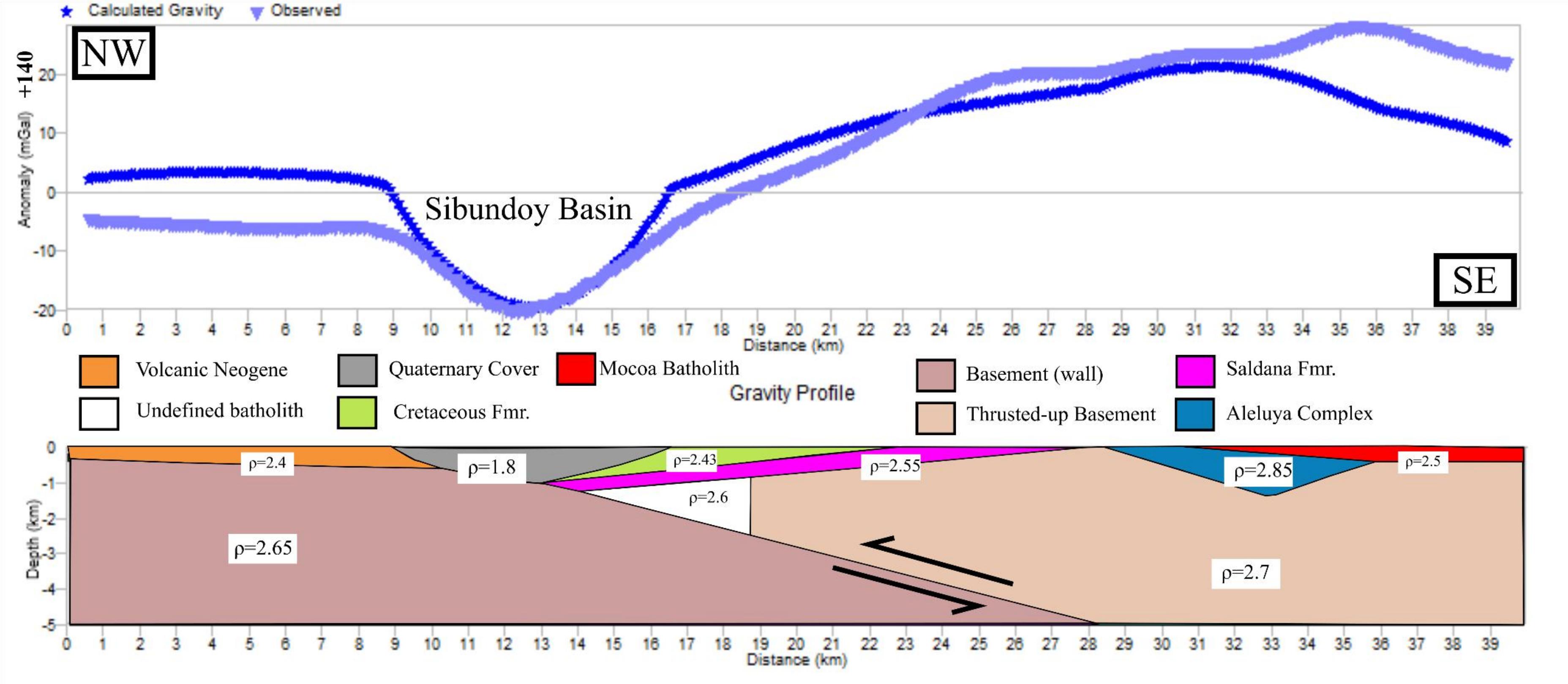

Figure 34 Model 1a shows the Complete Bouguer Anomaly values along a transect from point A to point B that overlays the northern part of the Sibundoy Valley with a NW to SE trend. The transect is approximately 39 km long. The calculated density measurements and the geology map were used to constrain this model, considering that the average of the basin infill is 1.8 g/cm^3. The geometries were changed until the calculated gravity best matches the observed gravity.

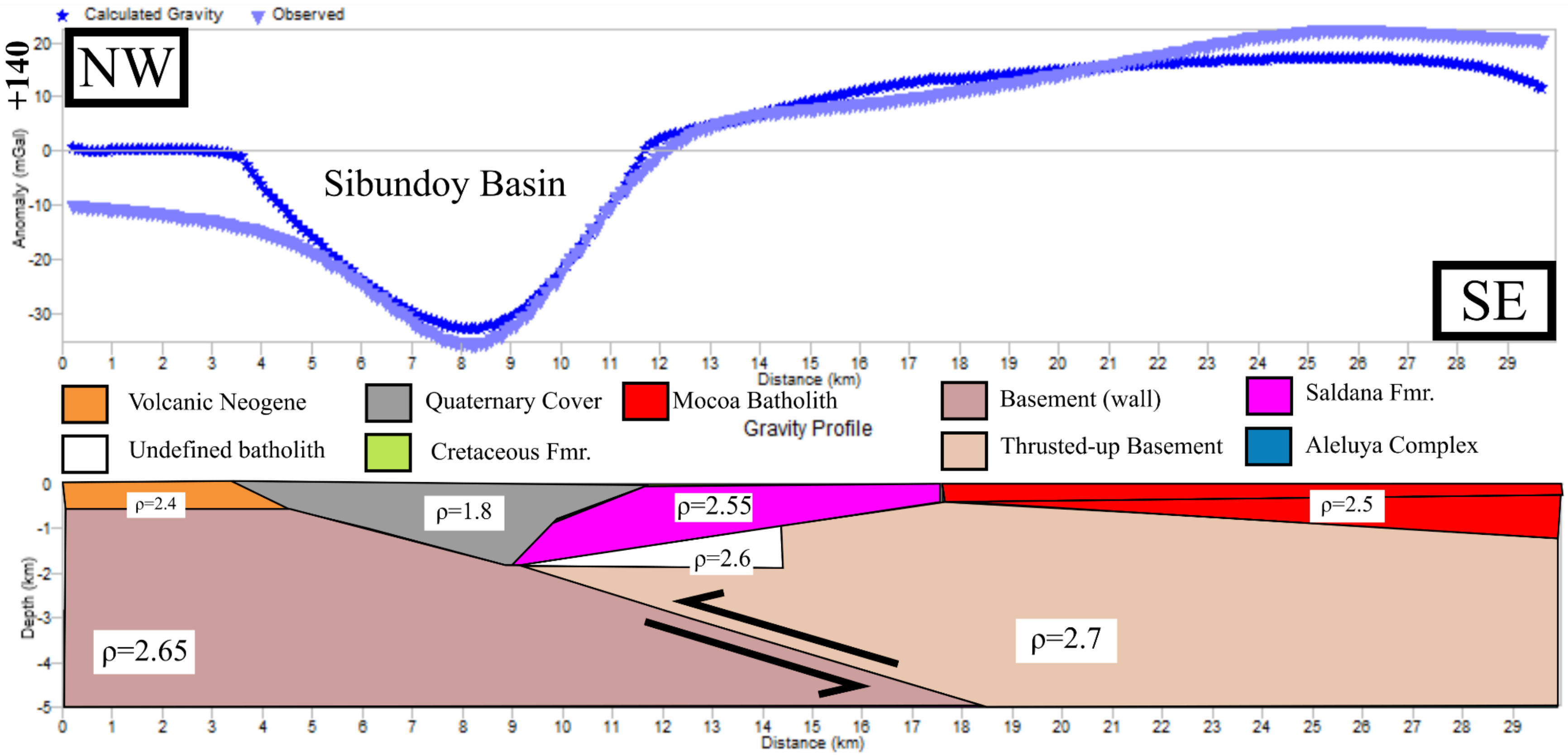

Figure 35 Model 3a shows the Complete Bouguer Anomaly values along a transect from E and F that overlays the southern part of the Sibundoy Valley with a NW to SE trend. The transect is approximately 29 km long. The calculated density measurements and the geology map were used to constrain this model, considering that the average of the basin infill is 1.8 g/cm3. The geometries were changed until the calculated gravity best matches the observed gravity.

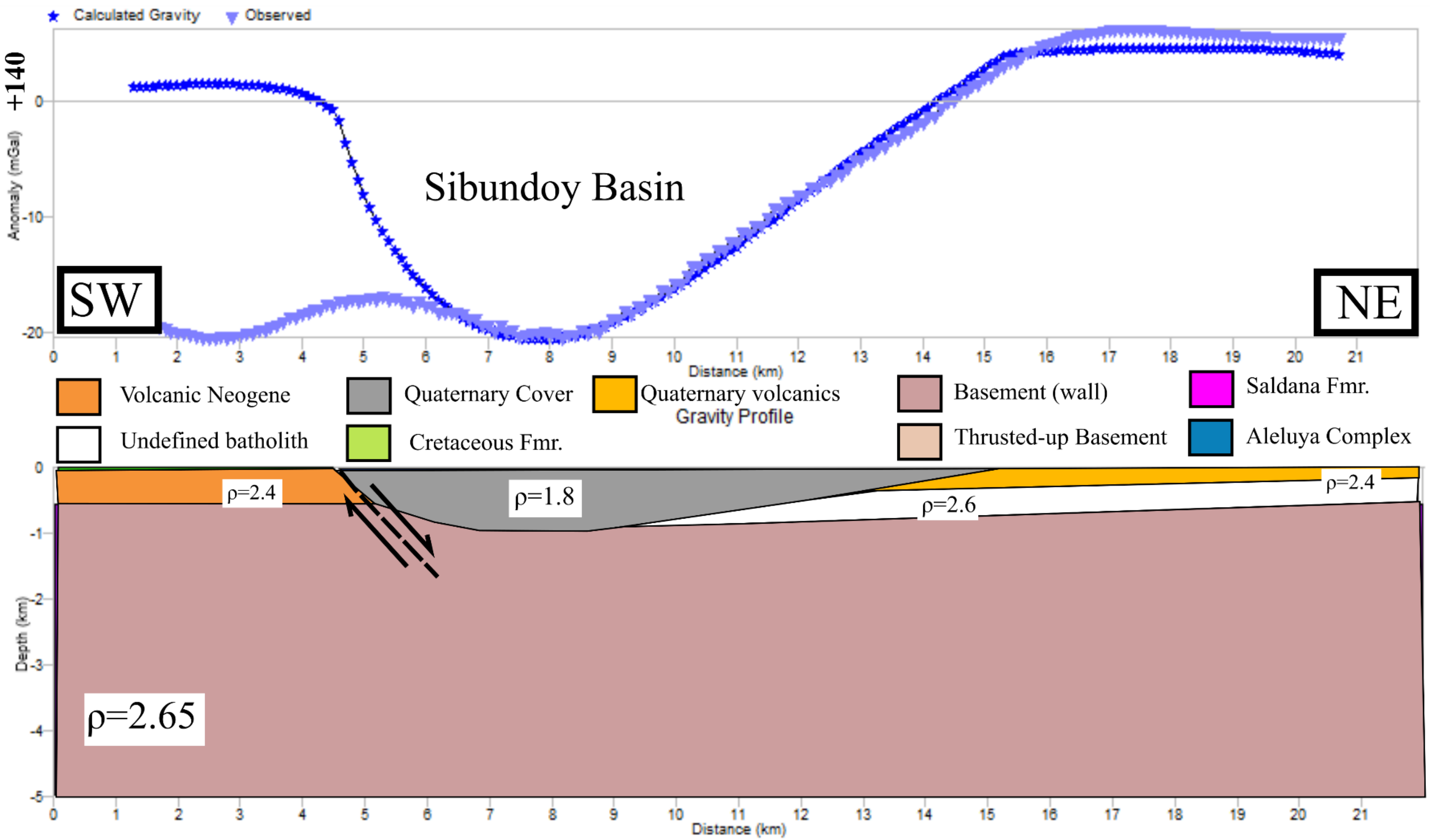

Figure 36 Model 4a shows the Complete Bouguer Anomaly values along a transect from G and H that overlays the western part of the Sibundoy Valley with a SW to NE trend. The transect is approximately 21 km long. The calculated density measurements and the geology map were used to constrain this model, considering that the average of the basin infill is 1.8 g/cm^3. The geometries were changed until the calculated gravity best matches the observed gravity.

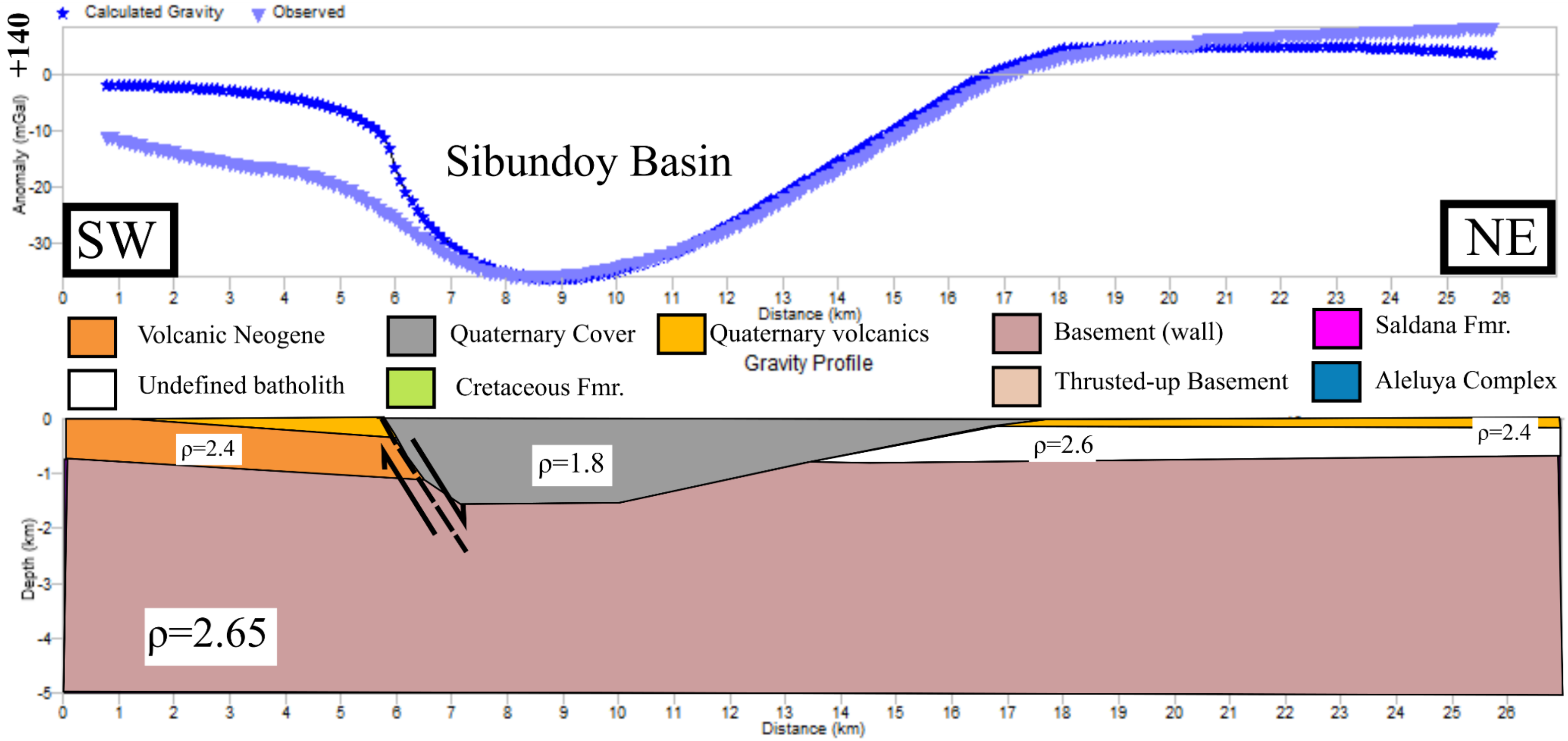

Figure 37 Model 5a shows the Complete Bouguer Anomaly values along a transect from point I and J that overlays the central part of the Sibundoy Valley with a SW to NE trend. The transect is approximately 26 km long. The calculated density measurements and the geology map were used to constrain this model, considering that the average of the basin infill is 1.8 g/cm^3. The geometries were changed until the calculated gravity best matches the observed gravity.

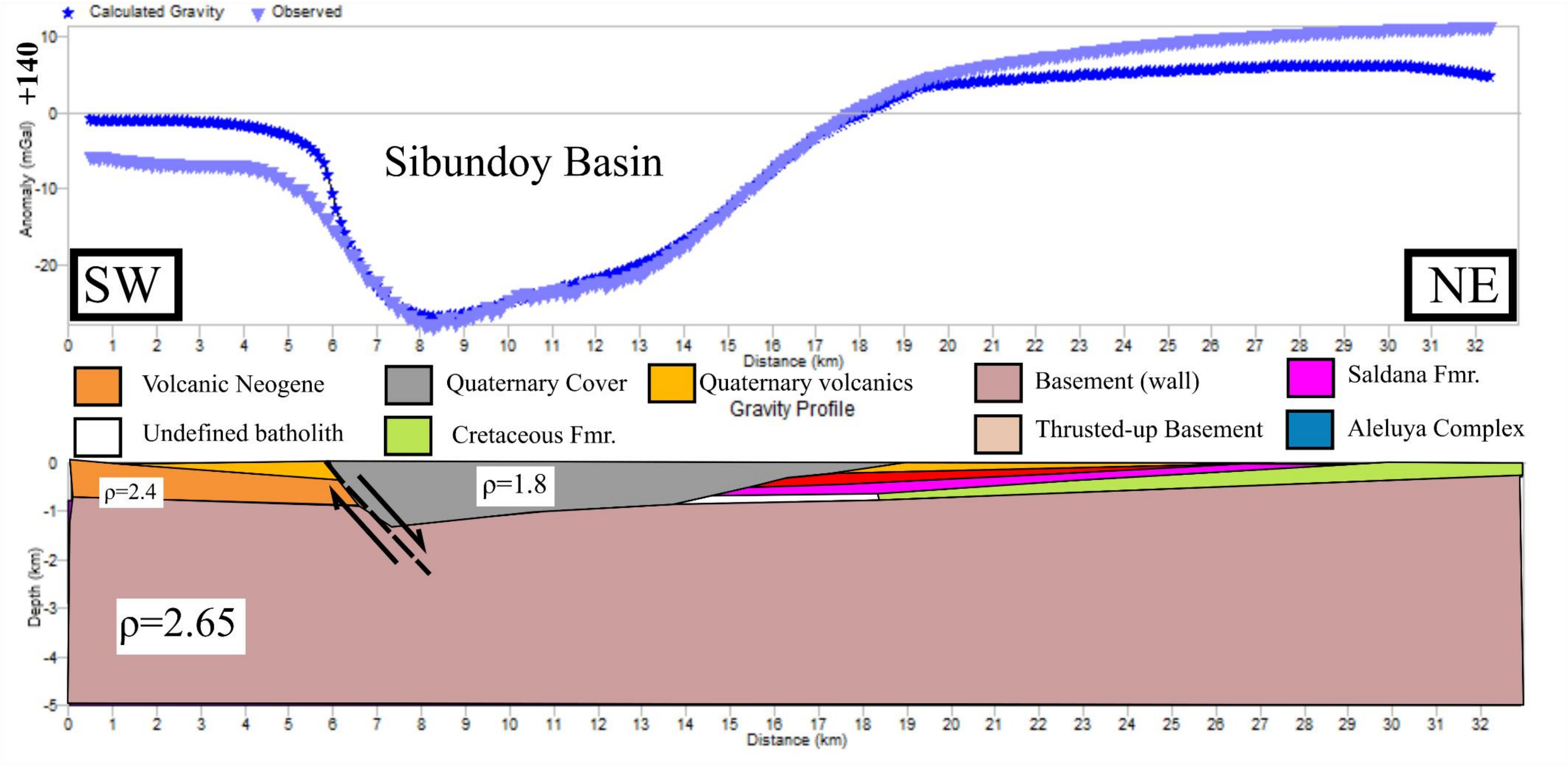

Figure 38 Model 6a shows the Complete Bouguer Anomaly values along a transect from point K and L that overlays the eastern part of the Sibundoy Valley with a SW to NE trend. The transect is approximately 32 km long. The calculated density measurements and the geology map were used to constrain this model, considering that the average of the basin infill is 1.8 g/cm^3. The geometries were changed until the calculated gravity best matches the observed gravity.

Models considering that the basin infill is 1.8 g/cm^3. Removal of regional trend.

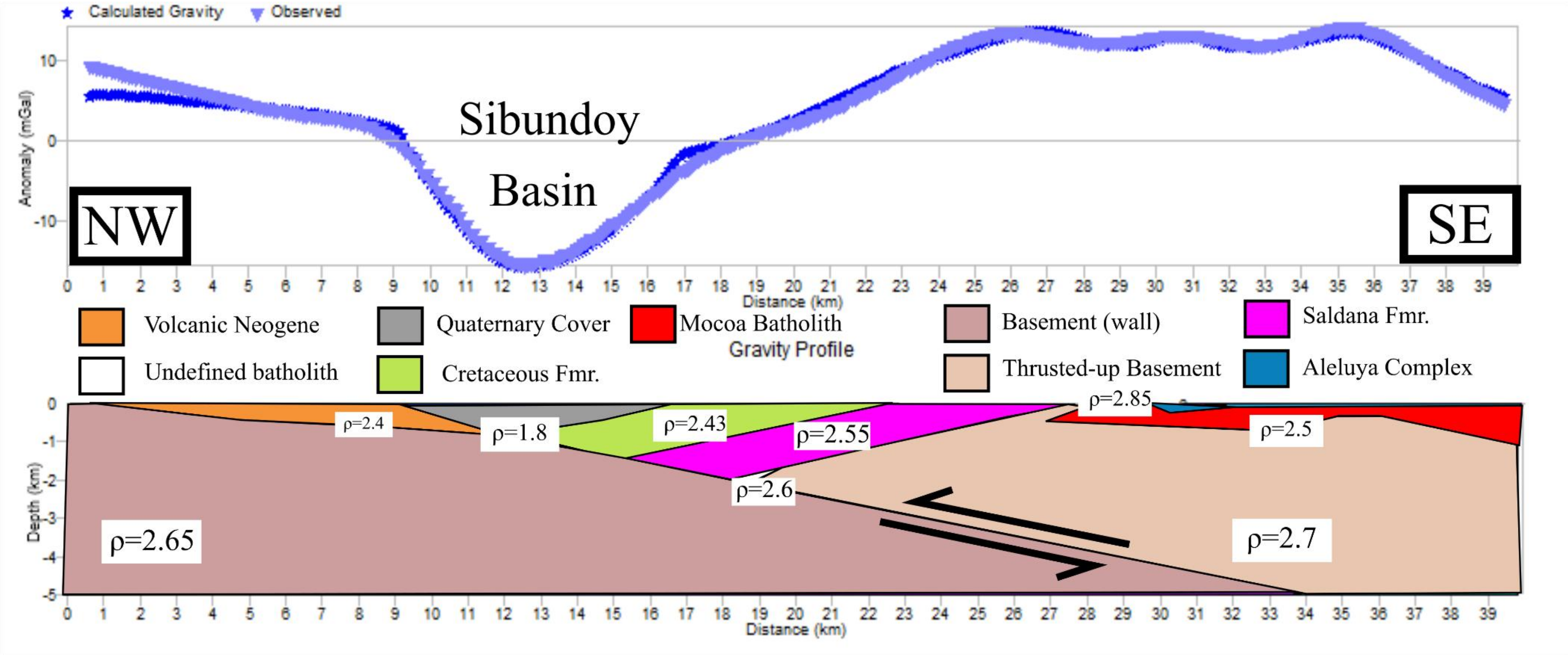

Figure 39 Model 1b shows the Complete Bouguer Anomaly values without the regional gravitational signature (taken from the best fit line from the BGI data), along a transect from point A to B that overlays the northern part of the Sibundoy Valley with a NW to SE trend. The transect is approximately 39 km long. The calculated density measurements and the geology map were used to constrain this model, considering that the average of the basin infill is 1.8 g/cm^3. The geometries were changed until the calculated gravity best matches the observed gravity.

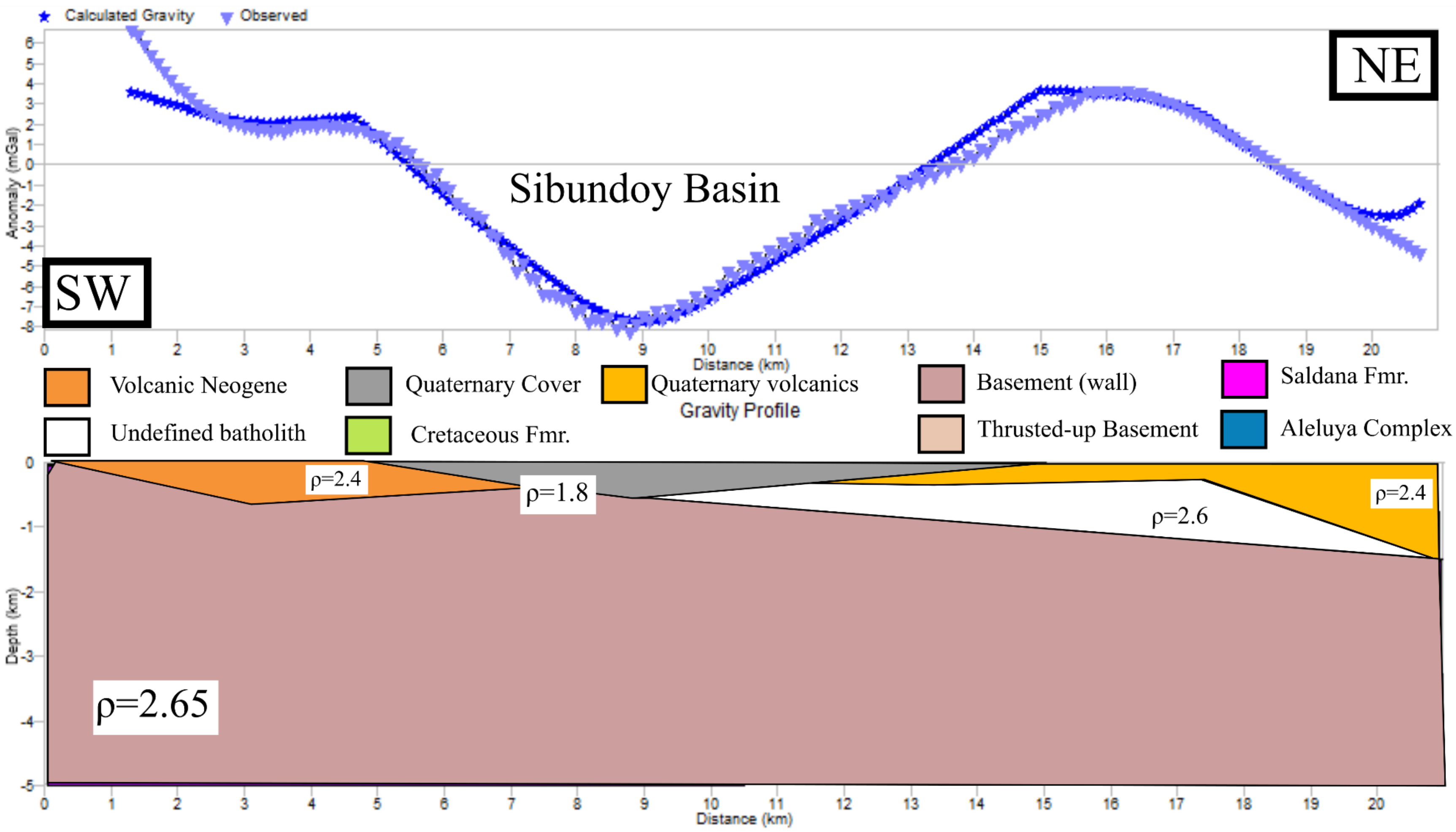

Figure 40 Model 4b shows the Complete Bouguer Anomaly values without the regional gravitational signature (taken from the best fit line from the BGI data), along a transect from point G and H that overlays the western part of the Sibundoy Valley with a SW to NE trend. The transect is approximately 32 km long. The calculated density measurements and the geology map were used to constrain this model, considering that the average of the basin infill is 1.8 g/cm^3. The geometries were changed until the calculated gravity best matched the observed gravity.

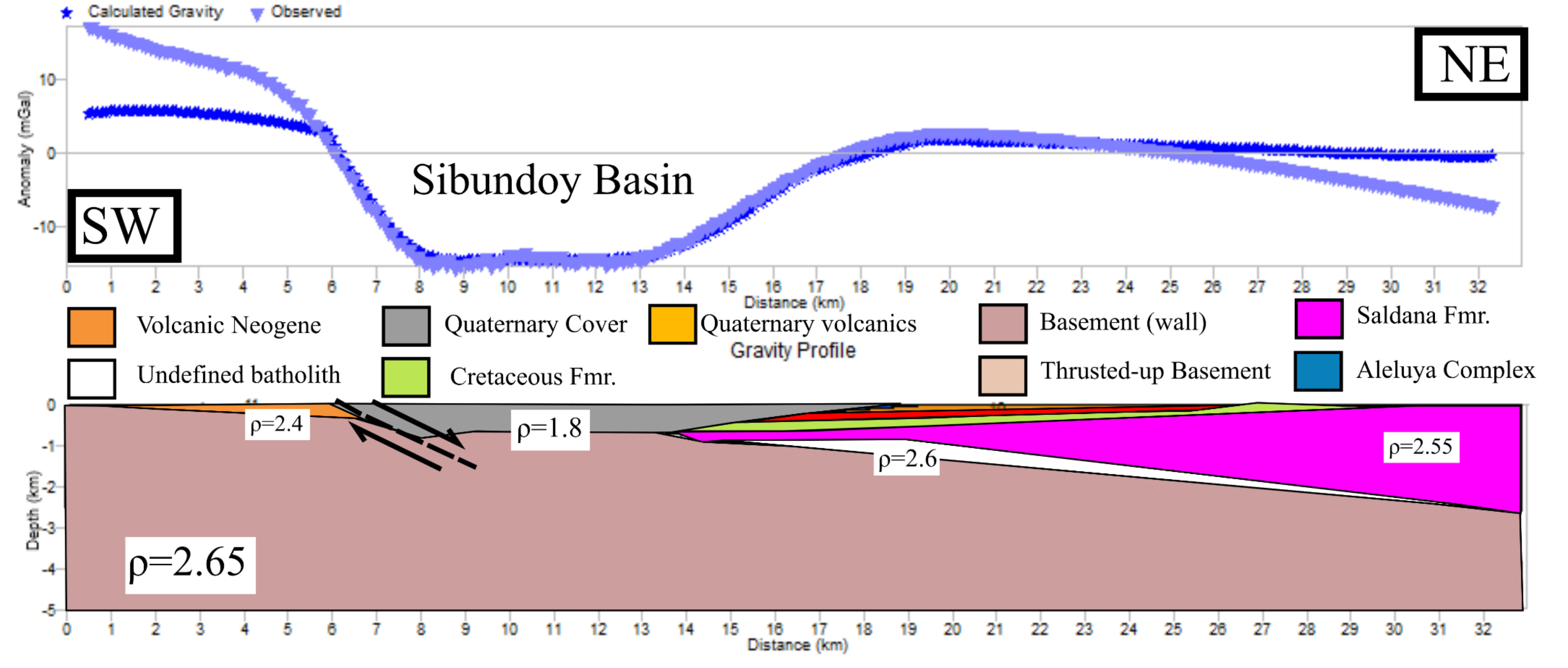

Figure 41 Model 6b shows the Complete Bouguer Anomaly values without the regional gravitational signature (taken from the best fit line from the BGI data), along a transect from point K and L that overlays the eastern part of the Sibundoy Valley with a SW to NE trend. The transect is approximately 32 km long. The calculated density measurements and the geology map were used to constrain this model, considering that the average of the basin infill is 1.8 g/cm^3. The geometries were changed until the calculated gravity best matched the observed gravity.

Models considering that the basin infill is 2.0 g/cm^3. Complete Bouguer Anomaly.

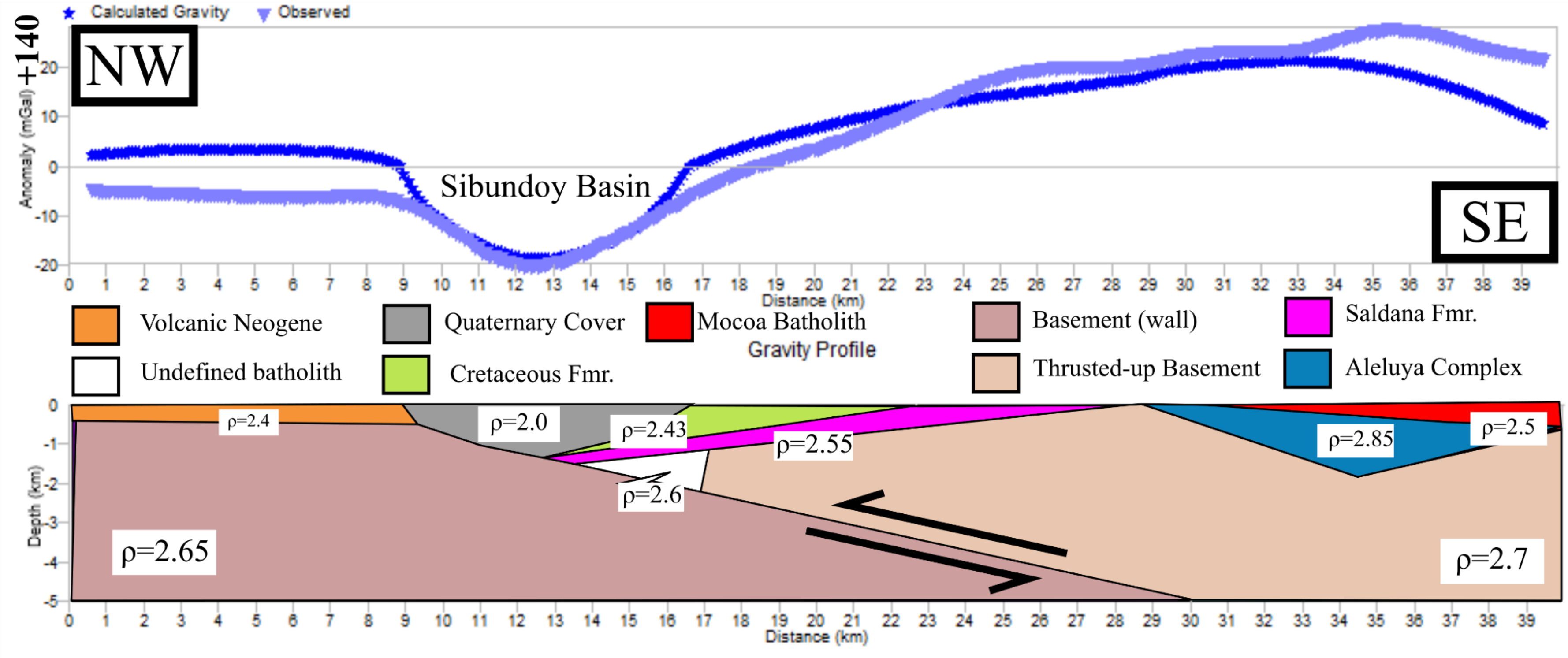

Figure 42 Model 1c shows the Complete Bouguer Anomaly values along a transect from point A and B that overlays the northern part of the Sibundoy Valley with a NW to SE trend. The transect is approximately 39 km long. The calculated density measurements and the geology map were used to constrain this model, considering that the average of the basin infill is 2.0 g/cm^3. The geometries were changed until the calculated gravity best matches the observed gravity.

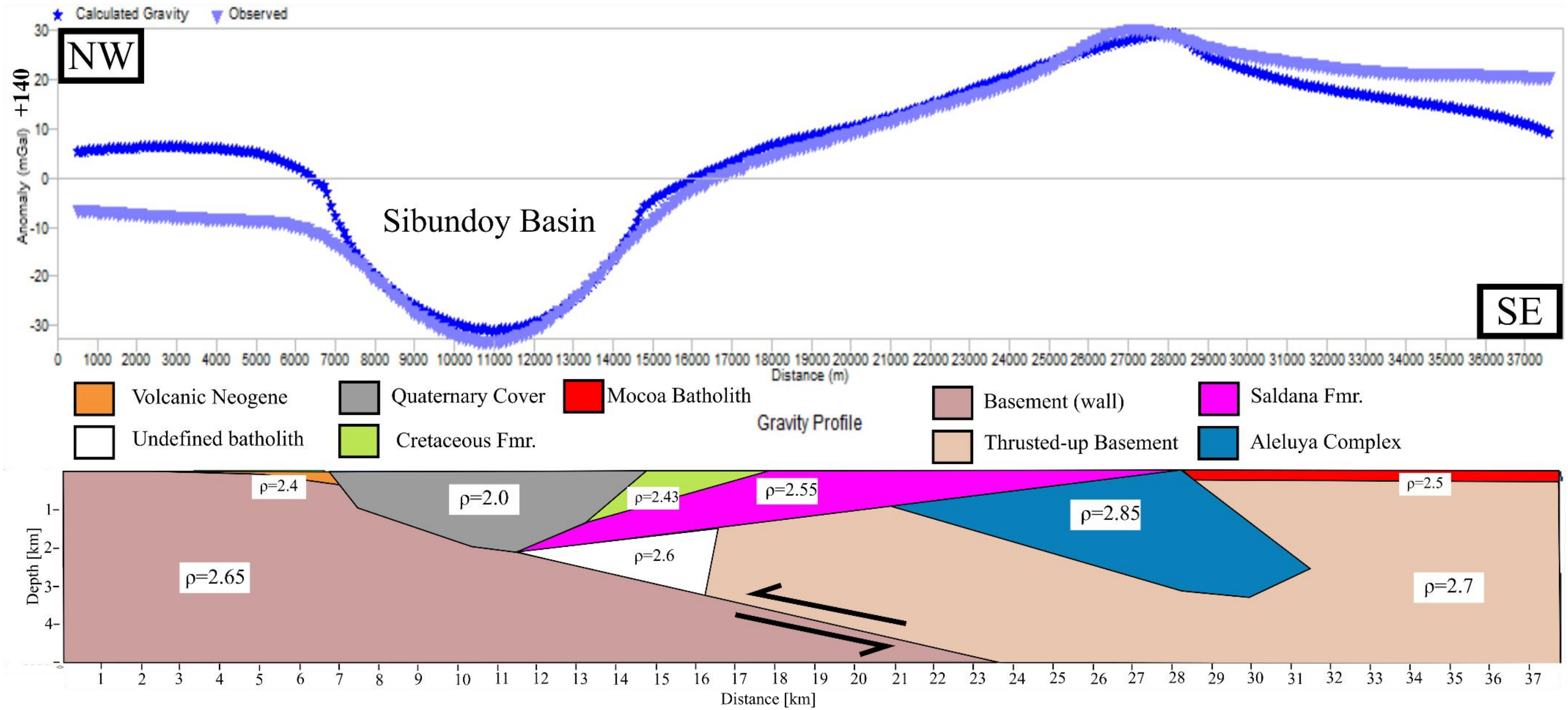

Figure 43 Model 2c shows the Complete Bouguer Anomaly values along a transect from point C and D that overlays the central part of the Sibundoy Valley with a NW to SE trend. The transect is approximately 38 km long. The calculated density measurements and the geology map were used to constrain this model, considering that the average of the basin infill is 2.0 g/cm^3. The geometries were changed until the calculated gravity best matches the observed gravity.

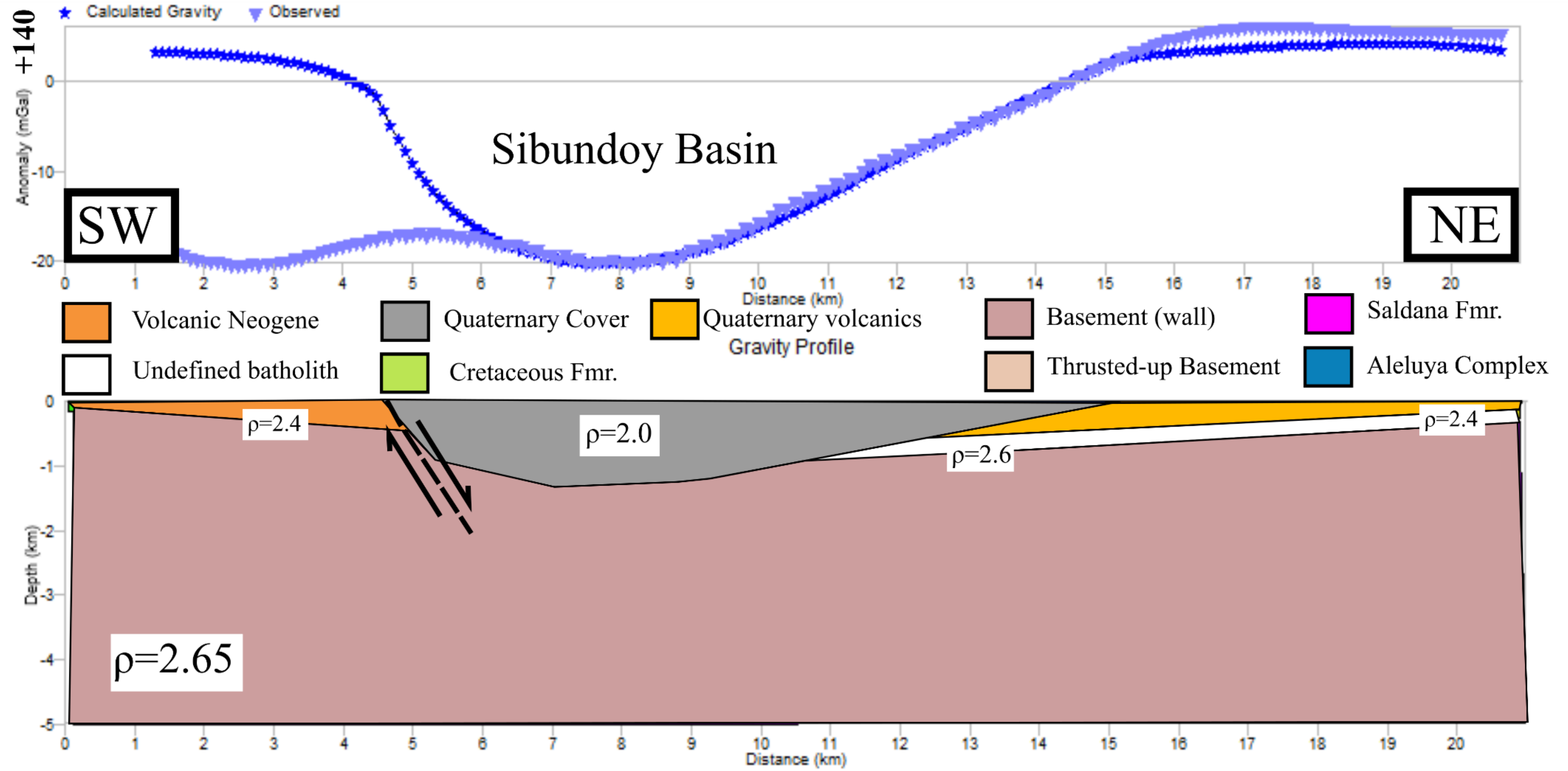

Figure 44 Model 4c shows the Complete Bouguer Anomaly values along a transect from point G and H that overlays the western part of the Sibundoy Valley with a SW to NE trend. The transect is approximately 21 km long. The calculated density measurements and the geology map were used to constrain this model, considering that the average of the basin infill is 2.0 g/cm^3. The geometries were changed until the calculated gravity best matches the observed gravity.

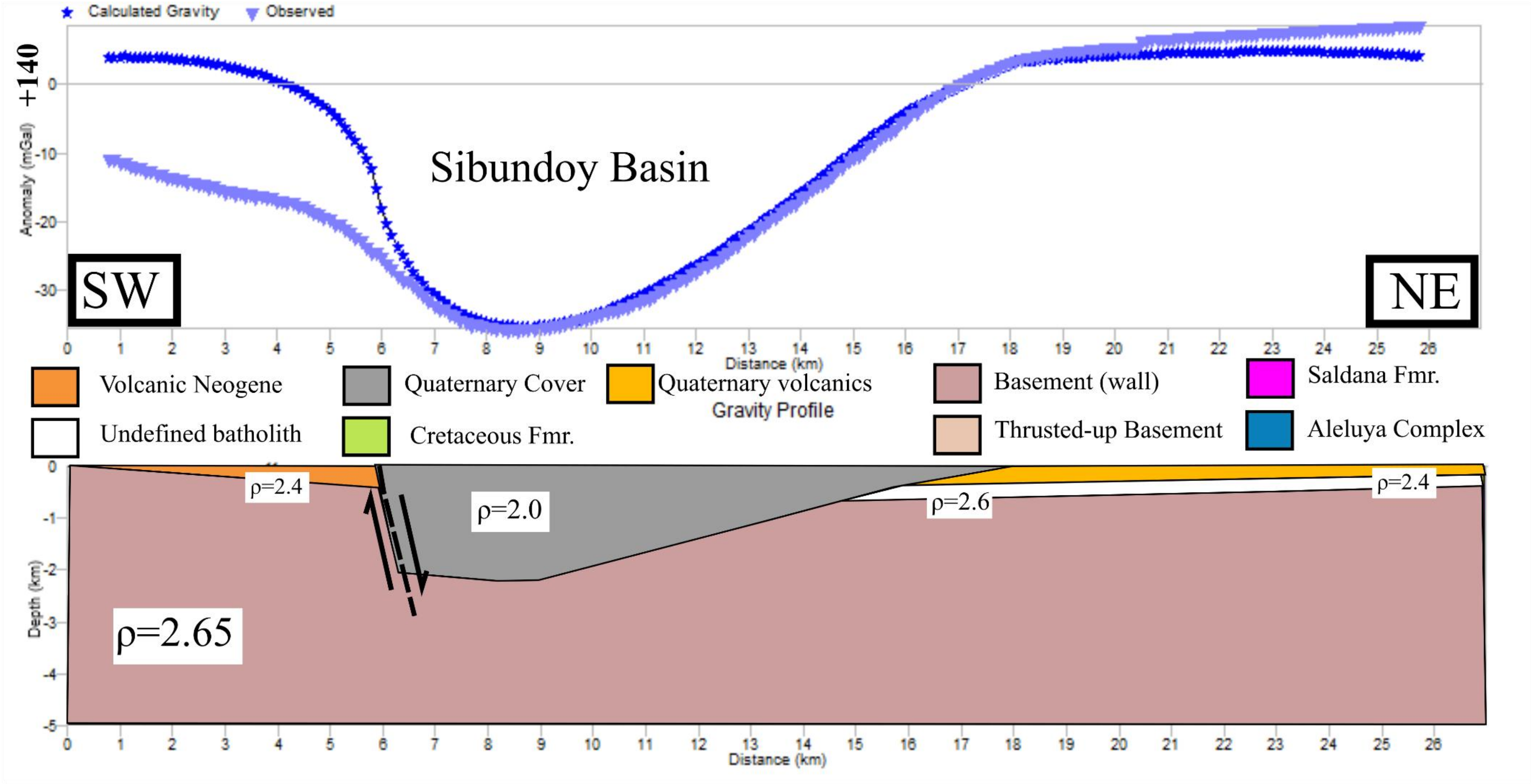

Figure 45 Model 5c shows the Complete Bouguer Anomaly values along a transect from point I and J that overlays the central part of the Sibundoy Valley with a SW to NE trend. The transect is approximately 26 km long. The calculated density measurements and the geology map were used to constrain this model, considering that the average of the basin infill is 2.0 g/cm^3. The geometries were changed until the calculated gravity best matches the observed gravity.

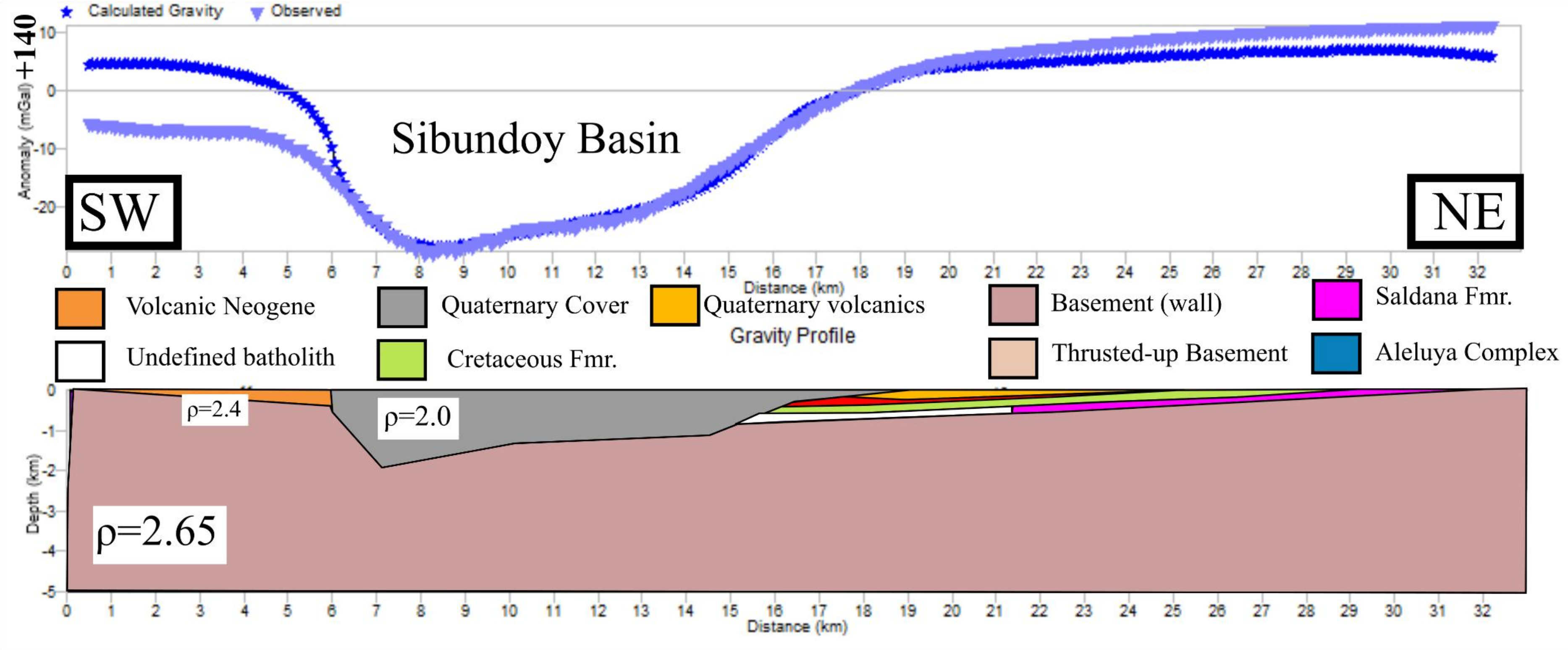

Figure 46 Model 6c shows the Complete Bouguer Anomaly values along a transect from point K and L that overlays the eastern part of the Sibundoy Valley with a SW to NE trend. The transect is approximately 32 km long. The calculated density measurements and the geology map were used to constrain this model, considering that the average of the basin infill is 2.0 g/cm^3. The geometries were changed until the calculated gravity best matches the observed gravity.

Models considering that the basin infill is 2.0 g/cm^3. Removal of regional trend.

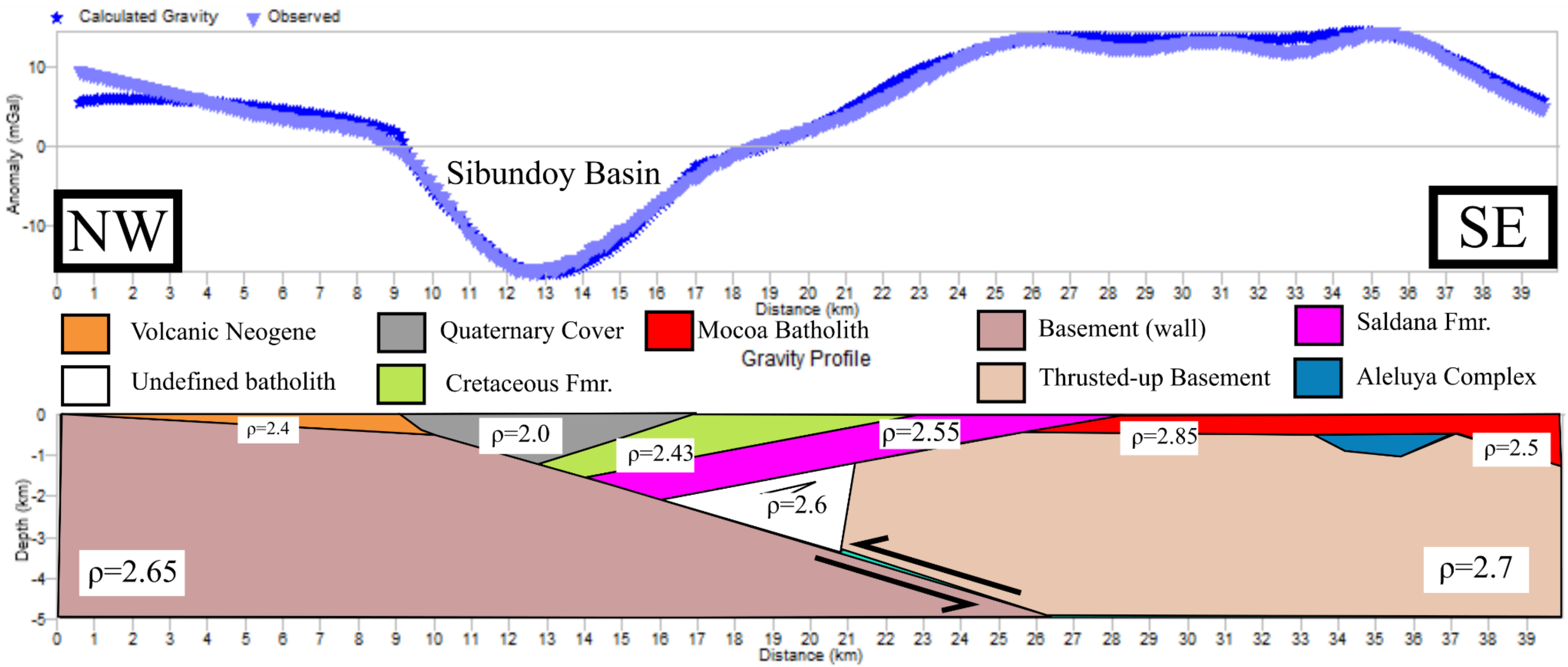

Figure 47 Model 1d shows the Complete Bouguer Anomaly values without the regional gravitational signature (taken from the best fit line from the BGI data), along a transect from point A and B that overlays the northern part of the Sibundoy Valley with a NW to SE trend. The transect is approximately 39 km long. The calculated density measurements and the geology map were used to constrain this model, considering that the average of the basin infill is 2.0 g/cm^3. The geometries were changed until the calculated gravity best matches the observed gravity.

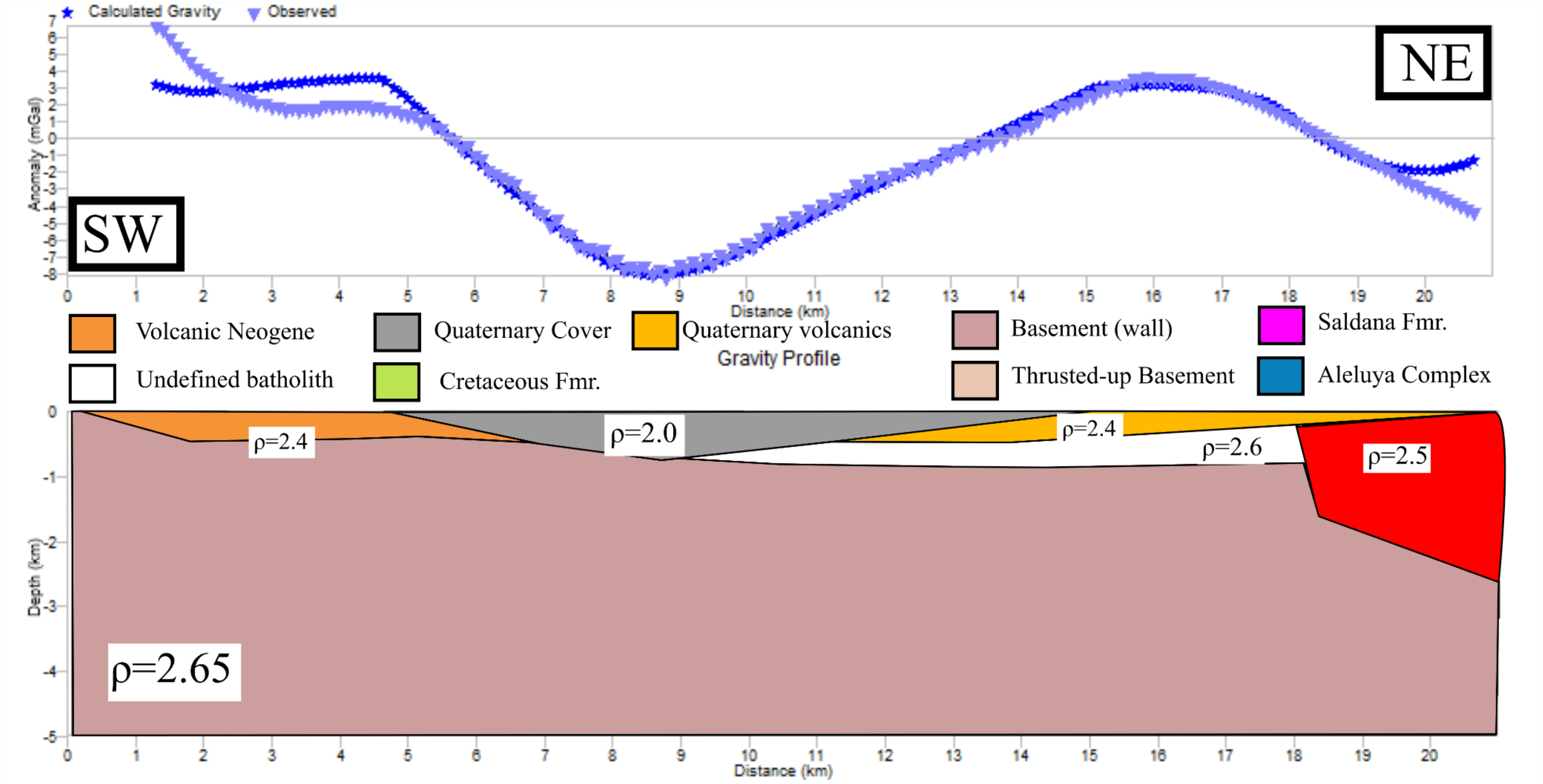

Figure 48 Model 4d shows the Complete Bouguer Anomaly values without the regional gravitational signature (taken from the best fit line from the BGI data), along a transect from point G and H that overlays the western part of the Sibundoy Valley with a SW to NE trend. The transect is approximately 20 km long. The calculated density measurements and the geology map were used to constrain this model, considering that the average of the basin infill is 2.0 g/cm^3. The geometries were changed until the calculated gravity best matches the observed gravity.

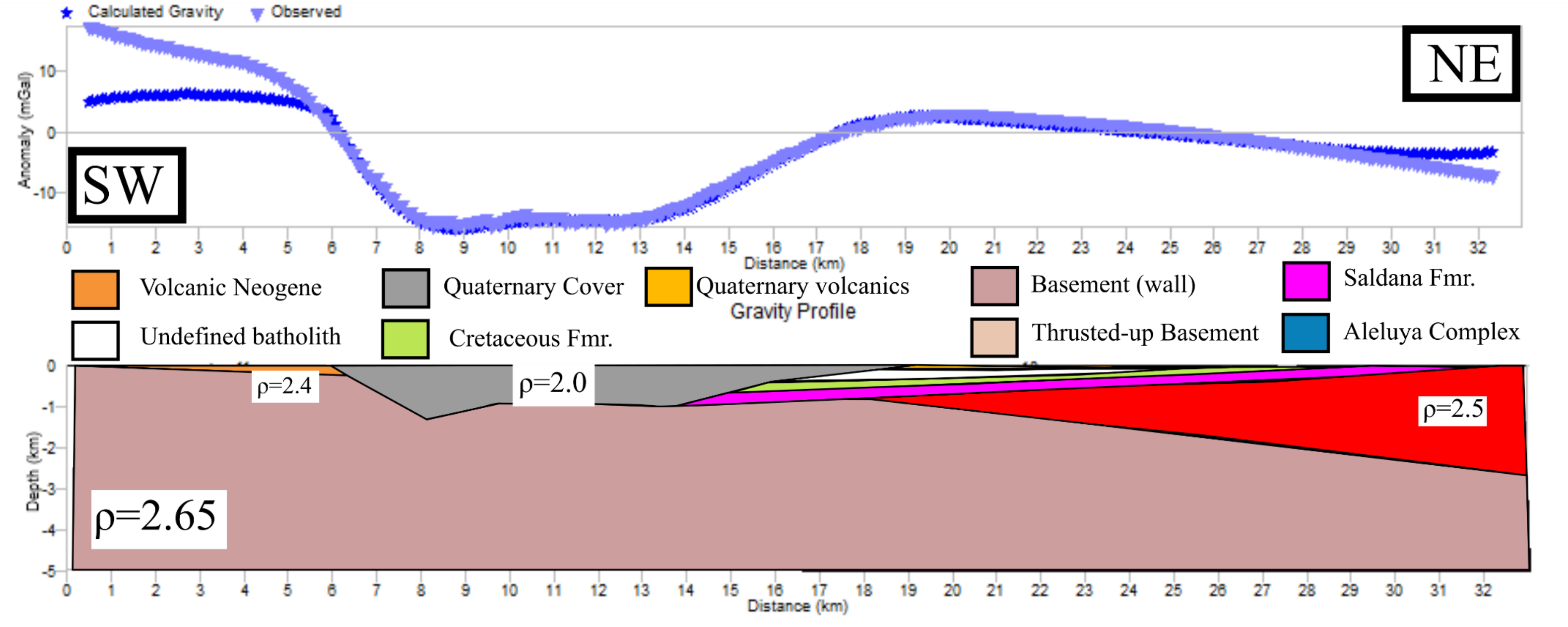

Figure 49 Model 6d shows the Complete Bouguer Anomaly values without the regional gravitational signature (taken from the best fit line from the BGI data), along a transect from point K and L that overlays the eastern part of the Sibundoy Valley with a SW to NE trend. The transect is approximately 32 km long. The calculated density measurements and the geology map were used to constrain this model, considering that the average of the basin infill is 2.0 g/cm^3. The geometries were changed until the calculated gravity best matched the observed gravity.